IVW - Schriftenreihe Band 59

Institut für Verbundwerkstoffe GmbH - Kaiserslautern

Konstantinos G. Gatos

Structure-Property Relationships in Rubber/Layered Silicate Nanocomposites

Bibliografische Information Der Deutschen Bibliothek

Die Deutsche Bibliothek verzeichnet diese Publikation in der Deutschen Nationalbibliografie; detaillierte bibliografische Daten sind im Internet über <http://dnb.ddb.de> abrufbar.

Bibliographic information published by Die Deutsche Bibliothek

Die Deutsche Bibliothek lists this publication in the Deutsche Nationalbibliografie; detailed bibliographic data is available in the Internet at <http://dnb.ddb.de>.

Herausgeber: Institut für Verbundwerkstoffe GmbH
Prof. Dr.-Ing. Alois K. Schlarb
Erwin-Schrödinger-Straße
TU Kaiserslautern, Gebäude 58
67663 Kaiserslautern
http://www.ivw.uni-kl.de

Verlag: Institut für Verbundwerkstoffe GmbH

Druck: Technische Universität Kaiserslautern
ZBT – Abteilung Foto-Repro-Druck

D 386

Als Manuskript gedruckt. Printed in Germany.

ISSN 1615-021X
ISBN 3-934930-55-7

Structure-Property Relationships in Rubber/Layered Silicate Nanocomposites

Vom Fachbereich für Maschinenbau und Verfahrenstechnik
der Technischen Universität Kaiserslautern
zur Verleihung des akademischen Grades

Doktor-Ingenieur (Dr.-Ing.)

genehmigte Dissertation

von

Dipl.-Phys. MSc. Konstantinos G. Gatos

aus Halkida, Griechenland

Tag der mündlichen Prüfung:	28. Oktober 2005
Dekan und Prüfungsvorsitzender:	Prof. Dr.-Ing. R. Renz
1. Berichterstatter:	Prof. Dr.-Ing. habil. Dr.h.c. J. Karger-Kocsis
2. Berichterstatter:	Prof. Z. A. Mohd Ishak

D 386

To my family

Στην οικογένειά μου

ACKNOWLEDGEMENTS

The present work was completed between October 2002 and September 2005 at the Institut für Verbundwerkstoffe GmbH (IVW) at the Technical University of Kaiserslautern.

First and foremost, I would like to express my special gratitude to my supervisor Prof. Dr.-Ing. habil. Dr.h.c. József Karger-Kocsis for his scientific support and constant interest on my work. Our fruitful discussions on polymer science and technology during my stay as PhD research assistant broadened my knowledge and enlightened the perspectives of this field.

I am thankful to Prof. Dr.-Ing. Rainer Renz for accepting the presidency of the examination committee. Many thanks are to the due to the co-referent of this PhD thesis Prof. Zainal Arifin Mohd Ishak for his constructive comments and remarks. I would like to express my special acknowledgements to Dr. Anton A. Apostolov and Dr. Ralf Thomann for the X-ray Diffraction Scattering (XRD) and Transmission Electron Microscopy (TEM) experiments, respectively. Their assistance and scientific skills accelerated the progress of this thesis significantly.

I would like to thank the German Science Foundation (DFG) for the financial support, as well as, the IVW GmbH for providing me all the appropriate means to realize this PhD work. Thanks are also due to the material donations for the following companies Lanxess Deutschland GmbH (Germany), Bayer AG (Germany), Nanomer Inc. (USA) and Southern Clay Inc. (USA). The support of the colleagues at the IVW is grateful acknowledged during my stay. Especially I would like to express my appreciation for the help and friendship to O. Gryshchuk, K. Kameo, P. Rosso, S. Wiedmer, I. Angelov, N. S. Sawanis and J. G. Martínez Alcázar.

Last but not least, I would like to convey my special thanks to my mother and my father, my brothers Vaggelis and Panos, as well as, to my fiancee Irini Koutmou who constantly supported and encouraged me.

Table of Contents

Acknowledgements I

Table of Contents III

Abstract/Kurzfassung VII

List of Abbreviations and Symbols XIII

1. Introduction……..…..1

2. Background……..……3

2.1 Elastomer Systems……..3

2.2 Types of Reinforcement……...……....4

2.2.1 Carbon Black…….5

2.2.2 Silica…….……6

2.2.3 Clay……..6

2.2.4 Surface Treatment…….8

2.3 Rubber/Layered Silicate Nanocomposites……...….9

2.3.1 Early Stage of Research……..……10

2.3.2 Current Stage…….11

2.4 Modeling of the Rubber Nanocomposites..……..12

2.4.1 Mechanical Performance……13

2.4.2 Gas Barrier Properties…….….15

3. Objectives……..……..17

4. Experimental……19

4.1 Materials…….....19

4.1.1 Rubber Matrix.....19

4.1.1.1 Ethylene Propylene Diene Monomer Rubber (EPDM).....19

4.1.1.2 Hydrogenated Acrylonitrile Butadiene Rubber (HNBR)…….20

4.1.1.3 Natural Rubber……21

4.1.2 Fillers……21
4.1.2.1 Conventional Fillers……21
4.1.2.2 Natural Clay and its Organophilic Versions……21
4.1.2.3 Synthetic Clay and its Organophilic Versions……22
4.1.3 Vulcanization Additives and Cure Recipes……23
4.1.3.1 EPDM……23
4.1.3.2 HNBR……23
4.1.3.3 NR……24
4.2 Compounding……25
4.2.1 Internal Mixer……25
4.2.2 Open Mill……25
4.3 Vulcanization……25
4.3.1 Rheometer……25
4.3.1.1 Monsanto Rheometer……25
4.3.1.2 Plate-Plate Rheometer……26
4.3.2. Hot Press……27
4.4 Mechanical Characterization……27
4.4.1 Tensile Experiments……27
4.4.2 Tear Test……27
4.4.3 Hardness……27
4.4.4 Cyclic Loading……28
4.5 Thermo Mechanical Characterization……28
4.5.1. Dynamic Mechanical Thermal Analysis (DMTA)……28
4.5.2. Thermo Gravimetric Analysis (TGA)……28
4.6 Oxygen Permeability Measurements……28
4.7 Micro- and Nano-structural Characterization……29
4.7.1 Scanning Electron Microscopy (SEM)……29
4.7.2 Transmission Electron Microscopy (TEM)……29
4.7.3 X-ray Diffraction (XRD)……29

5. Results and Discussion……30
5.1 Estimation of the Optimum Vulcanization Time: A New Method……30
5.2 Mechanisms Involved in Rubber/Organoclay Nanocomposite Formation……38

5.3 EPDM/Organoclay Nanocomposites……...39
5.3.1 Effect of Mixing Procedure……..…39
5.3.2 Effect of Polarity…….46
5.3.3 Effect of Vulcanization Accelerator…….49
5.3.4 Effect of Organoclay Intercalant…….56
5.3.5 Effect of Clay Loading……..60
5.4 HNBR/Organoclay Nanocomposites……64
5.4.1 Clay Dispersion in Sulfur Cured Systems ……..……..…64
5.4.1.1 Effect of Type of Organoclay Intercalant ……..……..65
5.4.1.2 Effect of Aspect Ratio of Clay Platelet ……....74
5.4.2 Clay Dispersion in Peroxide Cured Systems and Properties …….81
5.5 Modeling the Rubber/Organoclay Nanocomposite Behavior……...89
5.5.1 Mechanical Properties……..89
5.5.2 Gas Permeation……92

6. Summary and Outlook……...95

7. Appendix……...98

8. Literature……101

List of Publications 119

List of Student Support Works 121

Abstract

The scientific and industrial interest devoted to polymer/layered silicate nanocomposites due to their outstanding properties and novel applications resulted in numerous studies in the last decade. They cover mostly thermoplastic- and thermoset-based systems. Recently, studies in rubber/layered silicate nanocomposites were started, as well. It was presented how complex maybe the nanocomposite formation for the related systems. Therefore the rules governing their structure-property relationships have to be clarified. In this Thesis, the related aspects were addressed.

For the investigations several ethylene propylene diene rubbers (EPDM) of polar and non-polar origin were selected, as well as, the more polar hydrogenated acrylonitrile butadiene rubber (HNBR). The polarity was found to be beneficial on the nanocomposite formation as it assisted to the intercalation of the polymer chains within the clay galleries. This favored the development of exfoliated structures. Finding an appropriate processing procedure, i.e. compounding in a kneader instead of on an open mill, the mechanical performance of the nanocomposites was significantly improved. The complexity of the nanocomposite formation in rubber/organoclay system was demonstrated. The deintercalation of the organoclay observed, was traced to the vulcanization system used. It was evidenced by an indirect way that during sulfur curing, the primary amine clay intercalant leaves the silicate surface and migrates in the rubber matrix. This was explained by its participation in the sulfur-rich Zn-complexes created. Thus, by using quaternary amine clay intercalants (as it was presented for EPDM or HNBR compounds) the deintercalation was eliminated. The organoclay intercalation/deintercalation detected for the primary amine clay intercalants, were controlled by means of peroxide curing (as it was presented for HNBR compounds), where the vulcanization mechanism differs from that of the sulfur curing.

The current analysis showed that by selecting the appropriate organoclay type the properties of the nanocomposites can be tailored. This occurs via generating different nanostructures (i.e. exfoliated, intercalated or deintercalated). In all cases, the rubber/organoclay nanocomposites exhibited better performance than vulcanizates with traditional fillers, like silica or unmodified (pristine) layered silicates.

The mechanical and gas permeation behavior of the respective nanocomposites were modelled. It was shown that models (e.g. Guth's or Nielsen's equations) developed for "traditional" vulcanizates can be used when specific aspects are taken into consideration. These involve characteristics related to the platy structure of the silicates, i.e. their aspect ratio after compounding (appearance of platelet stacks), or their orientation in the rubber matrix (order parameter).

Kurzfassung

Es besteht heutzutage ein großes wissenschaftliches und industrielles Interesse an Polymer/Schichtsilikat-Nanoverbundwerkstoffen aufgrund ihrer ungewöhnlichen Eigenschaften, welche neue Anwendungsmöglichkeiten versprechen. Die Forschung und Entwicklung konzentrierte sich bislang auf Nanoverbundwerkstoffe mit thermoplastischen- und duroplastischen- Matrizes. Erst kürzlich wurden die Untersuchungen auf Elastomer/Schichtsilikat Systeme ausgeweitet. Trotz des weltweiten Interesses an solchen neuartigen Verbundwerkstoffen sind die Gesetzmäßigkeiten der Struktur-Eigenschaftsbeziehungen noch nicht ausreichend untersucht und genügend geklärt worden. Daher war es das Hauptziel der vorliegenden Arbeit, einen wesentlichen Beitrag zur Aufklärung der Struktur-Eigenschafts-Beziehungen in schichtsilikatmodifizierten Gummiwerkstoffen zu liefern.

Diese Arbeit beschäftigt sich mit verschiedenen EPDM Elastomeren polarer und apolarer Natur, sowie mit einem polaren HNBR Elastomer. Die Auswahl liegt darin begründet, dass die Polarität der Matrix die Herstellung und Eigenschaften der jeweiligen Nanoverbundwerkstoffe maßgeblich beeinflusst. Da das Schichtsilikat selber von polarer Natur ist kann somit dessen Verträglichkeit mit dem Elastomer durch die Anwesenheit von polaren Gruppen verbessert werden. Dies begünstigt die Dispersion des Schichtsilikates, d.h. fördert dessen Interkalierung und Exfolierung. Die polare Variante von EPDM diente dafür, den Einfluss der Mischungsparameter aufzuklären. Es wurde festgestellt, dass die im Mischkneter hergestellten Mischungen über bessere mechanische Eigenschaften verfügen als Mischungen, die auf einem Walzwerk präpariert wurden. Die mikrostrukturelle Untersuchung der Proben, welche im Mischkneter bzw. auf dem Walzwerk hergestellt wurden, deutete darauf hin, dass die Interkalierung des Schichtsilikates in erster Annäherung von der Thermodynamik abhängt. Ebenfalls trug die hohe Scherung, welche im Mischkneter vorherrscht, zum Aufbrechen der Schichtsilikatagglomerate bei. Je besser die Silikatdispergierung in der elastomeren Matrix war, desto deutlicher war der Verstärkungseffekt (Steifigkeit, Festigkeit) durch die Silikatplättchen.

Es wurde aufgezeigt, dass die Herstellung von Elastomer/Schichtsilikat Nanoverbundwerkstoffen ein sehr komplexes Verfahren darstellt. Die Deinterkalierung, welche in den EPDM/MMT-ODA Mischungen festgestellt wurde,

konnte auf eine Komplexbildung während der Schwefelvernetzung zurückgeführt werden. Weiterhin wurde indirekt nachgewiesen, dass das ODA während der Vulkanisation bei der Ausbildung eines Zink-Schwefel-Beschleuniger-Übergangskomplexes teilnimmt und dadurch sogar die ursprüngliche Interkalierung des MMT-ODA beeinflusst. Um diese Erklärung zu untermauern, wurden weitere Ergebnisse von Mischungen mit anderen Beschleunigern ohne Zinkgehalt (wie MBT und CBS) herangezogen, welche keine Deinterkalierung verursacht haben. Die deinterkalierten Stukturen, soweit vorhanden, lagen zusammen mit interkalierten und exfolierten Stukturen in der Matrix vor. Die Deinterkalierung der Schichtsilikate lässt sich durch Modifikatoren wenig hoher Reaktivität (quaternäre Aminverbindungen) kontrollieren. Daher führte die Verwendung von organophilen Schichtsilikaten (Organoschichtsilikate) mit den ursprünglichen Interkalanten (Modifikatoren) ODTMA und MTH zu keinerlei Deinterkalierung. Des Weiteren wurde festgestellt, dass die OH-Gruppen von MTH Wasserstoffbrücken mit der CN-Gruppe des HNBR bilden können, was zu einem höheren Dispersionsgrad und dadurch zu verbesserten Eigenschaften führte. Dies spiegelte sich unter anderem in einen höheren Modul (sowohl im DMTA- als auch im Zugversuch) des HNBR/MMT-MTH Nanoverbundwerkstoffes im Vergleich mit HNBR/MMT-ODA oder HNBR/MMT-ODTMA wider.

Die Überlegung bezüglich der oben angesprochenen Komplexbildung als Grund für die auftretende Deinterkalierung des Organoschichtsilikates wurde durch Untersuchungen an peroxidvernetzten Systemen (HNBR/MMT-ODA), wo Deinterkalierung nicht stattgefunden hat, verstärkt. In diesem Fall wurden nur interkalierte Silikatstrukturen in der Matrix wiedergefunden. Unter Betrachtung aller HNBR/Organoschichtsilikat Nanoverbundwerkstoffe konnte festgestellt werden, dass diejenigen, welche mit MMT-MTH modifiziert wurden, den höchsten Modul- und auch die niedrigste Sauerstoff-Permeabilität aufgezeigt haben.

Durch den Vergleich zweier Schichtsilikate mit unterschiedlichen Länge/Dicke-Verhältnissen (MMT und FHT) konnte festgestellt werden, dass je größer dieser Parameter ist, desto geringerer ist die Permeabilität und höher die Steifigkeit. Dies liegt in der ausgeprägteren „sekundären Struktur“ der dispergierten Silikatplättchen in der Matrix begründet. Es sei an dieser Stelle angemerkt, dass der gleiche organophile Interkalant, nämlich ODA, für diesen Vergleich benutzt wurde. Die

thermische Zersetzung (gemessen mittels TGA) der Elastomer/Organoschichtsilikat Nanoverbundwerkstoffe setzte verglichen mit dem unmodifizierten Material erst bei mehr als 10 Grad höheren Temperaturen ein.

Weiterhin wurde der Einfluss des Länge/Dicke-Verhältnisses der dispergierten Silikatstrukturen bzw. deren Volumenanteils auf die mechanischen Eigenschaften und Permeabilität ermittelt und zusätzlich modelliert. Als Ergebnis kann festgehalten werden, dass die Modul-Erhöhung bei dem HNBR/FHT-ODA Nanoverbundwerkstoff mit der modifizierten Guth Gleichung beschreibbar ist. Der Grund hierfür ist, dass dieses Model sowohl die weiche Matrix als auch die Plattenstruktur des Silikates berücksichtigt. Das modifizierte Nielsen's-Model (Bharadwaj's Model) wurde als optimal für die Beschreibung der Permabilität des HNBR/FHT-ODA Systems befunden. Die theoretischen Überlegungen des Bharadwajs Models stimmten mit den experimentellen Ergebnissen (gewonnen durch die Bildanalyse von TEM-Aufnahmen) gut überein.

List of Abbreviations and Symbols

Abbreviations

CB	carbon black
CBS	N-cyclohexyl-2-benzothiazole sulfenamide
CEC	cation exchange capacity
CN	acrylonitrile group
CTAB	cetyltrimethyl-ammonium-bromide
DBP	dibutyl-phthalate
DBPA	dibutyl-phthalate absorption
DMTA	dynamic mechanical thermal analysis
ENR	epoxidized natural rubber
EPDM	ethylene propylene diene rubber
EPDM-GMA	ethylene propylene diene rubber grafted with glycidyl methacrylate
EPDM-MA	ethylene propylene diene rubber grafted with maleic anhydride
FHT	fluorohectorite
FHT-ODA	fluorohectorite intercalated by octadecylamine
FKM	fluoro-elastomer
GMA	glycidyl methacrylate
H-bonds	hydrogen bonds
HNBR	hydrogenated acrylonitrile butadiene rubber
HT	hydrogenated tallow
JEF	Jeffamine®
MA	maleic anhydride
MBT	2-mercaptobenzothiazole
MgO	magnesium oxide
MMT-MTH	montmorillonite intercalated by methyl-tallow-bis(2-hydroxylethyl) quaternary ammonium salt
MMT-ODA	montmorillonite intercalated by octadecylamine
MMT-ODTMA	montmorillonite intercalated by octadecyltrimethylammonium salt
MRF	modulus reduction factor
MTH	methyl-tallow-bis(2-hydroxylethyl) quaternary ammonium
Na_2SiF_6	sodium hexaflorosilicate

NBR	nitrile rubber
NR	natural rubber
ODA	octadecylamine
ODR	oscillating disc rheometer
ODTMA	octadecyltrimethylamine
OH	hydroxyl group
OTR	oxygen transmission rate
PE	polyethylene
phr	parts per hundred parts rubber
PMMA	polymethylmethacrylate
PS	polystyrene
PVC	polyvinylchloride
rpm	revolution per minute
S_8	sulfur ring
SBR	styrene butadiene rubber
SEM	scanning electron microscopy
Si-OH	silanol group
TEM	transmission electron microscopy
TEOS	tetraethoxysilane
TGA	thermo gravimetric analysis
TMTD	tetramethyl thiuram disulfide
TOTM	trioctyl trimellitate
TTS	isopropyl tristearoyl titanate
XRD	wide angle X-ray diffraction scattering
ZDAC	bis(dialkyldithiocarbamato)zinc(II)
ZDEC	zinc diethyldithiocarbamate
ZMMBI	zinc methylmercaptobenzimidazole
ZnO	zinc oxide

Symbols

c	[1]	volume concentration
CEC	[meq/100g]	cation exchange capacity
d(001)	[nm]	interlayer spacing

E	[MPa]	Young's modulus
E'	[MPa]	elastic storage modulus
E*	[MPa]	complex modulus
f	[1]	shape factor
f	[rad/sec]	frequency
G*	[Pa]	complex shear modulus
G'	[Pa]	storage shear modulus
G''	[Pa]	loss shear modulus
M_L	[g.cm]	minimum torque
M_H	[g.cm]	maximum torque
ML	[1]	Mooney viscosity
n	[1]	reflection order
P	[cm^3.mm/m^2.day.atm]	permeation coefficient
R_L	[1]	minimum tanδ value
R_H	[1]	maximum tanδ value
T	[^oC]	temperature
t	[nm]	thickness
t_{90}	[min]	optimum curing time
t_2	[min]	scorch time
tanδ	[1]	mechanical loss factor
T_g	[^oC]	glass transition temperature
S	[1]	order parameter
w	[nm]	width

Greek Symbols

ζ	[1]	shape parameter
η	[Pa]	viscosity
θ	[^{o}]	angle
λ	[nm]	wavelength
φ	[1]	volume concentration
φ_{eff}	[1]	effective filler volume

1. Introduction

Practical applications of rubber appeared mainly after the discovery of its crosslinking with sulfur (i.e. vulcanization) in the year 1839 by Charles Goodyear (in USA). In the years followed, the first breakthrough in the rubber research was the first patent on synthetic rubber production in 1909 by F. Hofmann, in Germany.

Nowadays rubbers find a plethora of applications in automotive, agriculture, building/constructions and leisure mainly as tires, timing belts, sealing articles, water and fuel pipes, elastic binders/damping parts, etc. Therefore, to understand and predict the structure-property relationships in rubbers are of great practical relevance. In addition, this means at the same time a great scientific challenge.

The market demands cover a wide spectrum of rubber properties ranging from those of the unfilled vulcanizates (showing low modulus and high extensibility) up to highly filled vulcanizates (possessing high modulus and low elongation at break). Designing with rubber requires its property tailoring. This can be achieved by appropriate selection of the elastomer type, its vulcanization recipe and used fillers. Thus, a combined knowledge on chemistry, physics and engineering is the key for the successful application of rubber parts and products.

Since almost one century, fillers like carbon black and silica are widely used in the rubber industry. Carbon black guaranties high stiffness and strength whereas silica improves the rolling resistance. On the other hand, carbon black and silica are hazardous ingredients as compounding is an “open” process. As they are isometric fillers they do not affect the barrier properties on the final rubber part. In addition, their incorporation often results in low elongation at break values, at least for high filler loadings.

Therefore, there is a continuous search for new fillers, which may yield improved characteristics. In this respect, modified layered silicates are promising candidates. Low gas permeation properties (via the platy type structure), low filler loading for optimum mechanical performance (due to intercalation/exfoliation) and coloring possibility (usually they have off-white color) are some of their possible benefits. Last but not least, they become nanoscale dispersed only during compounding, which minimizes the health hazard effects. Disadvantageous is their higher cost compared to the inexpensive carbon black or silica grades. Further, little information is available

on the nanocomposite formation in rubber/layered silicate, which is a complex process influenced by many parameters.

Having a look at the producers of modified layered silicates, the number of which increases [global producers are Nanocor Inc. (USA), Southern Clay Inc. (USA), Süd-Chemie (Germany), FCC Inc. (China)], their price reduction is soon expected. On the other hand, this PhD work was conducted in order to contribute to the understanding of rubber/layered silicate nanocomposite formation. Elastomer types of different polarity (i.e. EPDM, EPDM-MA, EPDM-GMA, HNBR), layered silicates of different origin (i.e. MMT, FHT) and with various modifiers (i.e. –ODA, -ODTMA, -MTH), as well as, various vulcanization recipes (i.e. change in the accelerator type and vulcanization system) were used in order to shed light in how they affect the intercalation/exfoliation behavior (dispersed states). The most relevant properties of the rubber nanocomposites produced have been determined and traced to the dispersion of the layered silicates. Attention was paid at comparing the properties of the novel nanocomposites with those containing traditional fillers (silica). A further aim of this work was to find a correlation between the dispersion state (nanocomposite characteristics) and selected properties, as well as, to predict and model their performance.

2. Background

2.1 Elastomer Systems

Main characteristic of vulcanized rubber is the elastic behavior after deformation in compression or tension (elastomer). Having a moderate crosslinked network and assuming no change in the internal energy of the elastomer, the deformation process is governed solely by entropic elasticity.

It was early realized that just sulfur itself demanded prolonged curing times. However, the first patent for accelerated vulcanization was filed in 1912 by Hofmann and Gottlob. Since then, extensive research on this field resulted in many vulcanization recipes. Additives, assisting to the vulcanization procedure (e.g. activators, retarders, softeners), or improving the final properties (e.g. antioxidants) are also important [1-3]. Regarding sulfur curing, nowadays, conventional (2.0-3.5 phr sulfur with 1.0-0.5 phr accelerator), semi-efficient (1.0-2.0 phr sulfur and 2.5-1.0 phr accelerator) or efficient (0.2-0.9 phr sulfur and 6.0-2.5 phr accelerator) vulcanization system are usually in action [1, 4]. They differ from each other in the ratio of mono- (S), di- (S_2) and poly-sulfidic (S_x) links as schematically shown in Figure 2.1. Note that cyclic sulfur crosslinks or sulfur chains are also possible outcomes of rubber curing.

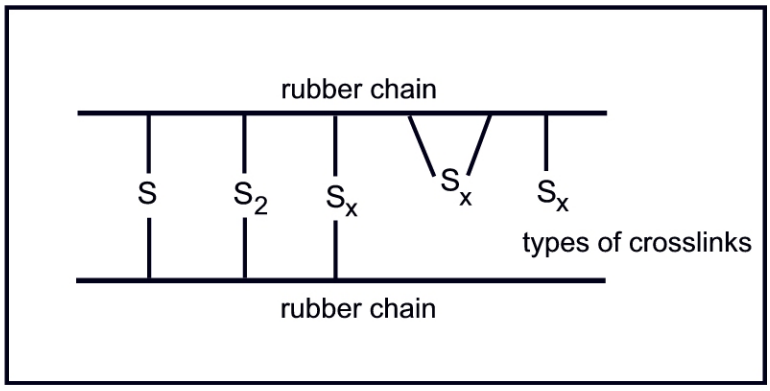

Figure 2.1: Scheme of the different crosslink structures obtained during vulcanization

Sulfur curing proceeds in three stages [5]. The first regime is the induction (scorch) period during which an accelerator complex forms [6-8]. The second period is that of the cure in which the crosslinked network is built (i.e. modulus increase; under- and

optimum- vulcanization regions in Figure 2.2), and the third one is the overcure (reversion) regime (cf. Fig. 2.2) [6]. The mechanisms involved in the vulcanization procedure and the contribution of each additive in the respective steps appear even nowadays as open research fields [9]. This fact is the main reason why every rubber company has its own formulations and keep them under secrecy.

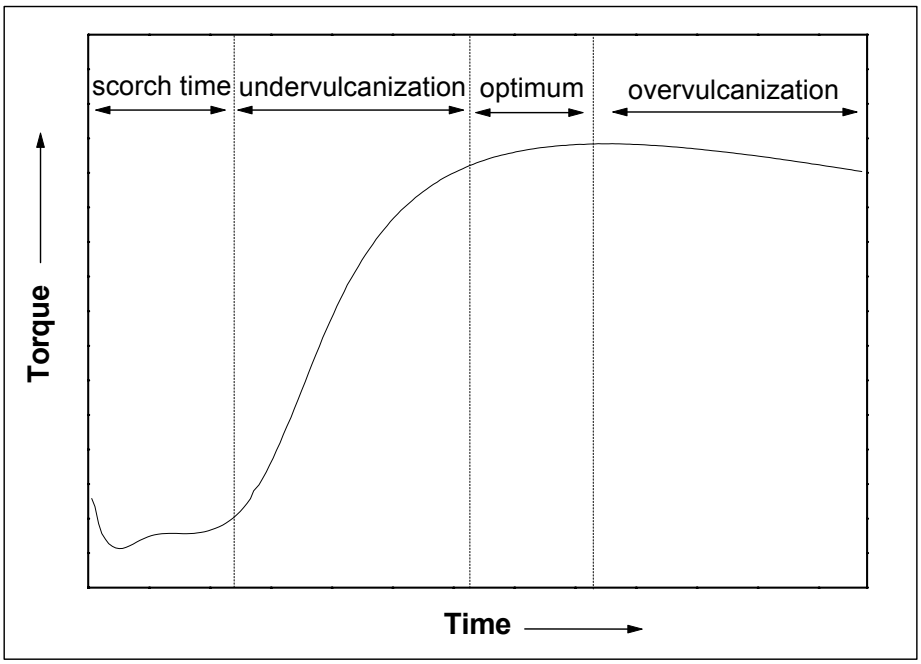

Figure 2.2: Stages of rubber vulcanization. Note that torque correlates with the crosslink density and shear modulus

Apart from sulfur, which demands the presence of an unsaturated polymer backbone to develop its action, vulcanization can be achieved by other means, like peroxide, resins or radiation [1, 4]. The related mechanism of crosslinking is different. For example in case of peroxide, crosslinking is initiated by the thermal decomposition of the peroxide, which generates free radicals on the rubber chains followed by their recombination [10-11].

2.2 Types of Reinforcement

Thinking in applications, rubbers articles should provide apart from the usual elasticity, properties fulfilling the operation demands (e.g. tensile and tear strength, low compression set, swelling resistance) [12]. For that purpose, rubbers are compounded with fillers, which ensure the desirable performance.

2.2.1 Carbon Black

The most popular filler for rubber reinforcement is by far the carbon black, covering all its variants (thermal, furnace, channel and acetylene blacks). Carbon black means elemental carbon (C) in the form of spherical particles of colloidal size. Its particles are coalesced into aggregates and agglomerates as carbon black obtained by the combustion or thermal decomposition of hydrocarbons [13]. The carbon blacks are distributive in nature regarding their particle size, aggregate form and aggregate shape between the different grades. About terminology, agglomerate comprised of a large number of aggregates, which are physically held together as opposed to the continuous graphitic structure, which links the particles within the aggregates [14].

Carbon blacks differ in their specific surface area, (generally expressed in m^2/g) affecting their reinforcing action in the polymer network. For its evaluation, the widely used techniques measure the adsorption of specific molecules (e.g. nitrogen, cetyltrimethyl-ammonium-bromide (CTAB) or iodine) on the carbon black surface [15].

In a rubber compound, the voids between the aggregates are filled with rubber. This occluded rubber is partly shielded from deformation and thus acts rather as part of the filler than as a part of the matrix. This parameter is related with the bulkiness of the carbon black. Thus, its estimation is based on the absorption of a liquid (dibutyl-phthalate, DBP) up to the point where the dry crumbly carbon black starts to cohere. At this point the liquid has filled the voids within and between the aggregates [15]. From the DBP absorption (DBPA), the related bulkiness can be evaluated by equation 2.1, where φ' corresponds to the CB volume fraction (φ) plus the occluded rubber.

$$\varphi' = \varphi\left(\frac{1 + 0.002139\,DBPA}{1.46}\right) \tag{2.1}$$

The degree of irregularity of the carbon black, the branching due to aggregation and the asymmetry of the aggregates results in the so-called “structure” of the carbon black. This is the reason why the term “bound rubber” has been introduced. Bound rubber is defined as the rubber portion in an uncured sample, which cannot be

extracted by a good solvent due to the adsorption (physical adsorption and chemisorption) of the rubber molecules onto the filler surface. In vulcanizates, the formation of an immobilized layer around the carbon structures is called “rubber shell”. The first term (bound rubber) refers to the whole molecule entangled with other molecules, which are attached to the filler, whereas the latter (shell) is related to the segments rather than the molecules the motion of which is affected by the filler [16].

2.2.2 Silica

Silica, which is amorphous, consists of silicon and oxygen arranged in a tetrahedral structure of a three dimensional lattice. There is no long-range crystal order, only short-range ordered domains in a random arrangement with neighboring domains. It appears also as traditional filler for rubber reinforcement yielding very good wet traction and rolling resistance.

The presence of the silanol groups (Si-OH) on the silica surface induces strong particle-particle interaction. By this way, the tendency for filler agglomeration rises [17]. The surface silanol concentration influences the degree of surface hydration. High levels of hydration can adversely affect the physical properties of the final compound. Most common preparation techniques of silica are the solution and the pyrogenic processes (fumed silica). For a better dispersion of the silica particles their in-situ generation is exploited by the sol-gel reaction using as silica precursor tetraethoxysilane (TEOS) [18-19].

2.2.3 Clay

As a non-black filler type, clay has been known for filling of rubbers since many decades ago [20]. In the literature the term clay denotes a textural class of minerals consisting of particles with an equivalent spherical diameter of less than 2μm, not all of which is crystalline. Majority of the clay minerals belongs to the category of layered silicates or phyllosilicates because their silica layers and alumina sheets joined together in varying proportions and in a certain way [21]. The principal building elements of the clay minerals are two-dimensional arrays of silicon-oxygen tetrahedra and two-dimensional arrays of aluminium- or magnesium-oxygen/hydroxyl octahedral superimposed in different fashions. In the silicon-oxygen

sheets, the oxygen atoms are located on the four corners of a regular tetrahedron with the silicon atom in the center. In this sheet three of the four oxygen atoms of each tetrahedron are shared by three neighboring tetrahedra. The fourth oxygen atom is shared by the Al octahedral sheet. There, the Al or Mg atoms are coordinated with six oxygen or OH groups, which are located around the Al or Mg atom with their centers on the six corners of a regular octahedron (cf. Figure 2.3). These groups lie in two parallel planes with Al or Mg atoms between them [22]. The combination of an octahedral sheet and one or two tetrahedral sheets is called a 'layer'. The repetition distance of the layers in the stack (i.e. between a certain plane in the layer and the corresponding plane in the next layer) is very important and is called the d(001) or basal or interlayer spacing.

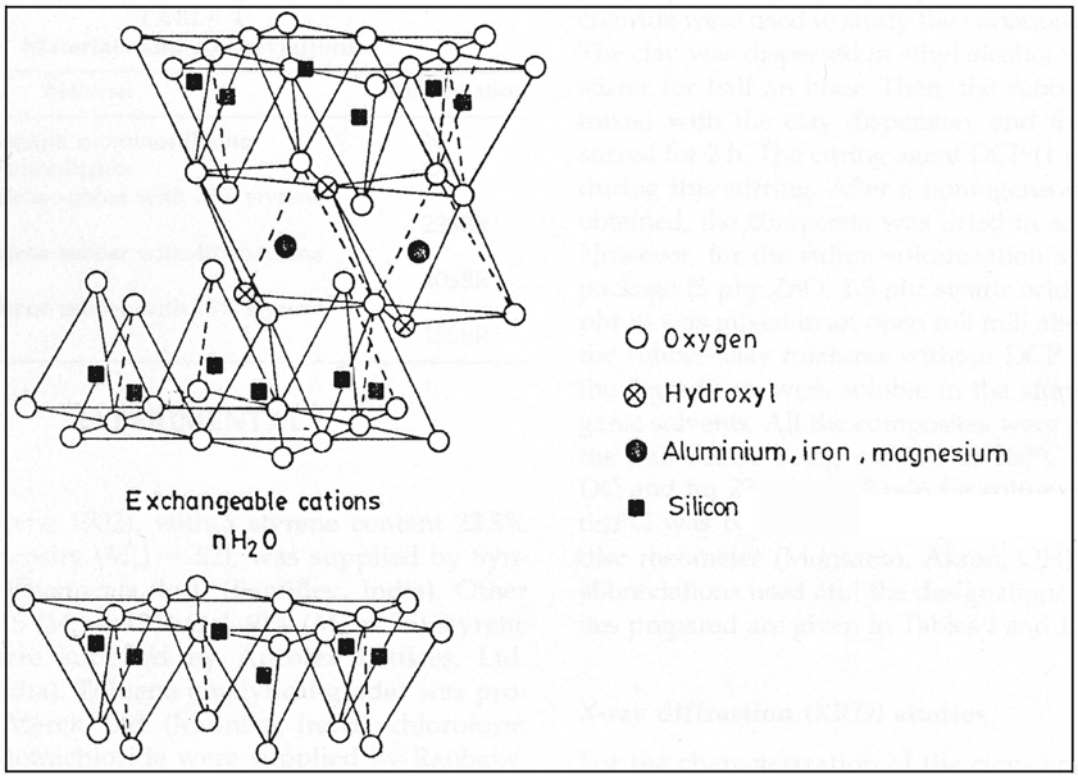

Figure 2.3: Layered silicate structure in an example of a 2:1 layered clay

Condensation in 1:1 ratio of a silica sheet with an alumina one gives rise to a 1:1 layer clay (e.g. kaolinite). In a 2:1 ratio, two silica sheets condense with an alumina one (e.g. pyrophyllite, smectite or montmorillonite, vermiculate, illite). Among the 2:1 layer clays, the montmorillonite possesses great significance because of its swelling capabilities. Partially replacement of trivalent Al by divalent Mg in the octahedral sheet results to a high negative surface charge of the layer. This fact renders the

space between the layer surfaces (i.e. gallery or interlayer) capable of accommodating cations. When montmorillonite clay is contacted with water or with water vapor, the water molecules penetrate between the layers (i.e. interlayer swelling) increasing its basal spacing. This phenomenon is likely related with the hydration energy. When it is released the van der Waals forces, which hold the layers in close packing together, are compensated. Furthermore, the charge compensating cations on the layer surfaces may be easily exchanged by other cations when available in aqueous solution; hence they called 'exchangeable cations'. The total amount of these cations is expressed in milliequivalents per 100 g of dry clay and is called the 'cation exchange capacity' (CEC) of the clay [22].

In the past, kaolins were mainly used for rubber filling (non-active reinforcement) [4]. Calendering a rubber stock with such anisotropic filler results in alignment of the filler particles in the direction of the calender grain [20]. In order to yield acceptable mechanical performance, high amount of clay incorporation is needed.

2.2.4 Surface Treatment

In order to enhance specific properties of the final rubber, the filler (type, characteristics) has to be selected carefully. This involves also the surface treatment of the fillers. For example, carbon blacks used for coloring high-quality coatings have to possess highly polar surfaces for optimum wetting by the binder. On the contrary, conductive applications need carbon black surfaces free from oxides [23].

For controlling the surface energy in case of silica, treatment with glycols, esterification with monofunctional alcohols or silane coupling agents have been extensively used [24-25].

Opposed to the active fillers (e.g. carbon black, silica), clays are considered as inactive ones. Accordingly their reinforcing ability in the rubber matrix is low and thus, high amount of clay is needed to reach pronounced property improvement. Surface treatment of clays has been known since many decades ago [22]. When an amine salt or a quaternary ammonium salt is added to a clay-water suspension, the organic cation replaces the inorganic cations (e.g. Na^+,K^+) which are originally present on the clay surfaces. Because of this exchangeable adsorption the amino groups are tethered on the clay surface while the hydrocarbon tail is positioned in the gallery space displacing the previously adsorbed water molecules (cf. Figure 2.4). By this

way, the clay is becoming compatible with organic molecules, i.e. organophilic. Note that this treatment expands the intergallery distance at the same time (cf. Figure 2.4). A widely accepted term of this treatment and its result is the ‘organoclay’.

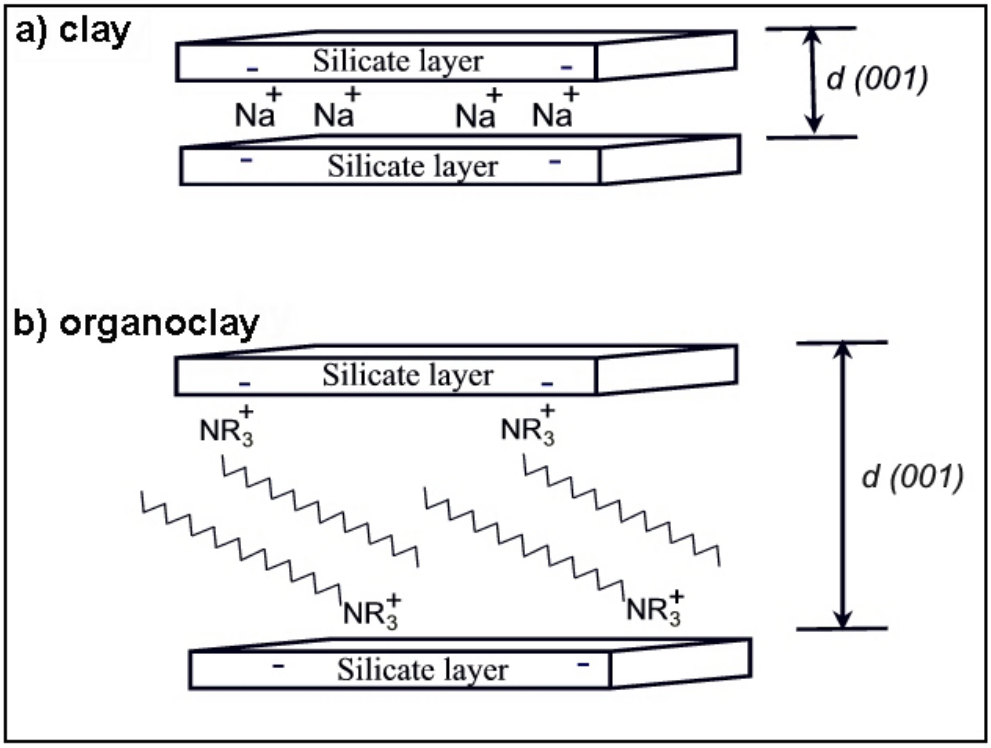

Figure 2.4: Scheme of a) clay and b) modified clay (i.e. organoclay). Note that R can be replaced accordingly by any chemical unit

Applications of such “clay-organic complexes” were first used in oil dispersions to manufacture lubricating grease. Main advantage of these systems is their better heat stability compared to conventional lubricating greases. Moreover, clay treated with coupling agents as the isopropyl tristearoyl titanate (TTS) has been also proposed to enhance the heat deflection temperature, mechanical performance and processability [26].

2.3 Rubber/Layered Silicate Nanocomposites

The special character of rubber, being a multi-component system (e.g. resin, curing agents, coagents), complicates the analysis of the parameters affecting the rubber/layered silicate nanocomposite formation. This was likely the reason for its late development compared to thermoplastic- or thermoset-clay nanocomposites.

Note that nanocomposite is obtained only when the polymer chains are intercalated into the intergallery spacing (cf. “intercalated” nanocomposite) or when the silicate layers are further pulled apart and appear exfoliated in the polymer matrix (cf. “exfoliated” nanocomposite) [27-29]. The possible outcomes are schematically depicted in Figure 2.5.

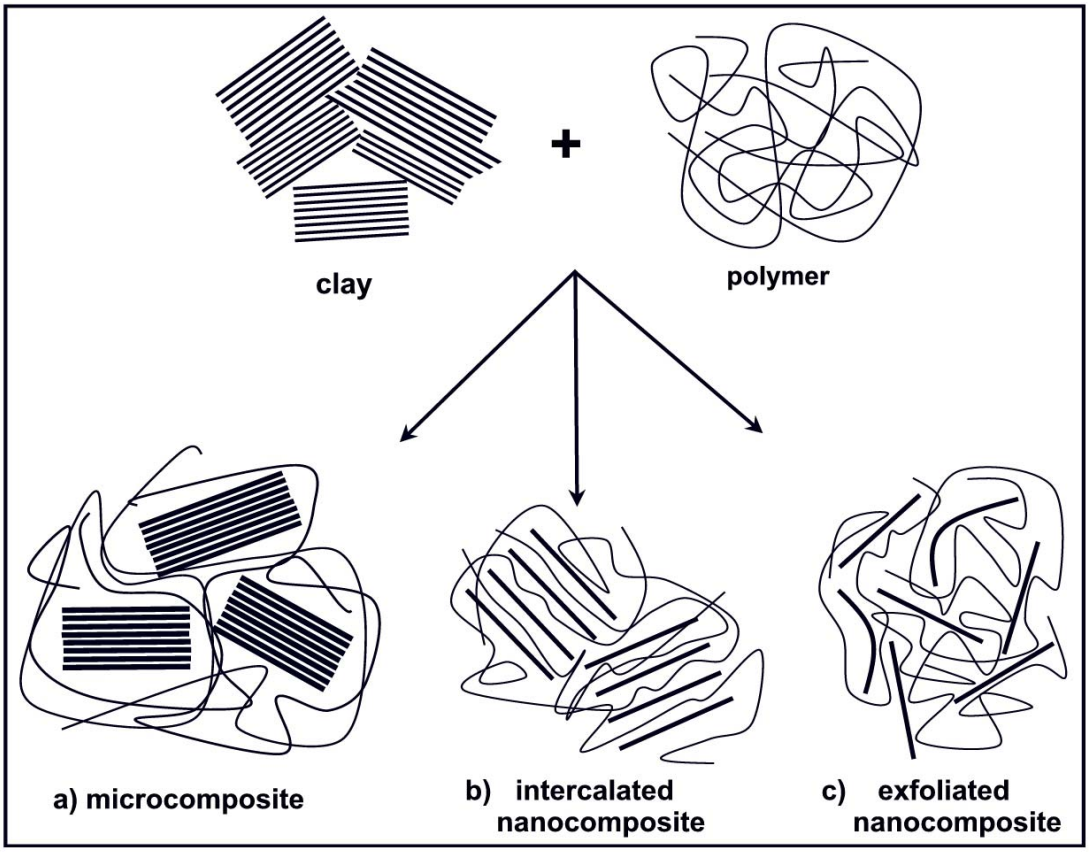

Figure 2.5: Scheme of possible dispersions of layered silicate in a polymer

2.3.1 Early Stage of Research

The reinforcing efficiency of the modified clays (i.e. organoclays) in the polymer matrix was fast recognized. In the beginning of the ‘60s montmorillonite modified with octadecylamine (MMT-ODA) was investigated in polymethyl methacrylate (PMMA) and polystyrene (PS) compounds [21]. Already that time, monomers, like methyl methacrylate, were mixed with MMT-ODA prior to their polymerization. Furthermore, polyethylene (PE) and polyvinyl chloride (PVC) were tested upon their performance after incorporation of surface-modified clays (mainly with modified kaolin). In the ‘70s, the production of clay filled polyamides, obtained by introducing catalytically active clay into the corresponding monomers has already been proposed. At the same time,

the mixing of polyester or epoxy resins with clays was done to improve heat and moisture resistance, as well as, to reduce the curing induced shrinkage and to avoid the cracking of the molded products. In case of elastomers, a very successful technique was to react the minerals with organosilanes. Using aminosilanes, the hydrolysed silanol group of the reagent was attached on the clay surface while the pendent amino group, at the other end of the molecule, was free to react with the rubber during vulcanization [21]. The mineral used for such type of rubber reinforcement was mainly non-swellable layered silicate (e.g. kaolin).

2.3.2 Current State

Tremendous boost to the polymer/layered silicate nanocomposites on both scientific and industrial levels was given at the beginning of '90s due to the researchers at the Toyota Central Research Laboratories (Japan). They reported on nylon 6/clay hydrids, which showed enhanced mechanical properties and high resistance to water permeation [30-32]. On the other hand, reporting on thermosets, researchers in the USA initiated the course on epoxy-silicate nanocomposites [33-35]. Research subjects of this 'second rally' (i.e. in the '90s) were mainly the modeling and simulation of the polymer clay interactions during the hybrid formation [36-41], as well as, their processing optimization and potential industrial use [42-47].

Regarding rubbers, less attention was put on them during the early research activities (i.e. '60s -'70s). Even during the "hot" period of the '90s, only some sporadic works appeared on rubber/layered silicate nanocomposites [48-50]. Since the proof of the enhanced performance of thermoplastic- and thermoset-organoclay nanocomposite systems, research has been initiated on rubber/organoclay nanocomposites [51-56].

In the past five years, several rubbers served as matrices in organoclay filled systems. Typical examples are styrene-butadiene- (SBR) [26, 51, 53, 56-62], ethylene-propylene-diene- (EPDM) [61, 63-67], fluoro- (FKM) [68], nitrile-butadiene- (NBR) [69-71] and natural- rubber [72-79]. The different methods to prepare a rubber/organoclay nanocomposite include solution mixing (i.e. solvent method) [69, 72, 75, 80-81], latex compounding (water assisted technique) [56, 82-86] and melt mixing (direct method) [58-59, 61-68, 70-71]. For the praxis, considering the portfolio of the rubber industries (i.e. application range) and the traditional compounding

methods, melt-mixing method emerges as the most promising one [87]. Further, latex compounding is a rather easy and inexpensive technique to produce nanocomposites (cf. use of pristine clay), which may gain industrial interest in the future.

As far as melt compounding concerns, rubber appears as a suitable model matrix because of its high molecular weight and the chemical reactions taking place during vulcanization. This thought is directly generated when the so-far advantages on thermoplastic- and thermoset-clay systems are pondered. It has been found for thermoplastics that the high molecular weight of the polymer [88], as well as, the polarity of the macromolecular chain backbone [89], favor the intercalation/exfoliation of the organoclay during mixing. Even better results can be achieved if mixing is performed at optimized processing parameters (shear rate and compounding time) [46-47]. On the other hand, in thermoset/organoclay nanocomposites, reactions between the curing agents and the clay surface modifier (i.e. clay intercalant) have been identified to affect the nanocomposite formation [33, 90-91]. Moreover, for both polymer categories, factors like the origin of the clay [35, 92-95] and the intercalant type [35, 91, 96-98] play crucial roles in respect to the final properties.

Although the research addressed rubber/layered silicate nanocomposites in the last five years, just few investigations focused on the mechanisms affecting the nanocomposite formation [61-64, 75] and even less brought some new ideas to this topic [64, 69, 74]. Transferring the knowledge, obtained in the last decade, on the mechanisms affecting the thermoplastic- and thermoset-clay nanocomposite formation to rubber compounds, rubber nanocomposites with strongly improved performance may be the result. Note that the vulcanization process itself may be a suitable tool [99-105], to control the morphology of the rubber/clay nanocomposites. After tailoring the properties of the rubber/clay nanocomposites, through the desirable dispersion grade, modeling of their behavior is the next step in order to deduce universal structure-property relationships.

2.4 Modeling of the Rubber Nanocomposites

Through the past decades, modeling of rubber and rubber composite behavior was imperative for predicting short- and long-term properties. Because of their highly non-linear elastic behavior under static loading and pronounced viscoelastic response

including hysteresis under cyclic loading, modeling of the physical properties of rubbers is even nowadays a complex task [106-108]. Among others, the modeling of the mechanical response and the gas permeability behavior has received considerable attention.

2.4.1 Mechanical Performance

A famous model to characterize the mechanical performance of rubber composites is based on the equation developed to describe the viscosity of colloidal suspensions and emulsions by Einstein in 1906 (cf. equation 2.2). This equation relates the viscosity of the emulsion and the solvent (η_c and η_m, respectively), as well as, the volume concentration *c* of the particles.

$$\eta_c = \eta_m \left(1 + 2.5c\right) \tag{2.2}$$

In case of rubber filled systems, this equation holds if the vulcanized rubber surrounding the filler can be considered as an isotropic elastic continuum having the same elastic properties as the rubber without filler. In addition, the filler should exhibit a spherical shape. Furthermore, it is postulated that the rubber wets completely the filler surface and no interaction between the filler particles takes place. To the above assumptions one has to add that the filler particles should be sufficiently large in order to neglect the molecular structure of the bound rubber. For small elongations and low filler loading, Smallwood [20] concluded the following equation:

$$E_c = E_m \left(1 + 2.5\varphi_f\right), \tag{2.3}$$

where E_c and E_m the modulus of the loaded stock and the rubber matrix, respectively, and φ_f is the volume fraction of filler. Guth and Gold modified the above equation to include interactions between the fillers [109]:

$$\eta_c = \eta_m \left(1 + 2.5c + 14.1c^2\right) \tag{2.4}$$

The η_c and η_m in the equation 2.4 can be replaced by the Young's modulus (E) or the shear modulus (G) as it was proved.
For rod-like filler particles embedded in a matrix Guth introduced a shape factor *f* (i.e. length/breadth) and thus, modified follow the equation 2.4 [109]:

$$E_c = E_m\left(1+0.67f\cdot c+1.62f^2\cdot c^2\right) \tag{2.5}$$

Irrespective to these modifications, a divergence between theory and experiments, especially for active carbon black, was the case. Medalia explained this difference by assuming that a part of the rubber was occluded in the interstices of the carbon black aggregates [15]. The occluded rubber is shielded/excluded from deformation and thus acts as a part of the filler. Thus, equation 2.4 has to consider the effective filler fraction:

$$E_c = E_m\left(1+2.5\varphi_{eff}+14.1{\varphi_{eff}}^2\right), \tag{2.6}$$

where φ_{eff} is the effective filler volume, which is greater than the initially added filler volume φ. It has to be mentioned that several alternative expressions were derived for the above hydrodynamic equation for rubbers in the past [110-112].

Apart from the rubber-specific models, classical equations, which are widely used to estimate reinforcement effects of filler in composites [e.g. Halpin-Tsai; cf. equation 2.7), have been also proposed to predict the mechanical performance of rubber/layered silicate nanocomposite [113-114].

$$\frac{E_c}{E_m}=\frac{1+\zeta\eta\varphi_f}{1-\eta\varphi_f}\ , \tag{2.7}$$

where E_c and E_m represent the Young's modulus of the composite and matrix, respectively, ζ is a shape parameter dependent upon filler geometry and loading direction, φ_f is the volume fraction of filler, and η is given by:

$$\eta = \frac{E_f / E_m - 1}{E_f / E_m + \zeta} \quad , \tag{2.8}$$

where E_f corresponds to the Young's modulus of the filler.

2.4.2 Gas Barrier Properties

The prediction of the gas barrier properties of polymers and polymers containing platelet-type fillers had always high priority [115]. For polymer/layered silicate nanocomposite systems, the application of the Nielsen's equation (cf. equation 2.9) proved to be a reliable estimate [116].

$$\frac{P_c}{P_m} = \frac{\varphi_m}{1 + (w/2t)\varphi_f} \quad , \tag{2.9}$$

where P_c and P_m is the permeability coefficient of the composite film and that of the unfilled polymer, respectively, φ_m and φ_f is the volume fraction of polymer and filler, and *w/t* is the width to thickness aspect ratio of the filler.

The mismatch of the experiments with the theoretical predictions was corrected by the modified Nielsen's model proposed by Bharadwaj [117]. The correction considers the order parameter [$S = \frac{1}{2}\left\langle 3\cos^2\theta - 1 \right\rangle$], which is well known for oriented aligned systems (e.g. liquid crystals). To fit to the current needs, θ represents the angle between the direction of the preferred orientation $\vec{n}$ and the sheet normal $\vec{p}$ unit vectors (cf. Figure 2.6). This function can range from 1 (θ=0), indicating perfect orientation of the sheet normal unit vectors $\vec{p}$ with $\vec{n}$, to -1/2 (θ=π/2), indicating perpendicular or orthogonal orientation of the sheets and a value 0, refers for a random orientation of the sheets (cf. Figure 2.6).

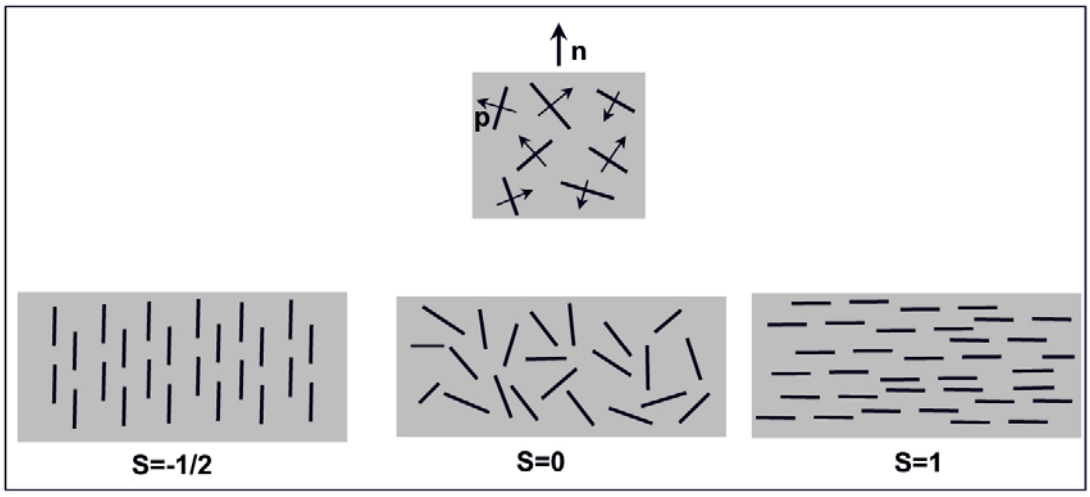

Figure 2.6: Preferred orientation (*n*) and the sheet normal (*p*) vector. The three characteristics values of the order parameter are also illustrated

The modified equation is as follows:

$$\frac{P_c}{P_m} = \frac{1-\varphi_f}{1+\frac{w}{2t}\varphi_f\left(\frac{2}{3}\right)\left(S+\frac{1}{2}\right)} \tag{2.10}$$

The above expression reduces to equation 2.9 when S=1 and converges to the permeability of the pure matrix characterized with S=-1/2.

3. Objectives

The demanding applications of rubber products, nowadays, trigger the search of even more effective rubber fillers. The conventional widely used fillers (e.g. carbon black, silica), reached some level of “saturation” with respect to R & D activity. The organoclays and organophilic layered silicates, on the other hand, represent a new type of filler the potential of which is not yet explored.

Incorporation of a few weight percentage organoclay in rubber stocks may lead to unique properties. This is due to platy structure of the clay (natural origin) and layered silicates (artificial origin). Thus, the elastomer/organoclay nanocomposite systems became a hot topic of the international research. However, the complexity of the rubber compounding and vulcanization processes mean great problems when universal aspects of the nanocomposite formation should be derived.

Objective of the current study is to investigate the rubber/organoclay nanocomposite formation, detecting and understanding the clay dispersion mechanisms. Note that by controlling the organoclay dispersion the final properties of the rubber nanocomposites could be tailored, as well.

Therefore, rubbers of different polarities (e.g. EPDM, EPDM-GMA, EPDM-MA, HNBR) and clays/layered silicates (e.g. MMT, FHT) bearing a wide spectrum of modifiers (e.g. ODA, ODTMA, MTH) were used. In order to shed light in the mechanisms involved in the rubber/organoclay nanocomposite formation an appropriate selection of the components and additives (e.g. curing agents) took place.

A further objective of this work was to determine the performance of rubber nanocomposite and thus to derive structure-property correlations. In order to show the property upgrade, a direct comparison with conventional fillers, like silica, was targeted. Further attempts were made to predict/model the micro/nanostructure-related physico-machanical properties like the mechanical performance and the oxygen permeation.

As far as rubber concerns, the optimum curing time is a parameter of great significance. Traditionally, such characteristics are delivered from Monsanto Rheometers. A part of the current analysis was to check the applicability of a Plate-Plate Rheometer as a curometer (i.e. measuring the cure characteristics).

4. Experimental

4.1 Materials

4.1.1 Rubber Matrix

To investigate the mechanisms involved in the rubber/organoclay nanocomposite formation, ethylene propylene diene monomer rubber (EPDM) and hydrogenated acrylonitrile butadiene rubber (HNBR) were mostly used. The related work includes also the use of modified/polar versions of EPDM. The natural (NR) and the epoxidized rubber (ENR) were used only to check whether or not a Plate-Plate Rheometer can be used as curometer, as described in the Section 5.1.

4.1.1.1 Ethylene Propylene Diene Monomer Rubber (EPDM)

The EPDM was a Buna® AP 451 with 50% ethylene and 8.6% ethylidene norbornene content supplied by Bayer AG, Leverkusen, Germany. This EPDM has a Mooney viscosity of ML (1+4) 125°C = 59.

EPDM grafted by glycidyl methacrylate (EPDM-GMA) was produced in our laboratory [118]. Its GMA content was 8.7 % based on the determination described elsewhere [119].

EPDM grafted maleic anhydride (EPDM-MA; Royaltuf 465A) with an ethylene/propylene ratio of 55/45 and MA content of 1 %, was supplied by Uniroyal Chemical, Louisiana, U.S.A. This EPDM-MA showed a Mooney viscosity of ML (1+4) 125°C = 60. All three types of EPDM are presented in Figure 4.1.

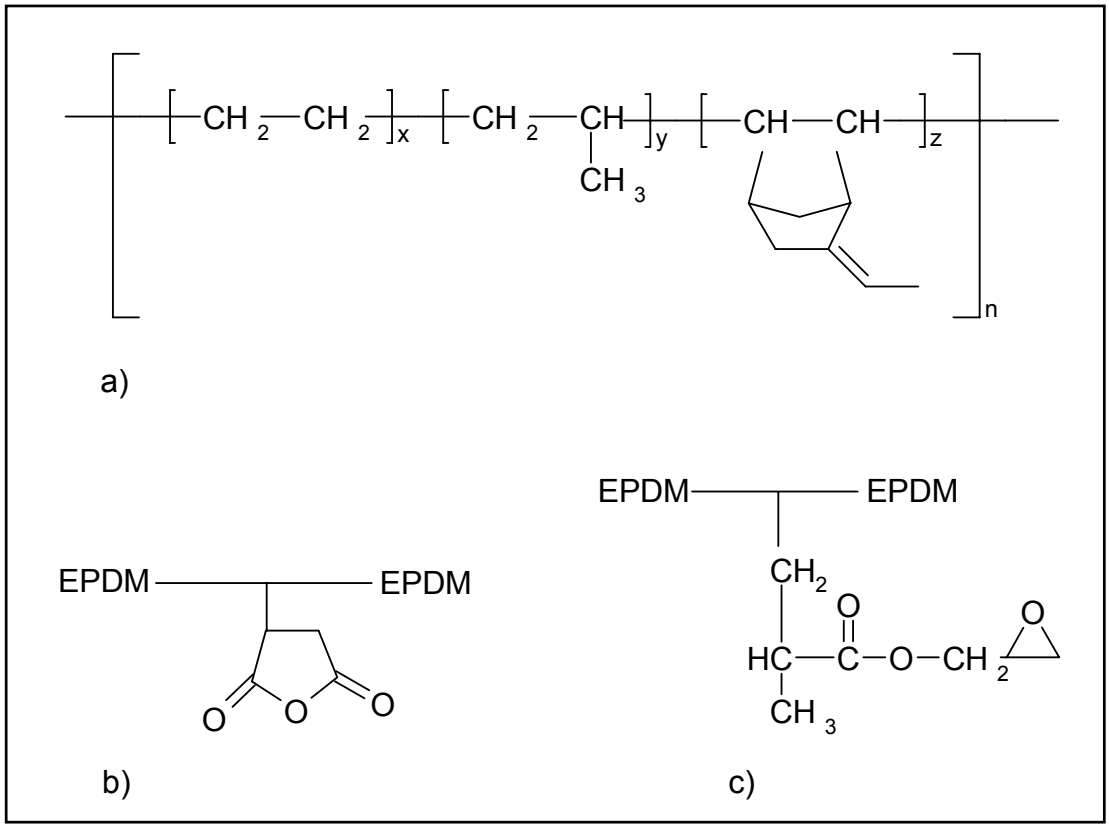

Figure 4.1: Schematic structures of a) EPDM b) EPDM-MA and c) EPDM-GMA structures

4.1.1.2 Hydrogenated Acrylonitrile Butadiene Rubber (HNBR)

Two types of HNBR were used each appropriate for sulfur and peroxide vulcanization. The HNBR for sulfur curing was a Therban® C 4367 (XN 532 C) having 43% acrylonitrile content and 5.5% residual double bonds. This shows a Mooney viscosity ML(1+4) 100°C = 60. HNBR structure is given in Figure 4.2.

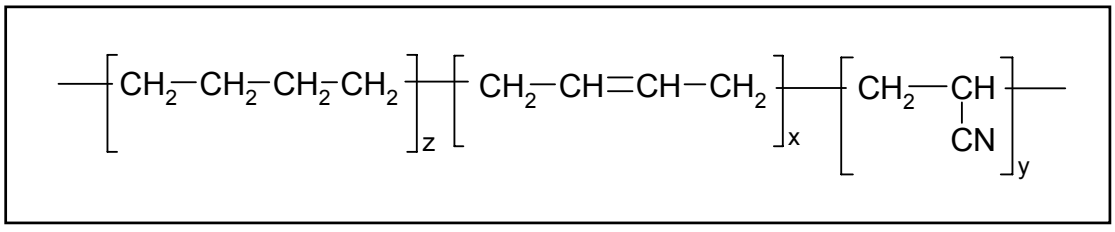

Figure 4.2: Scheme of the HNBR macromolecular chain

For the peroxide curing, a fully hydrogenated nitrile rubber (Therban® A 4307) (XN 532 A) having 43% acrylonitrile content and less than 1% residual double bonds was

selected. Both HNBR types have similar Money viscosity and were provided by Bayer AG, Leverkusen, Germany.

4.1.1.3 Natural Rubber

An epoxidized natural rubber with 50 mol % epoxidation (ENR-50) having a Mooney viscosity of ML (1+4) 100 ^{o}C = 140 and a natural rubber (NR) with Mooney viscosity of ML (1+4) 125^{o}C = 78, were used. Both rubbers were obtained from the company Kumpulan Guthrie, Malaysia.

4.1.2 Fillers

4.1.2.1 Conventional Fillers

Silica and carbon black were considered as conventional fillers in the current work. The silica was a synthetic amorphous one (Ultrasil VN2) supplied by Degussa (Frankfurt, Germany). Carbon black (grade: N330) was provided by the Rubber Research Institute of India, Kottayam, Kerala, India.

4.1.2.2 Natural Clay and its Organophilic versions

As unmodified natural montmorillonite (MMT) a sodium bentonite (EXM 757) having an interlayer spacing of 1.20 nm, supplied by Süd Chemie (Munich, Germany), was used.

MMT modified with octadecylammonium salt (MMT-ODA; Nanomer® I.30 P) and octadecyltrimethylammonium salt (MMT-ODTMA; Nanomer® I.28 E), respectively were donated by Nanocor Inc (Arlington Heights, IL, USA). MMT modified with methyl-tallow-bis(2-hydroxyethyl) quaternary ammonium salt (MMT-MTH; Cloisite® 30 B) was supplied by Southern Clay Inc (Gonzales, TX, USA). The interlayer spacing of the organoclays MMT-ODA, -ODTMA and –MTH was 2.10 nm, 2.50 nm and 1.80 nm, respectively. Their specific gravity was in the range of 1.8-1.9. The MMTs treated by Nanocor Inc and Southern Clay Inc present a cation exchange capacity of 120 and 90 meq/100g, respectively. The MMT intercalants are shown in Figure 4.3.

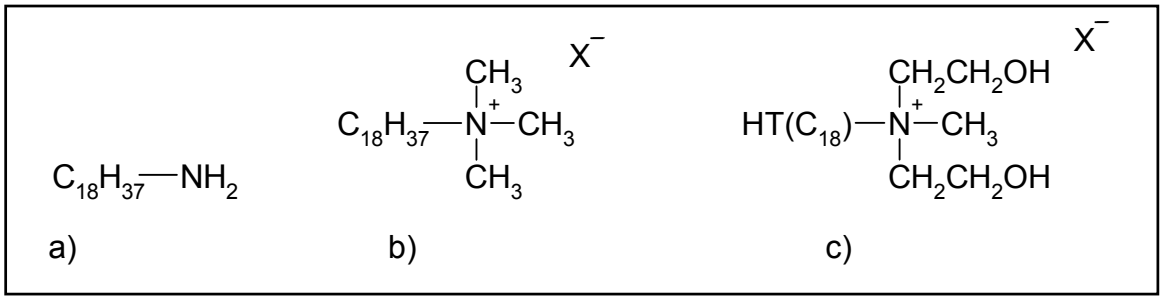

Figure 4.3: Molecular structure of the intercalants used to modify the Na-MMT by ion exchange. Designations: a) Nanomer® I. 30 P, b) Nanomer® I. 28 E, c) Cloisite® 30 B, commercial organoclays. HT (C_{18}) stays for hydrogenated tallow group attached to the nitrogen

4.1.2.3 Synthetic Clay and its Organophilic versions

A synthetic sodium fluorohectorite (FHT), prepared by heating talcum together with sodium hexaflorosilicate (Na_2SiF_6), having the trade name Somasif ME-100 of Co-op Chemicals (Tokyo, Japan), was selected. This has a cation exchange capacity of 100meq/100g and an intergallery distance of 0.95 nm.

FHT modified with octadecylamine (FHT-ODA) and Jeffamine 230, (JEF 230) (cf. Figure 4.4), all provided by the Freiburger Materialforschungszentrum, University of Freiburg, Germany, were involved in this work. Note that Jeffamine 230 is a polyoxypropylenediamine product of Huntsman Holland BV, Rotterdam, The Netherlands. (The JEF 230 was used only as filler in compounds for the determination of the optimum vulcanization time; chapter 5.1)

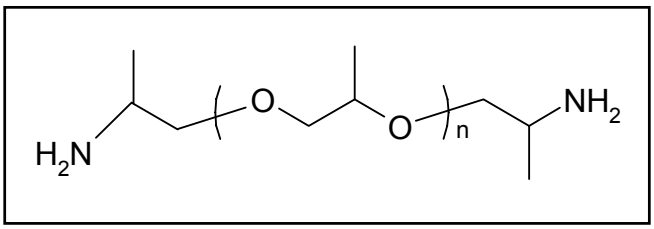

Figure 4.4: The molecular structure of JEF 230

4.1.3 Vulcanization Additives and Cure Recipes

4.1.3.1 EPDM

For the EPDM curing, the vulcanization curatives: zinc diethyldithiocarbamate (ZDEC; Vulkacit® LDA), N-cyclohexyl-2-benzothiazole sulfenamide (CBS; Vulkacit CZ), 2-mercaptobenzothiazole (MBT; Vulkacit Merkapto) stearic acid, zinc oxide (ZnO) and sulfur were donated by Bayer AG, Leverkusen, Germany. The mixing recipe used was as follows (in parts), rubber: 100, organoclay: various, ZnO: 5, stearic acid: 1, accelerator (different types): 1 and S: 2. The accelerator structures are shown in Figure 4.5.

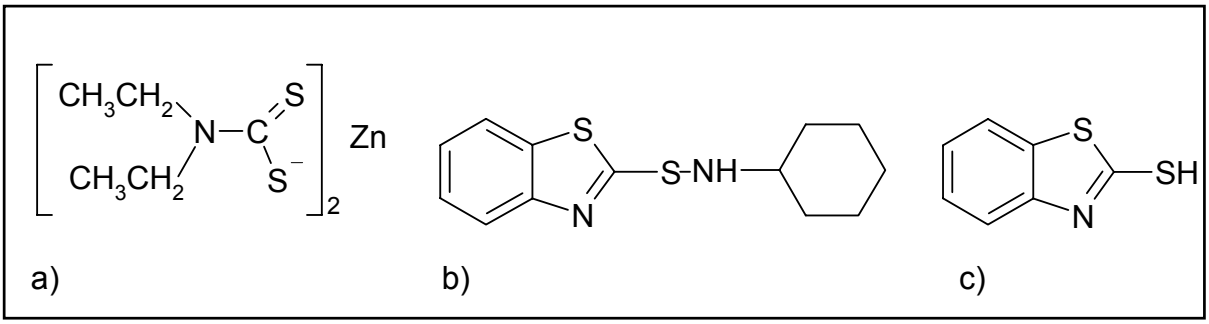

Figure 4.5: The molecular structures of the accelerators a) ZDEC, b) CBS and c) MBT

The plasticizer mineral oil (Kaydol) for the oil extended EPDM vulcanizates was supplied by Amco Chemicals Corp., Oakland, CA, USA. For the peroxide curing, dicumyl peroxide with 40% active compound (Perkadox, BC-40K-pd; Akzo Nobel Chemicals bv, Deventer, The Netherlands) was used.

4.1.3.2 HNBR

Two different recipes for sulfur and peroxide HNBR vulcanization presented in Table 1 and 2, respectively, were selected. Lanxess Deutschland GmbH, Leverkusen, Germany, supplied the related additives. These recipes include components, which offer heat stability and protection to aging, like diphenylamine and zinc methylmercaptobenzimidazole (ZMMBI), respectively. For a better processing of the HNBR, trioctyl trimellitate (TOTM; Plasthall®) was introduced as rubber plasticizer.

Table 4.1: Formulation of the sulfur cured HNBR mixes

Material	**Parts**
Therban® C 4367 (hydrogenated nitrile butadiene rubber) HNBR	100
Organoclay (various)	10
MgO	2
ZnO	2
Plasthall® TOTM (trioctyl trimellitate)	8
Vulkanox® ZMB-2 (zinc methylmercaptobenzimidazole) ZMMBI	1.5
Naugard® 445 (substituted diphenylamine)	1.5
Vulkacit® CZ (n-cyclohexyl-2-benzothiazole sulfenamide) CBS	0.5
Vulkacit® Thiuram (tetramethyl thiuram disulfide) TMTD	2
Sulfur	0.5

Table 4.2: Formulation of the peroxide cured HNBR mixes

Material	**Parts**
Therban® A 4307 (fully hydrogenated nitrile butadiene rubber) HNBR	100
Organoclay (various)	10
MgO	2
ZnO	2
TAIC® (triallyl isocyanurate)	1.5
Plasthall® TOTM (trioctyl trimellitate)	8
Vulkanox® ZMB-2 (zinc methylmercaptobenzimidazole) ZMMBI	0.4
Naugard® 445 (substituted diphenylamine)	1.1
Perkadox® BC-40K-pd	7

4.1.3.3 NR

The system used for the NR and ENR curing includes (in parts), rubber: 100, filler: various, ZnO: 5, stearic acid: 2, sodium carbonate: 0.3, S: 1.5, retarder (N-cyclohexylthio-phthalimide): 0.2, N-cyclohexylbenzothiazol-2-sulfenamide (CBS;

Vulkacit CZ): 1.5, antioxidant-HS (2,2,4-trimethyl-1,2-dihydroquinoline in polymerised form): 1.5, all supplied by Bayer AG, Leverkusen, Germany.

4.2 Compounding

4.2.1 Internal Mixer

An internal mixer type Brabender plasticorder PL 2000 (Brabender®, Duisburg, Germany) operating at 60 rpm was used. This internal mixer has an eight-shaped chamber in which two sigmoid, counter-rotating blades turn. The temperature of compounding has been varied (i.e. 30 or 100 ^{o}C).

4.2.2 Open Mill

A laboratory two roll mixing mill LRM-150/3E (Labtech, Bangkok, Thailand) with a nip clearance of 1 mm and friction ratio 1.3 (22/17 rpm) was used. In all of cases, the incorporation of the curatives took place at this equipment at room temperature.

4.3 Vulcanization

4.3.1 Rheometers

4.3.1.1 Monsanto Rheometer

Cure characteristics of the rubbers were determined on a Monsanto oscillating disc rheometer (ODR 2000). The parameters set were the followings: 8-10 grams of the compound was feeded in the chamber of the machine, which operated at a fixed frequency of 1.66 Hz and 0.5^{o} oscillation angle. The estimated optimum vulcanization time for the specimens used in chapter 5.1 is given in Table 4.3.

Table 4.3: Optimum curing time (t_{90}) of the mixes as evaluated by a Monsanto Rheometer

Nr.	Description of sample	t_{90} from Monsanto Rheometer (min)
1	ENR + MMT-ODA	3.8
2	ENR + carbon black	6.8
3	EPDM + MMT-ODA	6.9
4	EPDM + FHT-ODA	8.6
5	EPDM-MA50% + MMT-ODA (peroxide system)	10.5
6	NR + MMT	11.7
7	EPDM + silica	15.1
8	EPDM	17.1
9	EPDM-MA50% + MMT-ODA	17.5
10	EPDM-MA50% + oil (peroxide system)	17.7
11	EPDM-MA25%	28.5
12	EPDM-MA50%	29.0
13	EPDM + JEF 230	30.6
14	EPDM-GMA50% + silica	35.0

Note that in the Table 4.3, for the samples denoted EPDM-MA (GMA) 50% and EPDM-MA 25%, the EPDM-MA or the EPDM-GMA was added to the EPDM in 1/1 (50%) or 1/4 (25%) in an internal mixer and homogenized at 30 rpm for 4 min.

4.3.1.2 Plate-Plate Rheometer

The Plate-Plate Rheometer used was an ARES, Rheometric Scientific, Piscataway, NJ, USA. The samples were punched from the uncured batch in the form of circular discs with 25mm diameter and thickness of 2-3 mm, and mounted in the gap between the plates. Rheological tests were performed at a given temperature (isothermal) in strain and frequency sweeps in order to conclude the viscoelastic range. The time dependence of the complex shear modulus (G*) and its constituents (G', G'') were monitored in the linear viscoelastic range. The multiwave experiment was run with a basic frequency of 1 rad/sec and strains of 1 % for each harmonic.

The strain input was the sum of eight waveforms with frequencies ranging from 1 to 100 rad/sec.

4.3.2 Hot Press

The samples were cured in an electrically heated hydraulic press at 2 MPa pressure at various temperatures. The temperatures selected in respect with the type of rubber and its curatives. More specifically, 160^{o}C for the EPDM compounds, 170^{o}C and 180^{o}C for the HNBR when sulfur and peroxide cured, respectively, and 150^{o}C for the NR and ENR compounds were set. The curing time was either their optimum value (t_{90}), or 15 min for all samples of the HNBR stocks. The latter cure time was sufficient to well crosslink the HNBR compounds, as verified by means of the Plate-Plate Rheometer, without any sign of reversion.

4.4 Mechanical Characterization

4.4.1 Tensile Experiment

Tensile tests were performed on a Zwick 1445 (Ulm, Germany) universal testing machine at a cross-head speed of 100 mm/min. The specimens used were dumb-bells according to DIN 53504 standards. The tensile data (tensile strength, modulus and elongation at break) represent the average of five specimens.

4.4.2 Tear Test

On the above-mentioned machine, angle test piece DIN ISO 34-1 specimens were tested upon their tear strength. The tear strength was determined by the ratio of the plateau force, needed to tear the sample, to its respective thickness. Tear strength was derived from three parallel measurements using a deformation rate of 500 mm/min.

4.4.3 Hardness

For the hardness evaluation of the rubber films a Zwick Shore A tester (Ulm, Germany) was used. The measurements were according to the ISO 868 Standards.

4.4.4 Cyclic Loading

The cyclic testing was performed on a Zwick 1474 (Ulm, Germany) universal testing machine at a cross-head speed of 10 mm/min using small dumbbell specimens (DIN 53504). The experiment involves either three cycles up to 100% or 300% strain.

4.5 Thermo Mechanical Characterization

4.5.1 Dynamic Mechanical Thermal Analysis (DMTA)

DMTA spectra were recorded on rectangular specimens (length x width x thickness = 50 x 10 x ~1.2 mm^3) in tensile mode at a frequency of 10 Hz using an Eplexor 150 N device of Gabo Qualimeter, Ahlden, Germany. The DMTA spectra, viz. storage modulus and mechanical loss factor (tan δ) were measured in the temperature range from -100 to 120 ^oC at a heating rate of 2 ^oC/min.

4.5.2. Thermo Gravimetric Analysis (TGA)

Thermal degradation of the samples was investigated with a TG50, Mettler Toledo TGA device (Giessen, Germany). Temperature sweep tests were performed in the temperature range from 25 to 600 ^oC under air atmosphere at a heating rate of 20 ^oC/min and the weight decrease was measured.

4.6 Oxygen Permeability Measurements

For the permeation measurements a Systec Instruments apparatus, Model 8000 (Thame, Oxfordshire, England) was used. The sample test area and thickness were 50cm^2 and about 1mm, respectively, for all specimens. The oxygen transmission rate (OTR) was detected at 23^oC at 0% and 60% relative humidity. Multiplying the OTR value with the thickness, the permeation coefficient (P_c) can be determined. The permeability ratio referred is the P_c ratio of each rubber composite and the neat one.

4.7 Micro- and Nano-structural Characterization

4.7.1 Scanning Electron Microscopy (SEM)

The SEM equipment used was a JSM 5400 device (Jeol Ltd, Tokyo, Japan). The fractured surfaces for inspection were obtained by trouser tear test (length 60mm x width 30mm x thickness 1.5mm; 30mm cut in length direction) at a cross-head speed of 100 mm/min. These surfaces were sputtered with an Au/Pd alloy prior to SEM investigation.

4.7.2 Transmission Electron Microscopy (TEM)

TEM images were taken in LEO 912 Omega microscope (Oberkochen, Germany) with an accelerator voltage of 120kV. Thin sections (ca. 100nm) of the specimens were cryo-cut with a diamond knife at ca. –120^{o}C and used without staining.

4.7.3 X-ray Diffraction (XRD)

X-ray diffractograms (XRD) were obtained, using Ni-filtered CuK_{α} radiation (λ = 0.1542 nm) by a D500 diffractometer (Siemens, Germany) at 40kV and 35 mA. The samples were scanned in transmission in step mode by 1.5 °/min scan rate in the range of 2θ = 1 to 12 °. XRD spectra from the layered silicates and their organophilic versions were taken in reflection mode.

5. Results and Discussion

5.1 Estimation of the Optimum Vulcanization Time: A New Method

The creation of a crosslinked network in a rubber increases its stiffness and renders it elastic. The curing time at a specific temperature (i.e. vulcanization) is very important parameter with respect to the final properties of the rubber (cf. Figure 2.2). Cure characteristics are assessed by vulcameters such as the oscillating disc type Monsanto Rheometer. Here the disc oscillates at a constant angular displacement and the torque required is monitored as a function of time at a constant temperature [120]. Values like the minimum and the maximum torque are measured and parameters as the scorch time (t_2), the optimum curing time (t_{90}) or the cure rate (t_{90} - t_2) can be evaluated.

Change in the torque-time curve is related with the actual degree of crosslinking. Considering the fact that the complex shear modulus (viz. storage and loss constituents, G' and G'', respectively) are also linked with the microstructure of the material, they should also provide information on the crosslink density of the rubber. This suggests that a Plate-Plate Rheometer can also be used to determine the optimum curing time of rubbers. Note that this measurement covers the complete rheological characterization of the crosslinking rubber. So, this technique supplies additional information on the curing which conventional curemeters are unable to do. Although the Plate-Plate Rheometer has been already used for rheological characterization of rubbers [51, 53], no comprehensive work was dedicated to calculate the optimum curing time of crosslinkable rubbers.

The first step to proceed with the analysis is to determine the linear viscoelastic regime. For this purpose, strain sweep experiments were performed. Figure 5.1 shows characteristic G' vs strain curves measured at 10 rad/sec frequency at 160^{o}C on the example of an EPDM stock (sulfur curing). G' vs strain curves were recorded in the early, middle and final stages of vulcanization. Note that the t_{90} value at this compound was 17.1 min (cf. Table 4.3). One can see that the G' does not change practically with increasing strain in the early and middle stages of vulcanization (time is less than 25% of t_{90}). Beyond 1% strain in the late stages of vulcanization, the materials' behavior departs from linearity and the G' declines. This threshold strain

value (1%), in the linear viscoelastic regime, has been fixed when performing the frequency sweep tests.

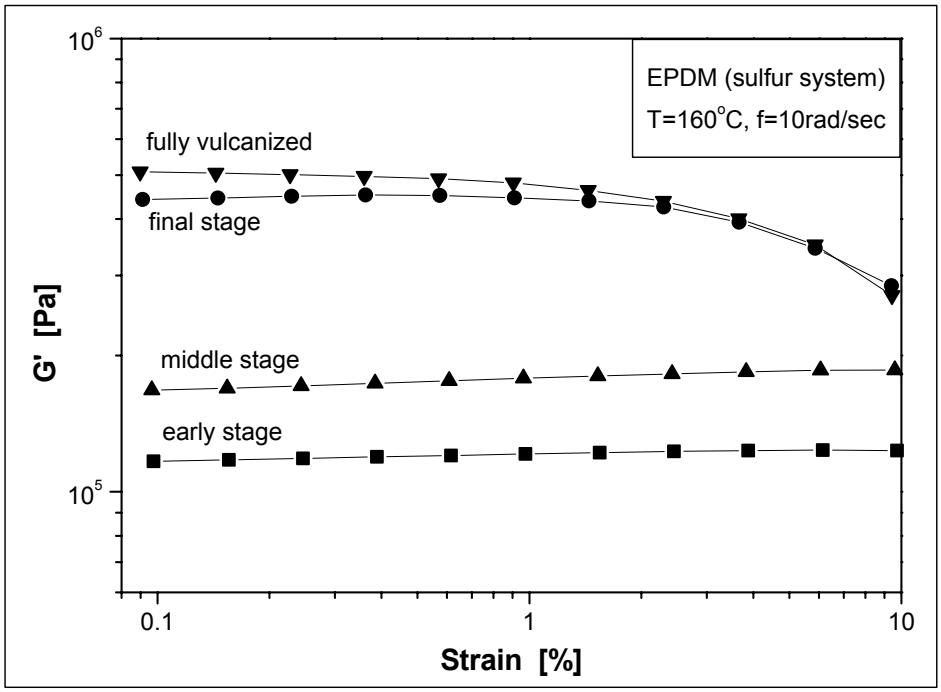

Figure 5.1: Storage modulus (G') against strain for an EPDM sample at different stages of crosslinking stage

The G' vs strain curves in Figure 5.1 clearly show how sensitive the shear storage modulus (G') reflects the degree of crosslinking. Recall that with increasing crosslinking G' monotonically increases. The scenario is somewhat different for frequency sweep tests at a fixed strain of 1%. Figure 5.2 displays the G' vs frequency curves on the example of the same EPDM stock indicated in Figure 5.1. Note that in the early and middle stages of crosslinking G' linearly increases with the frequency like for a typical viscoelastic polymer. On the other hand, G' does not change with frequency in the final stages of vulcanization, indicating the dominant elastic character and thus the loss of viscous characteristics. It should be mentioned at this point that each strain and frequency sweep test lasted ca.1-2 min therefore they are linked to various stages of curing.

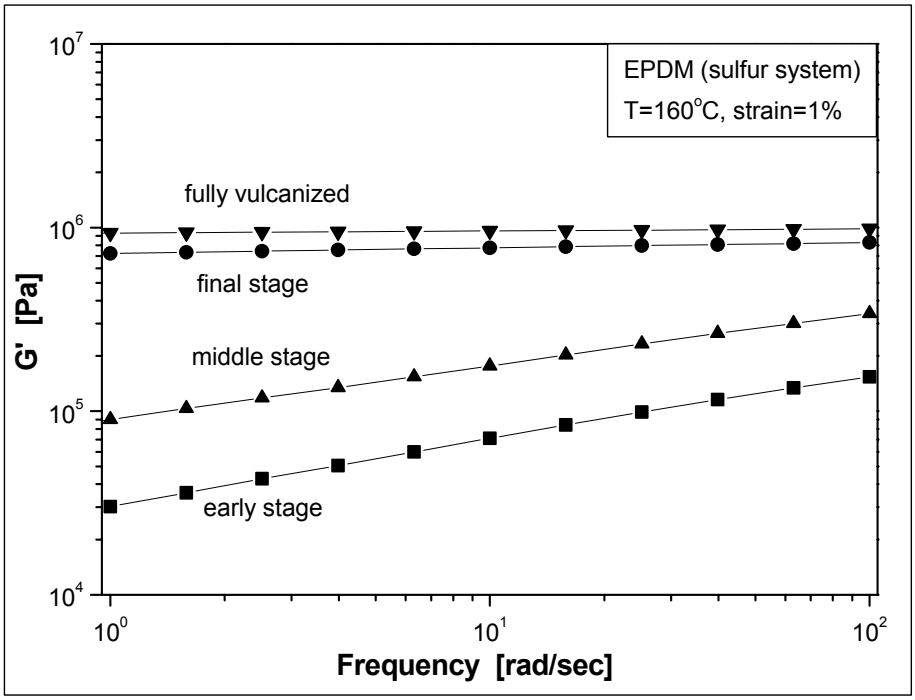

Figure 5.2: Storage modulus (G') against frequency for an EPDM sample at different stages of crosslinking

For monitoring the growth of the crosslink network the strain and frequency values (1% and 10rad/sec, respectively) were held constant and tests were performed under isothermal conditions. Shear moduli and mechanical loss factor (tanδ) of the elastomers were recorded as a function of time in order to deduce a direct relationship between the rheometric characteristics and optimum curing time. In Figure 5.3 the shear storage and loss moduli (Fig. 5.3a), as well as the tanδ and the torque (Fig. 5.3b) are presented for an EPDM reinforced with 10phr silica (sulfur cured). Note that both G' and G'' do not change within the first 10 min (Fig. 5.3a). The divergence in the first 2 min is owing to the time the material became fully tempered. After 10 min curing, the G' starts to increase whereas G'' decreases sharply till ca. 20 min. Afterwards, a gradual increase and decrease are observed up to 40 min for G' and G'', respectively. The trend of the complex shear modulus G* (not shown here) was like that of G' –none of them reached clearly a plateau value. The course of the torque and the tanδ as a function of time is presented in Figure 5.3b. As can be observed, the curve of tanδ vs. time ends in a plateau.

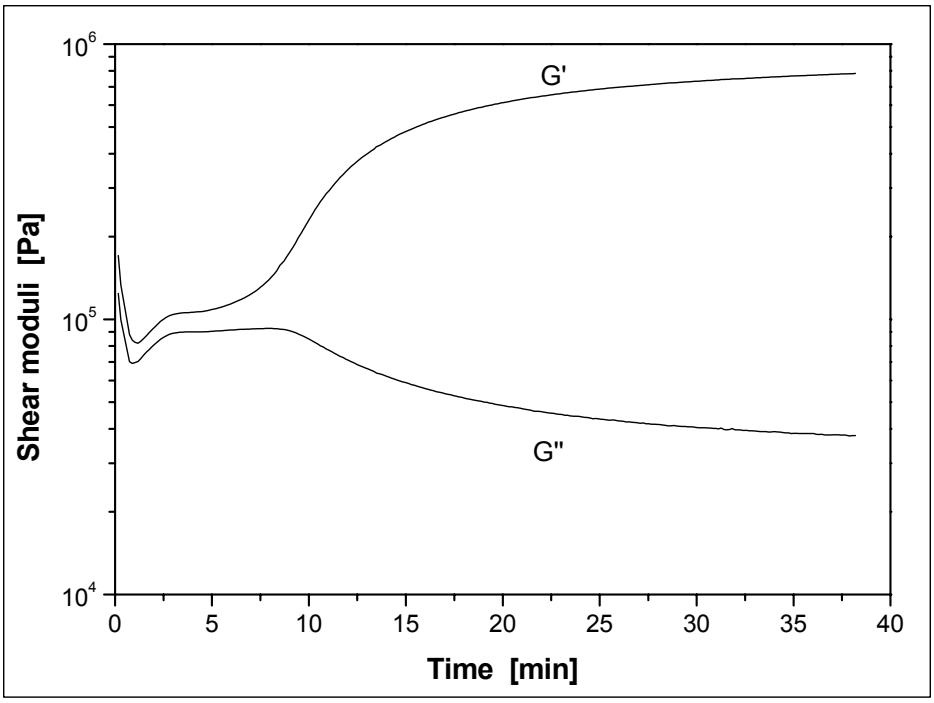

a)

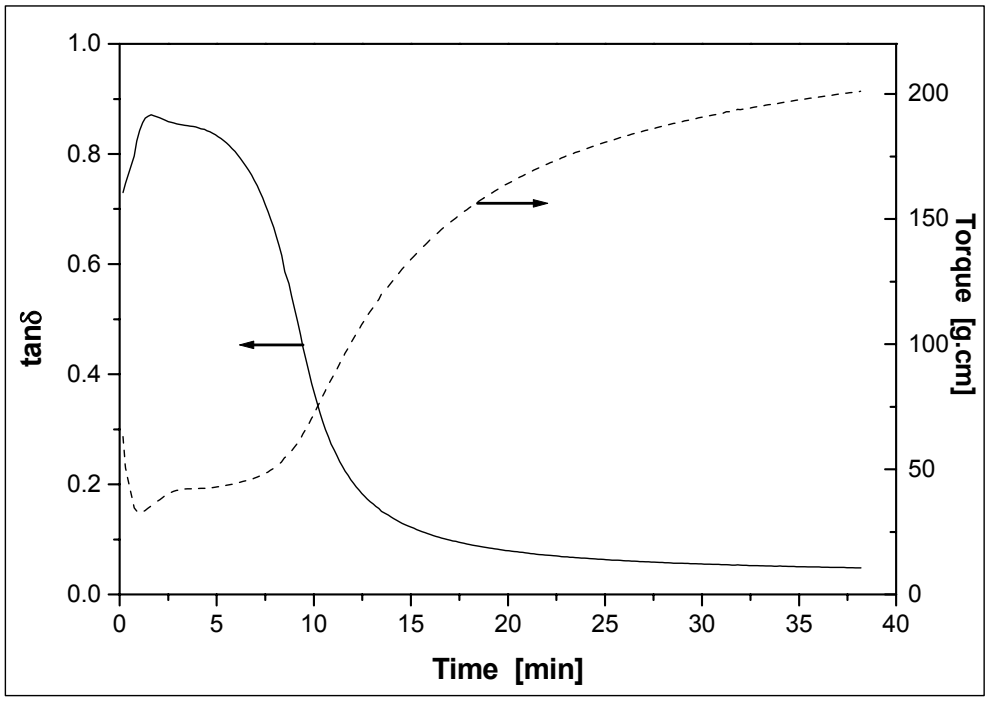

b)

Figure 5.3: Time dependence of the shear moduli (a) and tanδ and torque (b) during isothermal vulcanization of an EPDM reinforced with 10phr silica (sulfur cured)

These viscoelastic parameters and their change with time reflect directly the development of the crosslinking network within the rubber. Such interplay of the viscoelastic properties has been presented for thermoset resin composites during curing [121]. In the early stage of vulcanization, the so-called scorch time (cf. Figure 2.2), the parameters depicted in Figure 5.3 are rather constant in time (< 5min). The duration of this period depends on the type of the rubber, the curatives and the vulcanization temperature [122]. At the end of this scorch period (i.e. onset of vulcanization) a fast generation of ionic species was noticed for sulfur cured NR. This was monitored during on-line dielectric measurements and delivered useful insights in the vulcanization mechanisms [9]. While curing, crosslinks start to develop suppressing the mobility of the macromolecular chains and increasing the elasticity of the material. This is the reason why the storage modulus (G') and the torque are increasing. On the contrary, parameters presenting the energy loss to external excitation (e.g. G'', tanδ) are decreasing. Crosslinking is a process that leads usually to a plateau. Such a plateau was always well resolvable in the tanδ-time curves for all rubber mixes. In several cases an over-vulcanization was observed where both torque and modulus decreased after reaching a maximum (plateau) as a function of time [4]. The sensitivity of the Plate-Plate Rheometer was sufficient to record this over-cure phenomenon, as well. As presented in Figure 5.4 for NR reinforced with 10 phr bentonite (sulfur cured), the torque is decreasing after 20 min of curing. At the same time the tanδ increased marginally with the time.

The time to achieve a given degree of cure (as this is evaluated on conventional oscillating disc curometers like the Monsanto Rheometer from the recorded curve) is the time required for the torque to increase to [120]:

$$\frac{Y}{100}(M_H - M_L) + M_L \tag{5.1}$$

, where Y is the percentage cure required (usually 90% for a "practical" cure), M_H and M_L is the maximum (plateau) and minimum torque values, respectively. Considering the capability of the Plate-Plate Rheometer to monitor the formation of the crosslinking network, a similar formula should hold. Although the torque-time traces could also be used in our case, the related curves do not end always in a plateau (cf. Figure 5.3). This happens also with conventional curemeters, especially in case of peroxide cured rubber systems. For the Plate-Plate Rheometer, the parameter that

resulted a plateau as a function of time for all rubbers examined (peroxide and sulfur curing) was the tanδ. Therefore, formula 5.1 has to be adopted for the tanδ-time curve (cf. Figure 5.4):

$$R_H - \frac{Y}{100}(R_H - R_L) \tag{5.2}$$

, where now R_H and R_L is the maximum and the minimum (plateau) value of the tanδ, respectively. As shown in Figure 5.4, the t_{90} values as evaluated by the formulae 5.1 and 5.2 are right and left, respectively, from the t_{90} values measured by the Monsanto Rheometer. So, the 'underestimation' of the t_{90} value from the tanδ-time curve is likely due to the sensitivity of the tanδ on the detection of the crosslinked structure.

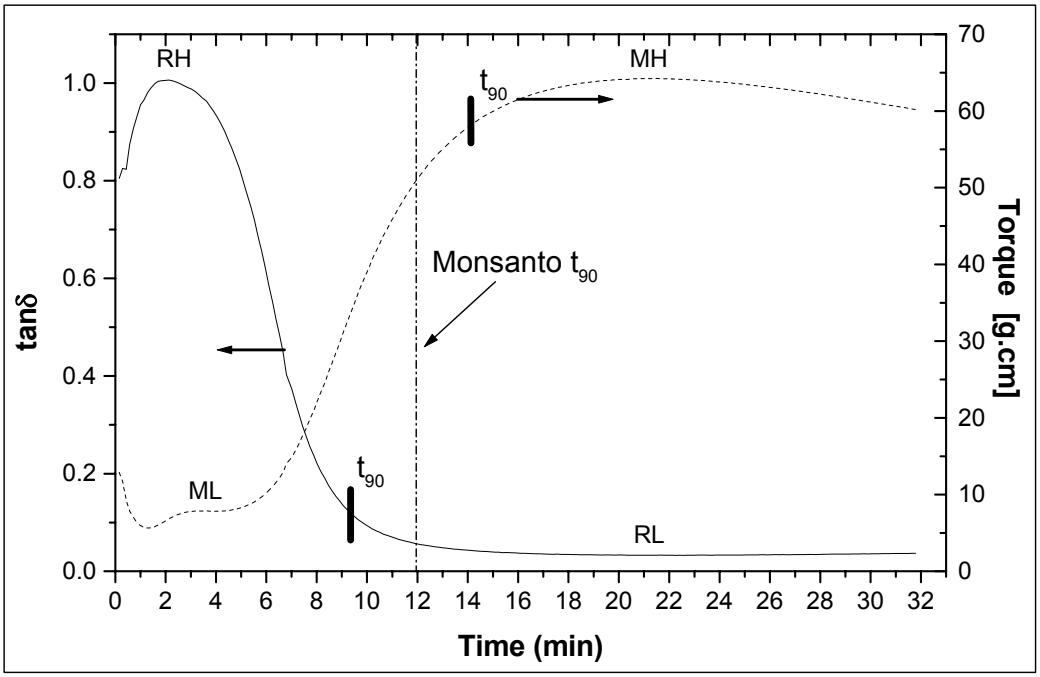

Figure 5.4: Change in tanδ and torque as a function of time in a time sweep test at 160°C for NR reinforced with 10phr bentonite (sulfur cured)

Figure 5.5 collates the optimum curing time derived from the measurements performed on the Monsanto vulcameter and Plate-Plate Rheometer. It is a time-time representation. The t_{90} Monsanto values are along the diagonal as they are linked to both x, y axes. On the other hand, the t_{90} Plate-Plate Rheometer values are linked only to the y axis in order to show the difference between the related t_{90} values for each rubber sample. As can be observed, the estimation of the optimum curing time for both techniques is almost the same for rubbers having less than 15 min t_{90} values,

whereas for higher t_{90} values the divergence is increasing. Note that the Monsanto data are always higher. It should be mentioned at this point that even different types of conventional curemeters present variation of optimum curing time for the same sample [1]. The line drawn in the graph in Figure 5.5 is the linear fit on the Plate-Plate Rheometer experimental data. Considering that the Plate-Plate Rheometer is a non-standard technique to determine the curing time, no calculation of further curing parameters (the scorch time or the cure rate) was tried. However, the above results corroborate that the tanδ vs time curves registered in the viscoelastic range under isothermal conditions can well be used to estimate the optimum curing parameters.

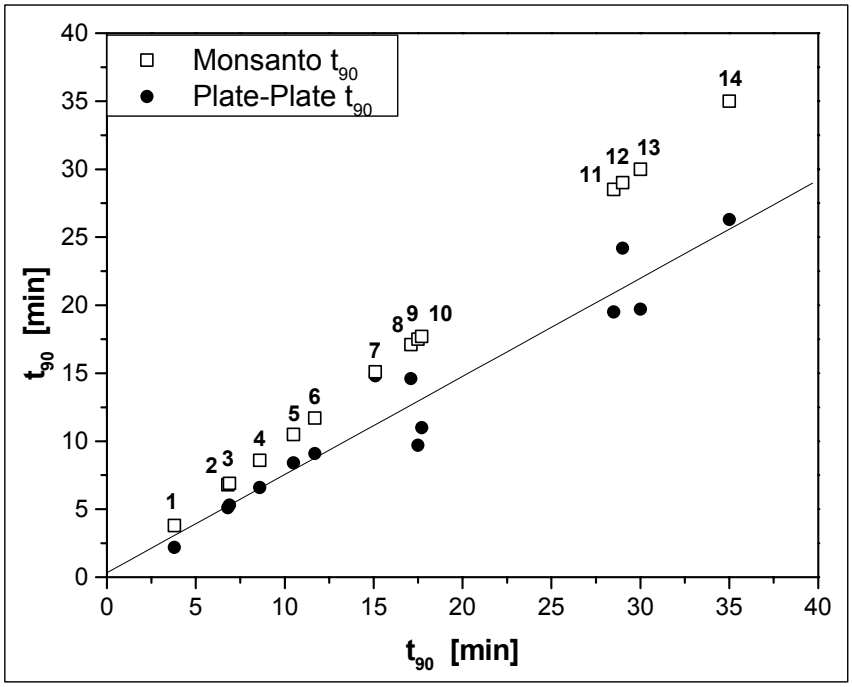

Figure 5.5: Time-time curve comparing the t_{90} values as measured by the Monsanto and the Plate-Plate rheometer (the t_{90} Monsanto values are on a diagonal array, where the t_{90} Plate-Plate values are in connection with the vertical axis). The numbers indicated on the graph correspond to the samples listed in Table 4.3

It should be mentioned at this point that the time required for rubber's optimum curing is different and greater than the gel time that corresponds to the sol-gel transition (Note that this term is usually used for systems presenting liquid to gel transition and thus, less used for rubbers). The transition between the liquid and the solid state (sol-gel) for crosslinkable systems is of great practical relevance, as the mould must be filled in the sol stage. The gel time is crucial for such systems but it lies markedly

lower than the optimum curing time needed for producing high performance rubbers. Application of the gelation study on rubber system was recently presented for resin cured chlorobutyl rubber [123]. For the evaluation of the gelation point in crosslinkable systems, the tanδ vs time curves measured at various frequencies are plotted [123-125]. Exploiting a multiple waveform dynamic experiment, based upon the Boltzmann superposition principle, the point that the tanδ curves intersect is independent of the frequency. The time at which this occurs is called the gel time. As shown in Figure 5.6, the tanδ traces recorded for an EPDM sample cured at 160°C (sulfur cured) do not seem to intersect at a single point but they just come close to one another after a specific time (during the scorch period), so no critical gel time is present. This may suggest a non-uniform gelation process for this chemically crosslinked rubber system [125-126].

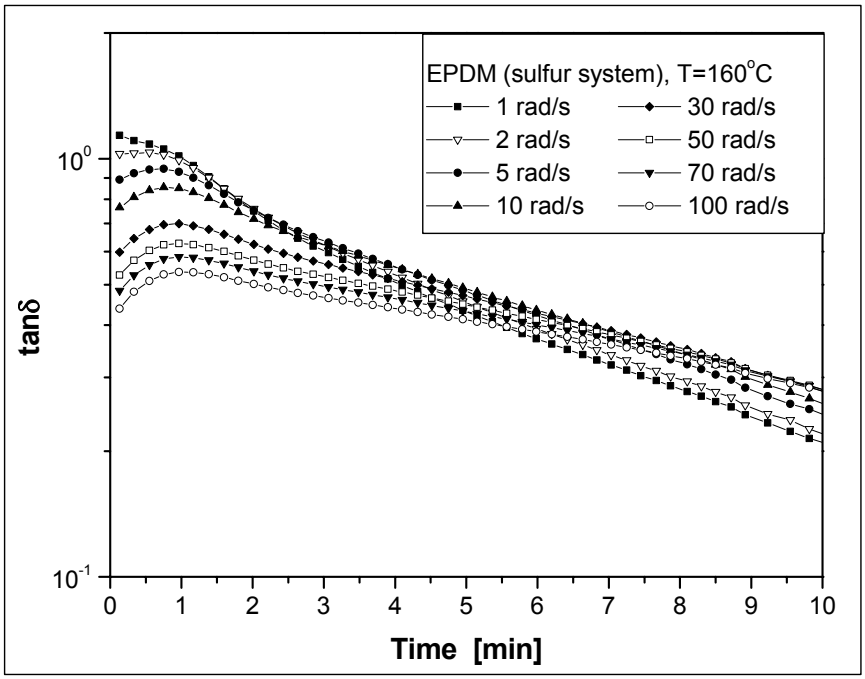

Figure 5.6: Multiwave dynamic rheological test on the time dependence of the tanδ for an EPDM sample cured at 160°C (sulfur cured)

It seems that the Plate-Plate Rheometer is capable not only of estimating the optimum curing time for rubbers, but moreover, for delivering information on gelation characteristics and mechanisms related with the scorch period.

5.2 Mechanisms Involved in Rubber/organoclay Nanocomposite Formation

The need of this separate chapter dedicated on introducing the mechanisms involved in the formation of rubber/organoclay nanocomposites is of high relevance in order to understand the idea behind the experiments, the results of which are summarized in the two following chapters. Considering the complexity of the rubber/organoclay nanocomposite formation, the effects of the constituents, i.e. rubber, organoclay, should be investigated accordingly. Their effects (combined and/or separately) on the structure-property relationships of the nanocomposite are determinant.

- Rubber:

There is a plethora of rubber types, which are usually classified according their chemical build-up. Their polarity is of high significance as it affects the processability during compounding and the wetting of the filler, the curing system selection, as well as, the final properties and possible applications. For that purpose, a non-polar EPDM and its polar versions, namely an EPDM-MA and an EPDM-GMA were initially chosen in order to investigate the polarity effect on the mixing technique and on the nanocomposite formation. Note that EPDM is an “engineering rubber”, finding applications in profiles/frames, cable jacketing and water hoses. To produce rubber articles, as discussed briefly in chapter 2.1, many additional ingredients should be always considered, which are important for the vulcanization procedure. In sulfur vulcanization, metal oxides (e.g. ZnO, MgO) have an important task as they assist the accelerators to develop their full potential during curing [4]. Moreover, the accelerator systems demand further activators like fatty acids, namely stearic acids, zinc soaps, etc. The above-mentioned EPDM rubber is indeed appropriate to be vulcanized by a sulfur system since bears unsaturated chain backbone (i.e. the diene group). Therefore, it was selected in order to study the effects of the accelerator type (viz. sulfur cured systems). Continuing the investigation on the rubber/organoclay nanocomposite formation, HNBR was chosen. It carries polar groups (i.e. no need of grafting compared to EPDM) and represents a high-tech elastomer with applications mainly in automotive and aerospace sectors. This rubber can be cured either by sulfur or peroxide and consequently it gave the opportunity some questions on the curing system to be solved. These questions were triggered by findings obtained from the tests performed on the EPDM-based nanocomposites.

- Organoclay:

The origin of the unmodified layered silicate may be one of the parameters affecting the nanocomposite formation. Thus, in the current analysis a MMT and FHT of natural and artificial origin, respectively, were investigated. Moreover, the modification of the silicates in combination with the rubber type should play a crucial role on the degree of silicate dispersion (i.e. intercalation/exfoliation). Intercalants of different reactivity, namely a primary amine (ODA) and quaternary polar (MTH) and non-polar ammonium compounds (ODTMA) were selected. Their action was investigated in combination with the polar and the non-polar version of above-mentioned rubbers. Further, the effect of the organoclay loading on the performance of the nanocomposite was checked.

By this way, via a straightforward selection of rubber and organoclay types, a wide spectrum of parameters, which influence the rubber/organoclay nanocomposite formation, could be studied. Thus, the results presented in the following chapters, including the discussion, can be transferred to the majority of rubber/organoclay nanocomposites. Accordingly, most of the results are of universal character.

5.3 EPDM/organoclay Nanocomposites

EPDM formulations served to study a) effects of compounding and recipe (i.e. mixing procedure, accelerator type, organoclay loading), and b) effects of the types of rubber and organoclay (i.e. rubber polarity and organoclay intercalant), on the corresponding nanocomposites.

5.3.1 Effect of Mixing Procedure

Table 5.1 presents the mechanical properties of the EPDM reinforced by 10phr organoclay. Note that in all these mixtures presented in Table 5.1, ZDEC was used as accelerator. This choice was based on the work of Usuki et al. [64], who investigated several types of accelerators (i.e. CBS, MBT, ZDEC), and found that the dithiocarbamate type proved to be the most promising to produce EPDM-clay hydrids. That was the major reason why the effects of mixing and temperature were studied in a formulation containing ZDEC.

The processing conditions, i.e. mixing technique and temperature, seem to have some effect on the mechanical properties of the EPDM samples. The tensile moduli

at 100%, 200% and 300% elongations are less influenced by the mixing techniques and temperature. On the other hand, mixing in the internal mixer at 100^{o}C increased both the tensile strength and elongation at break (cf. EPDM stocks in Table 5.1).

Table 5.1: Mechanical properties of EPDM/organoclay (10phr) compounds, prepared under different conditions with and without MA grafted EPDM as compatibilizer

Properties	Processing conditions (mixed with 10phr MMT-ODA)							
	Open mill				Internal mixer			
	30°C		100°C		30°C		100°C	
	EPDM	EPDM-MA	EPDM	EPDM-MA	EPDM	EPDM-MA	EPDM	EPDM-MA
Tensile strength (MPa)	3.9	6.6	5.2	8.1	4.9	10.5	7.1	14.9
Modulus (MPa) at:								
100% Elong.	1.5	2.0	1.6	2.7	1.5	3.9	1.6	5.4
200% Elong.	2.3	3.3	2.3	4.6	2.0	7.3	2.3	9.3
300% Elong.	3.0	4.9	2.9	6.9	2.6	9.9	3.0	12.1
Elongation at break (%)	380	395	495	360	520	321	645	403

As obvious in Table 5.1, the use of EPDM-MA compatibilizer resulted in markedly higher values of tensile strength and stiffness at all processing temperatures and mixing methods. This is related with the functional group MA that rendered the polymeric chain polar. This “polarity” facilitates the intercalation/exfoliation phenomena. Clear advantage of the MA grafting was observed for compounding in the internal mixer. The tensile strength of the EPDM-MA was more than doubled when mixed either at room temperature or at 100^{o}C. Moreover, the EPDM-MA mixed at 100^{o}C in the internal mixer possessed the highest tensile strength of 14.9 MPa. These results are in accordance with the work of Yoon et al. [127]. They noticed on polystyrene/clay hydrids that the shear applied during mixing does not contribute to

the intercalation when no or only weak interactions exist between the polymer and the silicate.

Considering a parallel increase in the tensile moduli at all elongations, the stress-strain behaviour of the composites has been changed (Fig. 5.7). Such tremendous change in the stress-strain curves is usually observed for intercalated and/or exfoliated rubber nanocomposites.

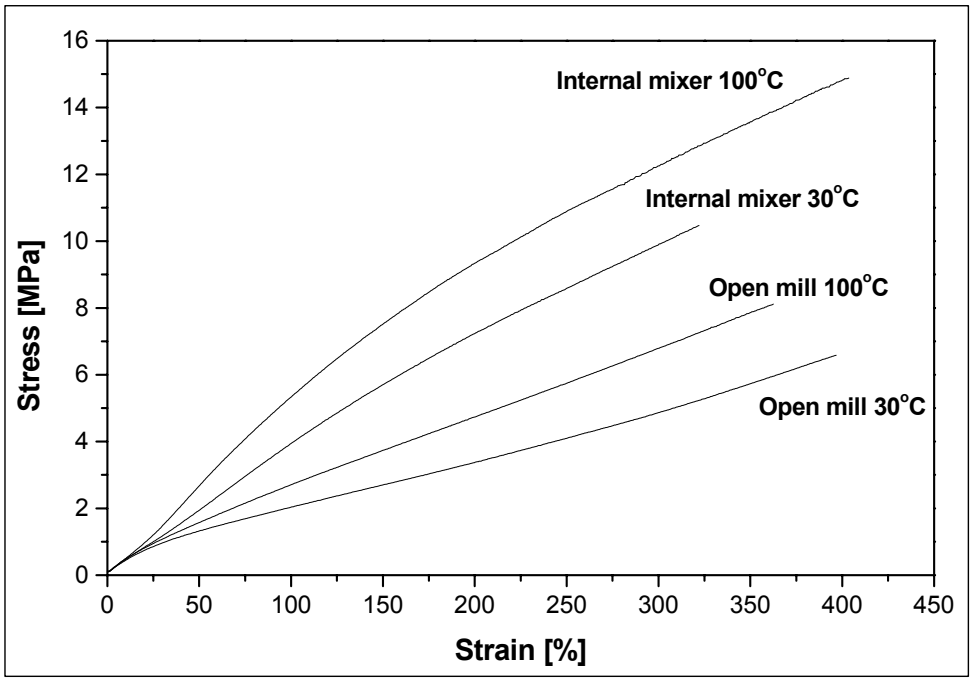

Figure 5.7: Stress-strain curves of EPDM-MA/organoclay reinforced systems prepared at different conditions

As can be seen in Figure 5.8, the main reason for the large difference in the stress-strain response shown in Figure 5.7 (i.e. between the compounding in the internal mixer at 100 °C and that on the open mill at 30°C) should attributed to the degree of organoclay dispersion. Compounding in the internal mixer at 100 °C (cf. Fig. 5.8a) yields a nanocomposite, opposed to that mixed on the open mill where a microcomposite containing big agglomerates developed (cf. Fig. 5.8b).

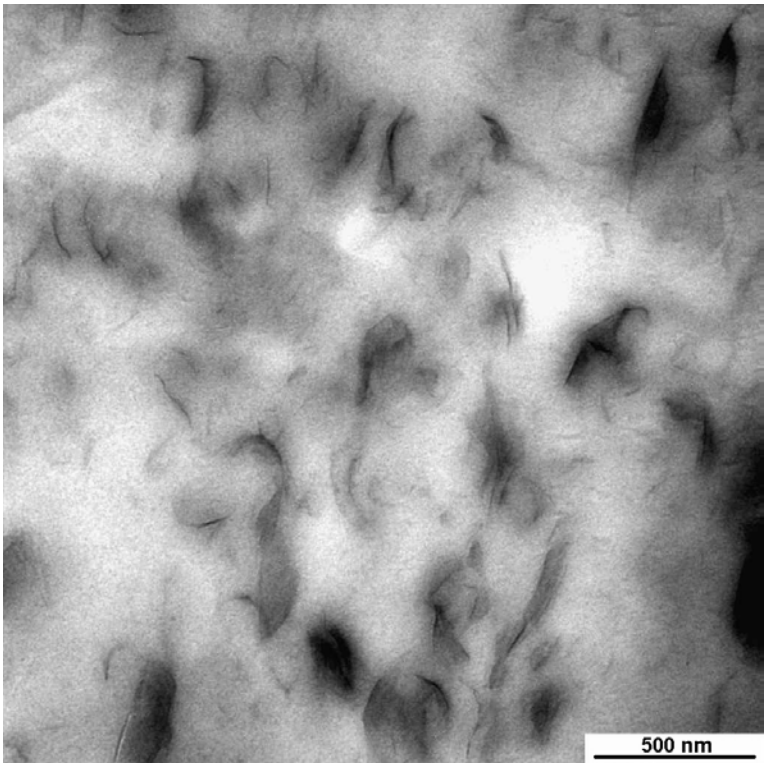

a)

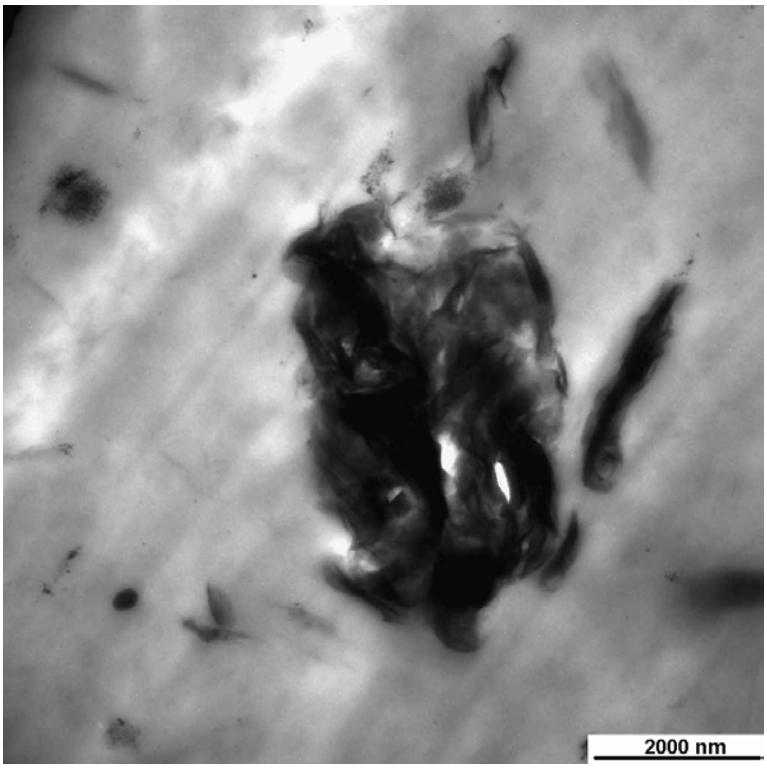

b)

Figure 5.8: TEM images of EPDM-MA/MMT-ODA nanocomposite prepared a) in the internal mixer at 100^{o}C and b) mixed on the open mill at 30°C (room temperature)

In order to investigate further the agglomerates observed by TEM (cf. Figure 5.8), the organoclay was subjected to SEM observation. As shown in Figure 5.9, the MMT-ODA particles delivered (powder form) have a diameter less than 40 μm. A closer view reveals the complex structure of the organoclay particles (Fig. 5.9b).

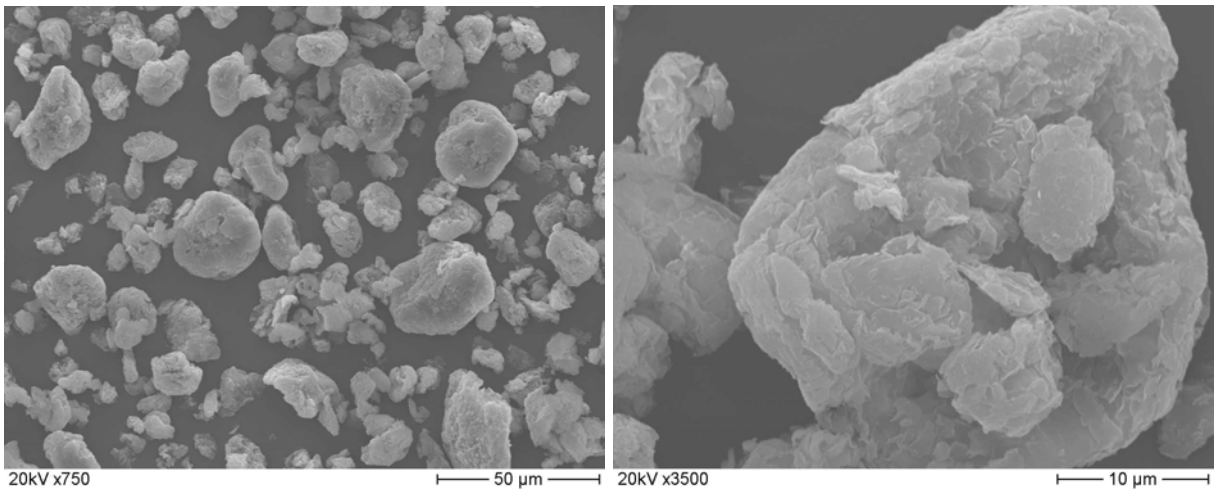

a) b)

Figure 5.9: SEM images from the organoclay (MMT-ODA) particles at (a) low and (b) high magnification

SEM photos taken from the fractured surface of EPDM-MA/MMT-ODA compounds produced on the open mill (Fig. 5.10) show that big organoclay agglomerates are dispersed in the rubber matrix. This is in accordance with the TEM images showed before (cf. Figure 5.8b).

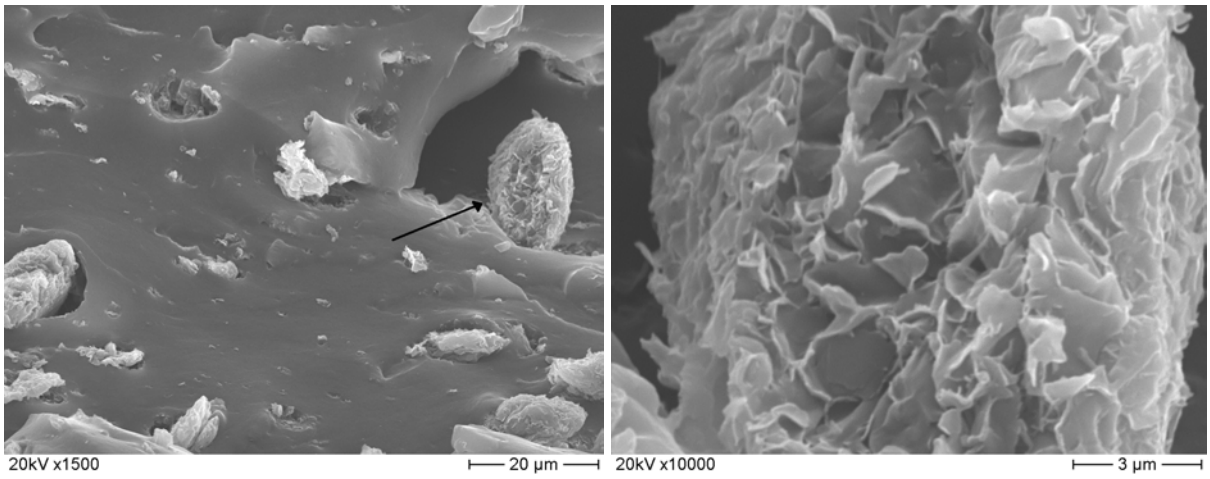

a) b)

Figure 5.10: SEM images taken at low (a) and high magnifications (b) from the EPDM-MA/MMT-ODA nanocomposite mixed on the open mill (accelerator: ZDEC)

A closer look at the aggregate (Fig. 5.10b) shows that its structure differs from that of the initial one (cf. Figure 5.9b). The primary particles appear in Figure 5.10b like flakes, suggesting that some macromolecular chains have been intercalated within the primary particles. A totally different morphology was found for the same rubber when compounded in the internal mixer. As presented in Figure 5.11, in this case some very regular well-shaped crystal-like particles appeared. Elemental mapping analysis of the particles revealed that these are, indeed, silicates. These large crystal-like structures suggest that even aspects related to mineralogy should be considered (e.g. illitization [128-129], face/face and edge/edge aggregation [130]). It is interesting to observe one platelet in the middle of the photo (indicated by arrow in Figure 5.11) that is supposed to have a width of ca.100 nm. These crystal-like agglomerates along with individual and stacked silicate layers (the latter derived from the TEM analysis) are dispersed in the rubber matrix.

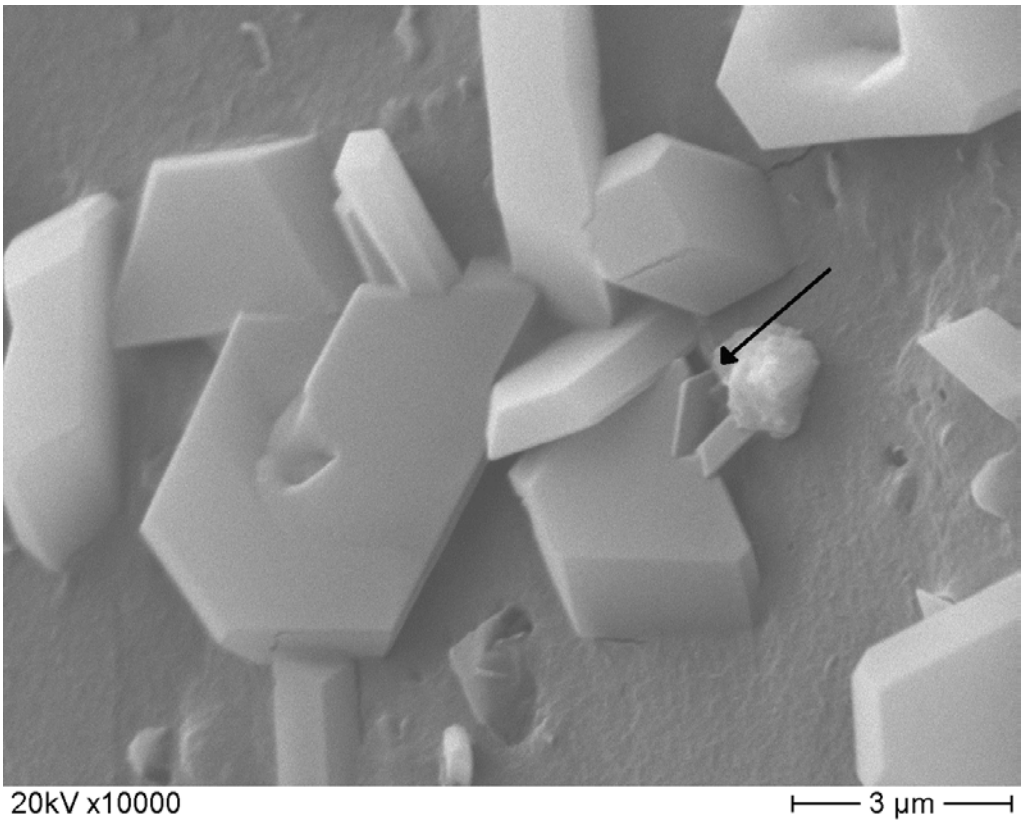

Figure 5.11: SEM image on the fractured surface of the EPDM-MA/MMT-ODA nanocomposite produced in the internal mixer (accelerator: ZDEC)

To investigate whether the organoclay was intercalated in the vulcanizates, the XRD analysis is the appropriate tool. As shown in Figure 5.12, the dispersion of both vulcanizates is almost identical presenting broad scattering at low angles and an asymmetric peak around 6.5^{o} (2θ scatter angle). The scattering at low 2θ values indicates likely some exfoliated populations, whereas the latter presents an interlayer spacing of 1.29 nm, lower than the initially MMT-ODA organoclay (viz. 2.10 nm). This fact signifies that somehow deintercalation of the organoclay took place. Moreover, the asymmetric shape hints that the surface coverage of the clay has been altered [131]. It has to be emphasized here that the terminology, “confinement” covers the collapse of the silicate layers up to the initial basal spacing, whereas a further collapse in the nanocomposite is termed deintercalation (“extraction” of the initial intercalant from the organoclay).

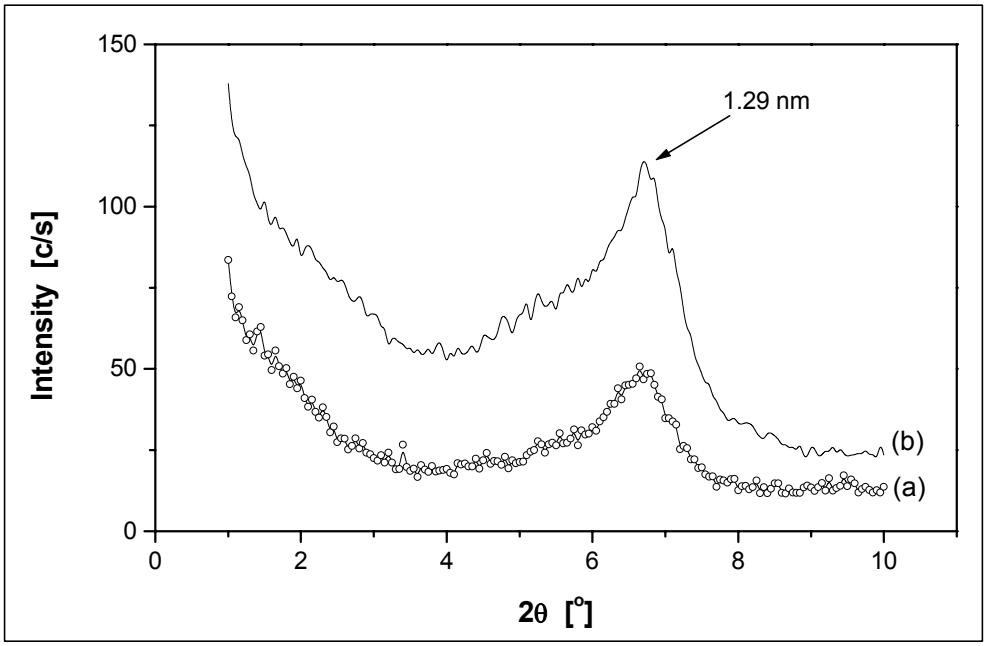

Figure 5.12: XRD spectra of the EPDM-MA/MMT-ODA vulcanizates when initially mixed (a) on the open mill and (b) in the internal mixer

The similarity of the XRD spectra for the EPDM-MA/MMT-ODA vulcanizates compounded on the open mill and in the kneader is opposed to their different dispersion grades proved by TEM and SEM. Thus, it can be claimed that during compounding the organoclay particles (cf. Fig. 5.9b) are intercalated by EPDM-MA macromolecules. As this effect is governed by thermodynamics, the role of the

mixing techniques is marginal. As the shear forces increase during the compounding in the kneader, the intercalated agglomerates (cf. Fig. 5.10b) break down and become finely dispersed in the rubber matrix. The outcome is a more efficient reinforcement owing to the intercalated/exfoliated organoclay layers and stacks.

5.3.2 Effect of Polarity

After having defined well-suited conditions for the mixing (viz. internal mixer) the effect of the rubber polarity was studied. It should be mentioned that ZDEC accelerator and MMT-ODA organoclay (in 10 phr) were used in all these compounds. The mechanical performance of the mixes is shown in Figure 5.13. One can clearly see that the incorporation of both grafted EPDM rubbers strongly improved the strength and stiffness characteristics of the composites compared to the non-polar EPDM rubber. Moreover, the MA group delivered higher tensile strength and moduli values than the GMA group. This can be attributed to the enhanced intercalating action of the MA group linked with its higher polarity.

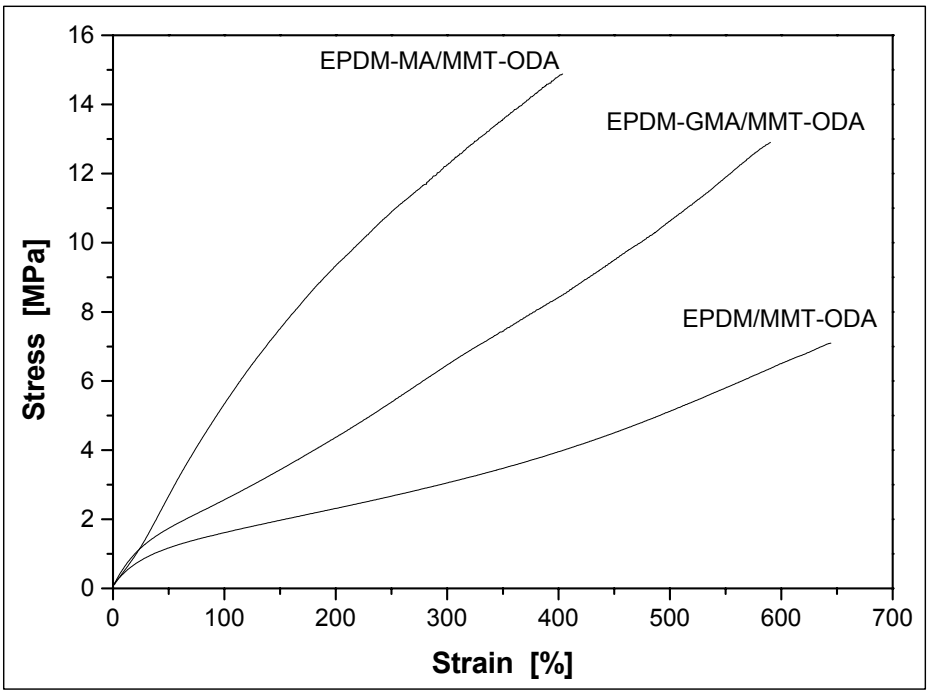

Figure 5.13: Effect of grafted polar groups on the EPDM macromolecular chain backbone. Note that MMT-ODA was incorporated in 10phr and in the vulcanization recipe ZDEC served as accelerator

The XRD in Figure 5.14, spectra supply valuable information for the above-mentioned nanocomposite structures. The diffraction peak of MMT-ODA appears at ca. 4°, which corresponds to an interlayer spacing of 2.10 nm. For the EPDM/clay nanocomposite two peaks can be observed. One around 2.7° (≈ 3.28 nm) that indicates the intercalation of the layered silicate, and the second at 5.8° (≈ 1.51 nm), which suggests some deintercalation of the silicate layers. The XRD pattern of the EPDM-GMA/clay nanocomposite presents also two distinct peaks like the EPDM/organoclay system. The first peak raises at 2.2° (≈ 3.92 nm) and the second broad peak is in the region of $2\theta \approx 5\text{-}7^{o}$ (peak position of ≥ 1.29 nm). It is worth of noting the XRD spectrum of EPDM-MA/organoclay, which showed the best mechanical behavior, exhibited only one distinct peak at 6.9° (≈ 1.29 nm) and a broad scattering at low diffraction angles ($2\theta < 3°$). Considering the work of Yoon et al. [127], the appearance of such a peak (i.e. at ≈1.3nm) can be likely attributed to the monolayer arrangement of the intercalant (ODA in this case). They report on styrenics/organophilic montmorillonite (modified with dimethyl benzyl hydrogenated tallow ammonium compound) nanocomposites, where the authors assigned the peak in the XRD spectrum at around 6.2° (≈ 1.42 nm) to the onset of a monolayer arrangement instead of bilayer structure of the intercalant.

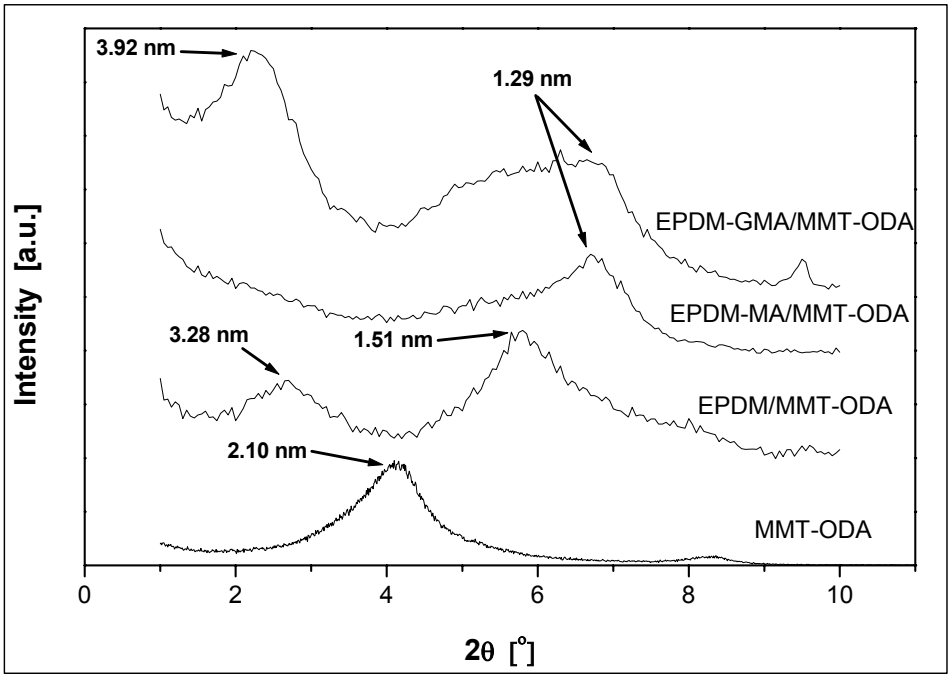

Figure 5.14: XRD patterns of EPDM compounds with and without compatibilizers (MA and GMA grafted EPDM) after mixing in an internal mixer at 100°C and using ZDEC as accelerator for sulfur curing

Figure 5.14 demonstrates that a better clay intercalation occurred in the recipes containing EPDM-MA or EPDM-GMA compatibilizers. Both functional groups, i.e. anhydride and epoxy, may react with the primary amine functionality of the ODA intercalant. These chemical reactions obviously contribute to the intercalation (and even exfoliation, which the XRD is not a suitable tool for) via entropy gain for the ODA.

Further evidence about the polarity effect of the rubber was supplied by TEM. As shown in Figure 5.15a, the EPDM reinforced by MMT-ODA has a nanocomposite structure. Compared with Figure 5.8a, one can notice that in presence of polar macromolecular chains the silicate layers delaminate more easily and become better dispersed in the EPDM matrix. In case of EPDM-GMA/organoclay nanocomposites, which possess a highly intercalated structure (cf. XRD spectrum-Figure 5.14) the high magnification TEM images resolve well both the widened and deintercalated (layer stacks) interlayer galleries (Fig. 5.15b).

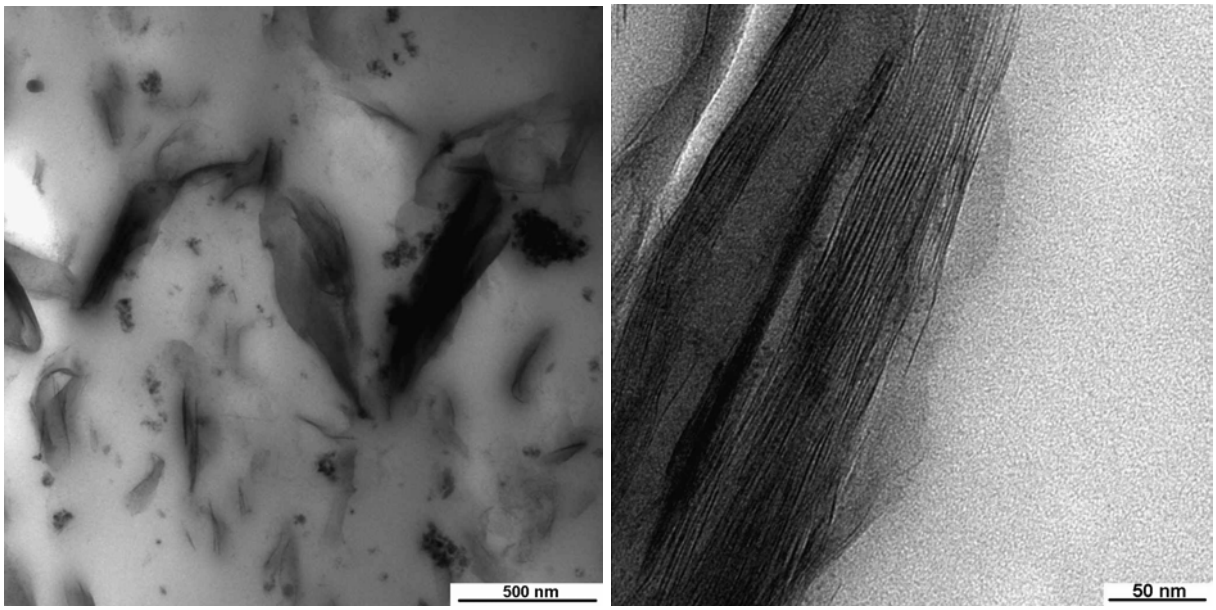

a) b)

Figure 5.15: TEM image of (a) EPDM/organoclay and (b) EPDM-GMA/organoclay nanocomposite vulcanizates

During investigating the effect of the rubber polarity the question raised: what is the origin of the deintercalation observed (cf. XRD spectra and TEM images-Figures 5.14 and 5.15). This aspect will be addressed in the following sections (i.e. 5.3.3 and 5.3.4).

5.3.3 Effect of Vulcanization Accelerator

As the vulcanization accelerator has been found to play an important role in the rubber/organoclay nanocomposite formation [64], its role was further investigated. The EPDM rubber, as well as, its polar versions reinforced by 10phr of MMT-ODA was checked upon the effect of the vulcanization accelerators. The mechanical performance was tested and the results are summarized in Table 5.2. Comparing the CBS, MBT and ZDEC the best mechanical properties appear in case of the latter for all three types of EPDM rubbers. Stiffness characteristics were improved parallel to the maintenance of the high elongation at break values.

Table 5.1: Mechanical properties of EPDM reinforced by 10phr MMT-ODA using different grafted EPDMs as compatibilizers and accelerators

Properties	Nanocomposites with 10phr MMT-ODA								
	EPDM			EPDM-MA			EPDM-GMA		
	CBS	MBT	ZDEC	CBS	MBT	ZDEC	CBS	MBT	ZDEC
Tensile strength (MPa)	5.3	7.0	7.1	11.6	12.0	14.9	8.8	9.7	13.0
Tensile modulus (MPa)									
100% Elong.	1.6	1.3	1.6	2.3	2.9	5.4	1.9	1.9	2.7
200% Elong.	2.1	1.7	2.3	4.6	5.2	9.3	2.8	2.8	4.5
300% Elong.	2.6	2.1	3.0	6.6	7.4	12.1	3.9	3.9	6.5
Elongation at break (%)	636	733	645	583	553	403	655	708	590

Investigating the effect of the vulcanization accelerator on the microstructure of the EPDM-MA/MMT-ODA vulcanizates, it seems that the superior action of ZDEC is linked with the dispersion grade of the organoclay (Fig. 5.16). The CBS and MBT accelerators produced intercalated nanocomposites, whereas the ZDEC, as has been already discussed (cf. Fig.5.14), gives exfoliated and deintercalated clay structures. The peaks at 1.60 and 1.75 nm for MBT and CBS, respectively, should be attributed reflections at higher order, i.e. *d(002)*.

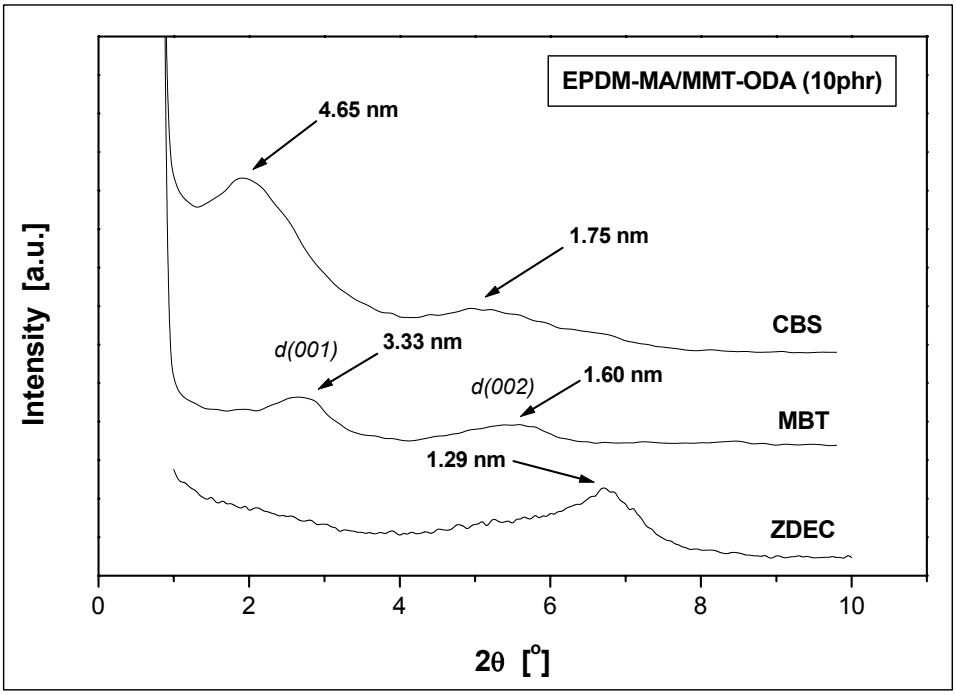

Figure 5.15: XRD patterns of EPDM-MA/MMT-ODA (10phr) nanocomposites compounded with different vulcanization accelerators

Observing the TEM images of the EPDM-MA/MMT-ODA nanocomposites vulcanized with ZDEC and CBS, the clay dispersion grade appears rather similar. Both present an exfoliated structure, however, stacks of platelets are also well resolved.

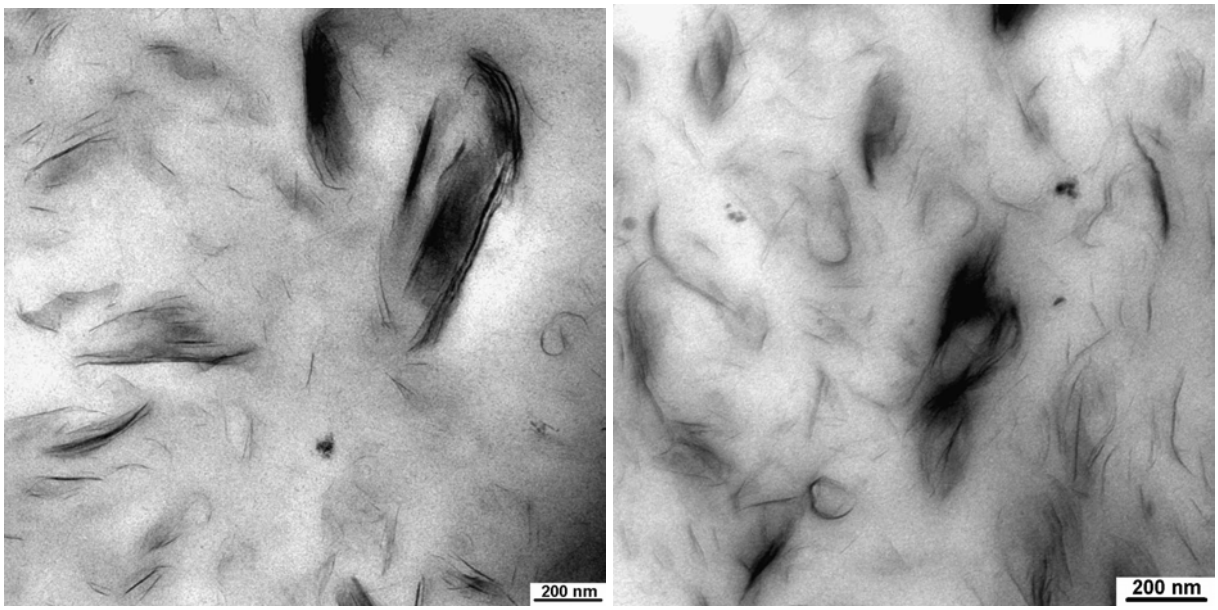

Figure 5.16: TEM images of EPDM-MA/MMT-ODA nanocomposites vulcanized with (a) ZDEC and (b) CBS

The XRD results indicate that the deintercalation phenomena are related mostly with the Zn containing accelerator (i.e. ZDEC), which may “extract” the ODA intercalant from the intergallery spacing. This type of curative is rich in Zn^{2+} and dissociate at high temperatures in presence of ZnO. In order to increase the action of ZnO on the dissociation of the ZDEC, ZnO was added during the compounding stage of the EPDM-MA with the MMT-ODA in the internal mixer for 10 min. By this way a better ZnO dispersion in the rubber matrix can be reached, which should act beneficially on the acceleration process. It has to be mentioned that ZnO works as lubricant as it reduced the torque during compounding by ca. 40%. In the XRD spectrum, trace B (Figure 5.17) represents that mixture to which the ZnO was added in the kneader. This system shows, apart from the asymmetric peak in the region 5-7^{o} (already discussed in chapter 5.3.1), also a second sharp one corresponding to an interlayer spacing of 0.94 nm. In this case the ODA intercalant has been totally removed from the galleries, which thus further collapsed. Moreover, for the XRD spectrum B no scattering at low angles appears. This hints that mostly deintercalated silicate stacks created with no sign of any intercalated rubber/organoclay nanocomposite structure.

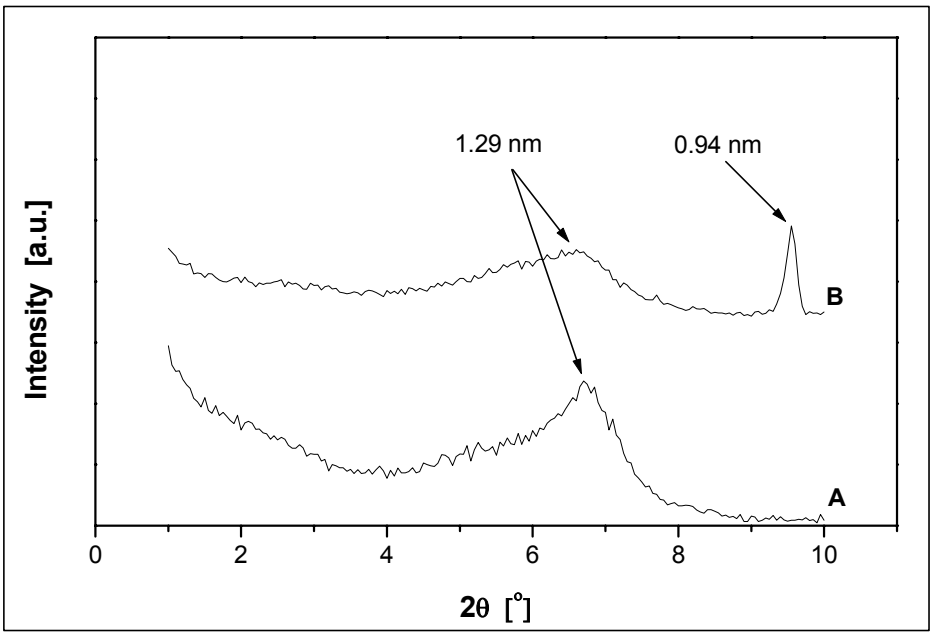

Figure 5.17: XRD spectra recorded from the EPDM-MA/MMT-ODA vulcanizates where the ZnO was added as usual on the open mill together with all the other curatives, designated with A, and when it was added during the internal mixer procedure, designated with B

Until now solely rubber vulcanizates were subjected to XRD investigations. At deeper understanding on the intercalation, confinement and deintercalation, XRD spectra were taken in different steps of rubber compounding. The related stocks contained ZDEC as accelerator. As presented in Figure 5.18, the basal spacing of the initial MMT-ODA slightly increased during mixing of the EPDM with the organoclay (10 phr) in the kneader. This limited penetration of the EPDM into the clay galleries was observed also for other non-polar polymers, like polypropylene (PP) [89].

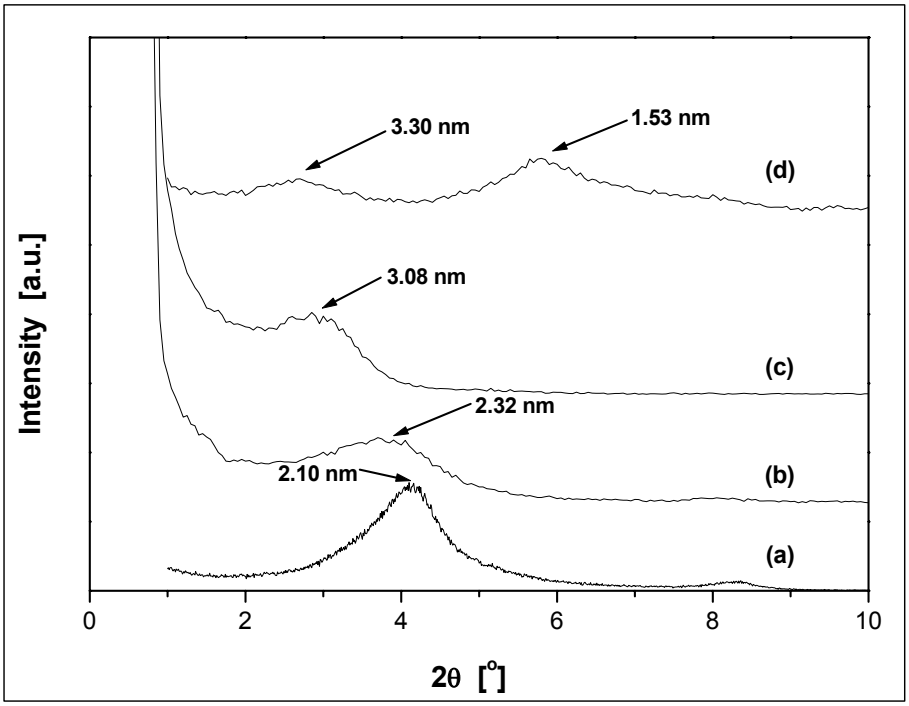

Figure 5.18: XRD patterns of (a) the MMT-ODA and (b)-(d) the EPDM/MMT-ODA (10 phr) nanocomposite at the different stages of processing: (a) MMT-ODA powder, (b) mixing of the EPDM and the MMT-ODA (10 phr) in the internal mixer, (c) after addition of the curatives on the open mill and (d) after vulcanization at 160 ^{o}C

After the second stage of compounding, i.e. incorporation of the curatives and further ingredients on the open mill, a shift in the XRD peak towards lower 2θ values occurred. This indicates further opening of the clay galleries. But what can be the reason for this 0.76 nm gallery expansion that is observed between the first and second stage? Considering the fact that EPDM alone does not favor intercalation, as it was proven during the first step, further compounding (i.e. on the open mill) should not contribute to a better intercalation. The parameter that changed during the second step was the addition of the curatives, i.e. ZnO, ZDEC, stearic acid and

sulfur. Nanoparticles of ZnO was found by Németh et al. [132] to intercalate in kaolinite and montmorillonite layers. Note that ZDEC is quite polar and stearic acid is also a polar low molecular mass compound. Sulfur is rather inactive in its original form (ring of eight atoms) at room temperature. Conclusively, the observed layer expansion of the organoclay might be related, indeed, with the “adsorption” of the curatives in the clay galleries. Adsorption of such agents has been reported on silica particles surfaces [133]. The further layer separation between the first and the second processing step has been observed recently by Zheng et al. [63] and Usuki et al. [64] for EPDM mixed with MMT-ODA and MMT-ODTMA, respectively. These authors attributed this phenomenon to the prolongation of the compounding. After vulcanization, as presented in Figure 5.18-trace d, apart from a peak that can be attributed to the nanocomposite formation (3.30 nm), another one at higher 2θ appeared (1.53 nm). This suggests some confinement of the clay galleries.

To check the role of the polar MA group during the stages of compounding the same procedure as above was followed for the EPDM-MA recipe. As shown in Figure 5.19, the beneficial action of the polar chains appears already in first stage (i.e. mixing in the internal mixer). After this step, an increase up to 3.15 nm interlayer spacing is observed (cf. Figure 5.19-trace b). Adding the curatives (trace c) did not change practically the degree of intercalation. Trace d in Figure 5.19 reflects the effect of vulcanization. There the only XRD peak at higher 2θ corresponds to a basal spacing of 1.29 nm. This is markedly lower than the initial interlayer spacing of the MMT-ODA (2.10 nm).

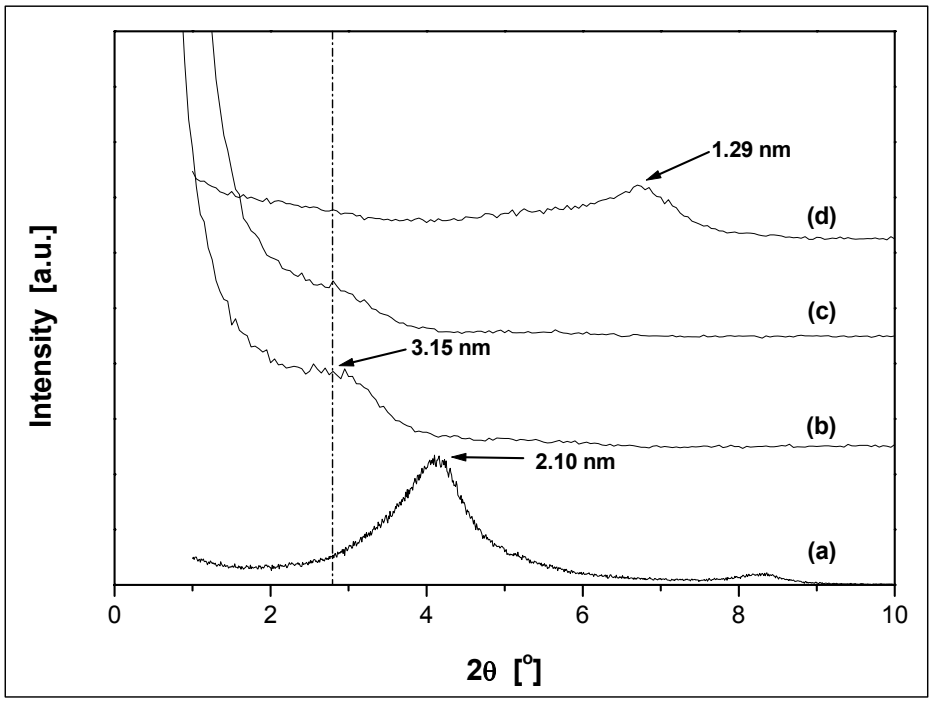

Figure 5.19: XRD patterns of (a) the MMT-ODA and (b)-(d) the EPDM-MA/MMT-ODA (10 phr) nanocomposite at the different stages of processing: (a) MMT-ODA powder, (b) mixing of the EPDM-MA and the MMT-ODA (10 phr) in the internal mixer, (c) after addition of the curatives on the open mill and (d) after vulcanization

To step forward with the investigation the role of the curatives between the first and the second processing stage should be examined. Do they indeed interfere with the intercalation process or just the prolonged compounding on the open mill is the key aspect? Are the curatives present in the gallery environment before vulcanization as it was speculated above?

To elucidate these questions, samples were prepared similarly as before, but changing the compounding in the first stage. So, instead of compounding the rubber and the MMT-ODA (10 phr) in the internal mixer for 10 min, their mixing was performed on the open mill for the same time. As can be seen in Figure 5.20-traces a and c, just by working on the open mill does not support the intercalation because after 10 min of processing, both EPDM and EPDM-MA produce identical results. This result was expected for the EPDM compound, as this rubber does not favor intercalation due to its apolarity (compare Fig. 5.18-trace b with Fig. 5.20-trace a). On the other hand, in case of EPDM-MA the results are in contrast to those achieved in the internal mixer (compare Fig. 5.19-trace b with Fig. 5.20-trace c). It is now

interesting to observe that just by adding the vulcanization curatives, Figure 5.20-traces b and d, the XRD peak shifts to lower 2θ for both EPDM and EPDM-MA. Note that the addition of the vulcanization curatives took place on the open mill at room temperature (typical procedure) and lasted between 5 and 10 min.

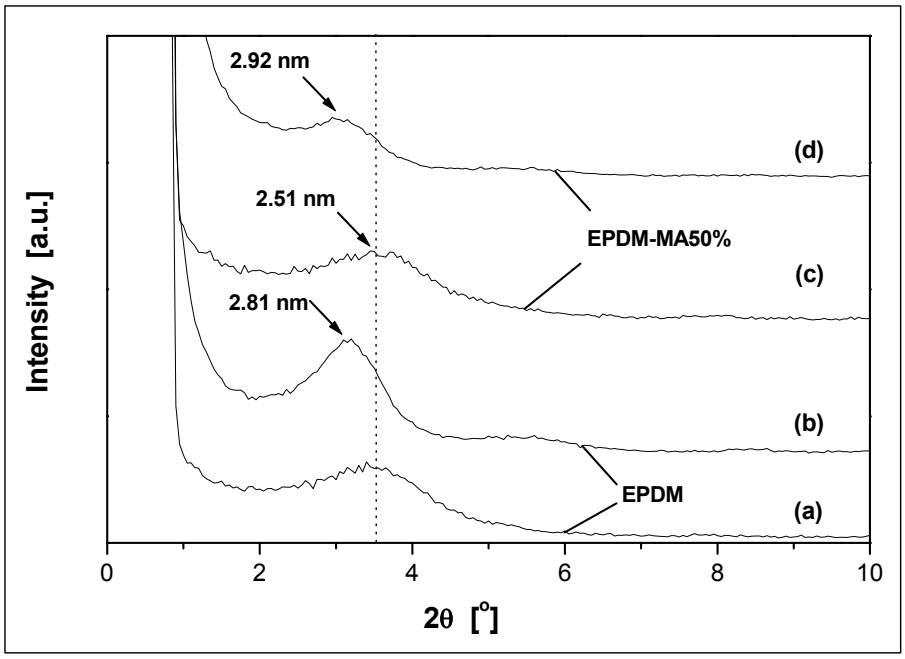

Figure 5.20: XRD patterns of (a) the EPDM mixed with MMT-ODA (10 phr) for 10 min on the open mill, (b) further addition of the curatives, (c) the EPDM-MA mixed with MMT-ODA (10 phr) for 10 min on the open mill and (d) further addition of the curatives

These data evidence the decisive role of the curatives and makes clear their presence in the clay galleries. Proceeding further with the vulcanization of these samples, the related XRD spectra were similar to those presented as d traces in Figures 5.18 and 5.19. Recall that the above-mentioned results were deduced on EPDM-based mixes containing MMT-ODA as filler. To step further, the effect of the organoclay intercalant was addressed.

5.3.4 Effect of Organoclay Intercalant

It is known that the sulfur-vulcanization of rubber proceeds in three stages (cf. chapter 2.1). Nieuwenhuizen and co-workers have presented the role of zinc accelerator complexes in sulfur-vulcanized systems [101, 103] underlining the action

of amines. They refer a mechanism where a nucleophilic attack of an amine on the carbon atom of the thiocarboxy group of a bis(dialkyldithiocarbamato)zinc(II) (ZDAC) yields an amine-dithiocarbamic intermediate from which, in the case of primary amines, thiourea products are obtained [103]. Tertiary amines were found not to react with ZDACs. A rough scheme of the catalytic action of primary amines on the vulcanization procedure is given in Figure 5.21.

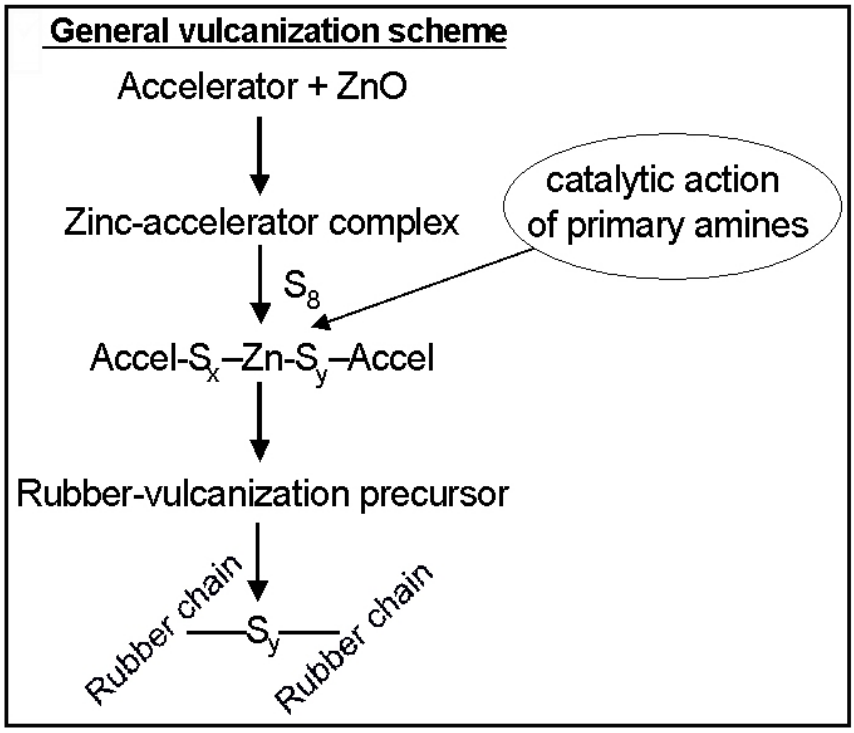

Figure 5.21: Scheme of the vulcanization steps and the stage where a primary amine acts catalytically

In our system, primary amines can be found only inside the clay galleries (i.e. ODA intercalant). The presence of the curatives either inside or at the edges of the silicate layers (cf. chapter 5.3.3) could generate such complexes. By this way, the tethered ODA chain should leave the clay surface in order to participate in the vulcanization intermediate. This occurs either by migration into the rubber matrix (resulting in confinement or deintercalation of the galleries) or causing rubber crosslinking inside the galleries (inducing better clay dispersion via layers separation or delamination/exfoliation). If the above scenario holds, then using a quaternary amine as modifier, creation of such type of complexes excluded and thus no confinement/deintercalation take place.

As shown in Figure 5.22, when MMT-ODTMA is used as organoclay (following the basic compounding procedure, i.e. internal mixer followed by open mill) the XRD spectra of the vulcanized EPDM rubbers strongly differ from those produced with MMT-ODA (cf. Figure 5.14). The spectra in Figure 5.22 indicate intercalated nanocomposite structures presenting *d*-spacing (i.e. *d(001)*) of 4.20 nm and 4.69 nm for EPDM and EPDM-MA, respectively. At the same time, peaks at 2θ = 4.4° and 6.6° were observed. We speculate that the additional peaks in Figures 5.22b and c are related on both reflections at higher order (especially for EPDM/MMT-ODTMA; Fig. 5.22b) and some deintercalation phenomena due to the high sulfur content (especially for EPDM-MA/MMT-ODTMA; Fig. 5.22c). Note that the right positions (calculated) of the reflections at higher order, as well as, the measured ones are indicated in Figure 5.22 and were estimated based on the Bragg's equation (eq. 5.3).

$$n\lambda = 2d\sin\theta \tag{5.3}$$

, where *n* is the reflection order term, *d* is the interlayer spacing, *λ* is the wavelength and θ is the scattering angle of the beam.

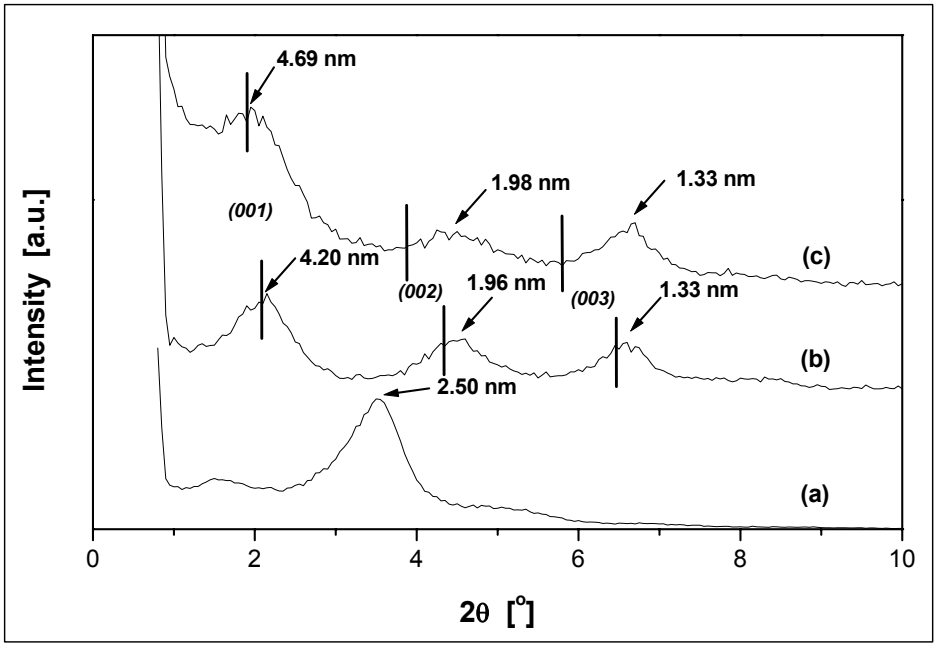

Figure 5.22: XRD patterns of (a) the MMT-ODTMA, (b) the EPDM/MMT-ODTMA after vulcanization and (d) the EPDM-MA/MMT-ODTMA after vulcanization (clay loading in 10 phr)

The TEM image taken from the EPDM-MA/MMT-ODTMA (Figure 5.23) presents a nanocomposite containing also exfoliated clay layers.

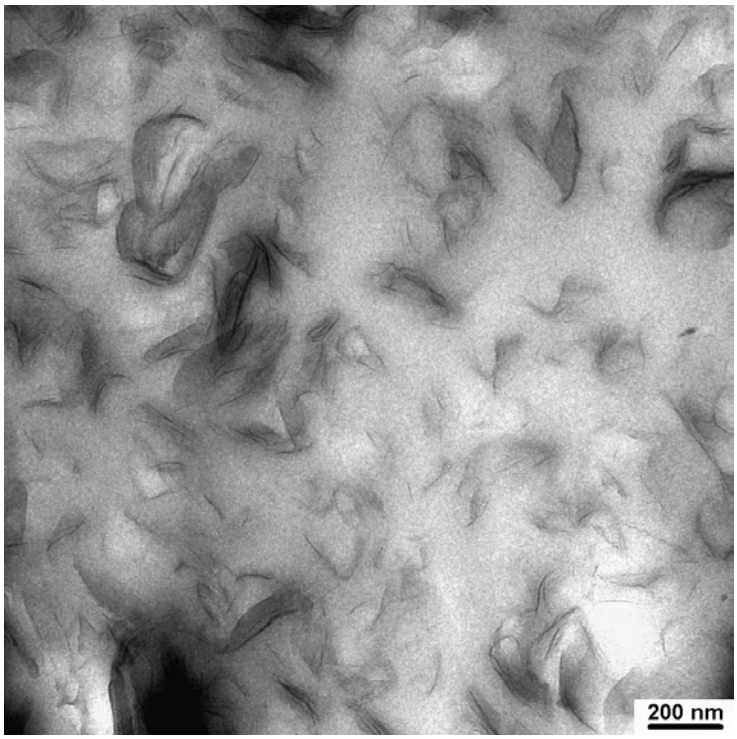

Figure 5.23: TEM image on an EPDM-MA/MMT- ODTMA (10 phr) vulcanizate

It is believed that the primary amine of MMT-ODA created a complex with the vulcanization curatives during the curing (see Figure 5.24). This may yield deintercalation of the clay. Based on the XRD spectra, the EPDM/MMT-ODA (viz. primary amine as intercalant) compounds resulted in both intercalated and deintercalated structures (Figure 5.14) opposed to the EPDM/MMT-ODTMA (viz. quaternary ammonium as intercalant), which produced highly intercalated populations (Figure 5.22). On the contrary, in EPDM-MA/MMT-ODTMA intercalated and deintercalated (cf. XRD spectra-Figure 5.22), as well as, exfoliated structures (cf. TEM images-Figure 5.23) were generated. Moreover, for the EPDM-MA/MMT-ODA only exfoliated and deintercalated structures (cf. XRD spectra-Figure 5.14 and TEM images-Figure 5.8a) were obtained. Thus, the special role of the MA group appears.

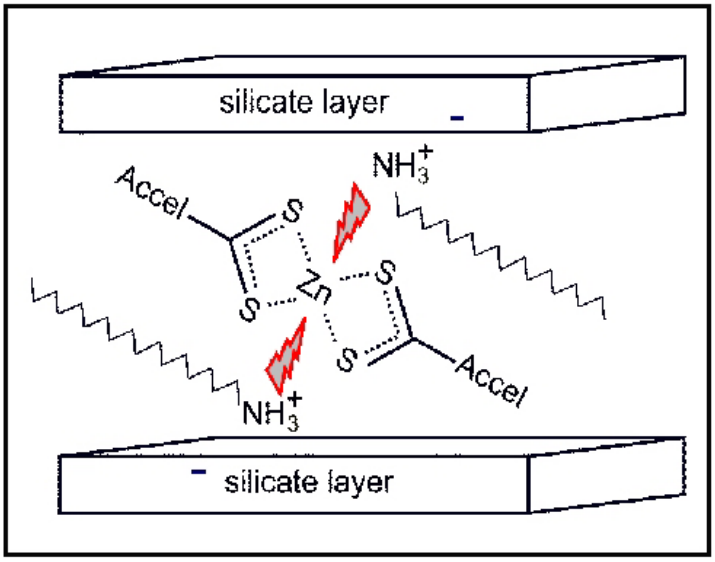

Figure 5.24: Scheme of the interaction between the sulfur-rich Zn complex and the primary amine intercalant within the silicate gallery

The increased polarity of the EPDM alone does not support the exfoliation, as it was shown for EPDM grafted with glycidyl methacrylate, where mostly clay intercalation was achieved (cf. chapter 5.3.2). It can be assumed that the MA ring opened and affected by this way the complex formation. It is well known that the maleic anhydride reacts with the primary and secondary amine groups of polymers [134]. In this reaction the MMT-ODA may also be involved [135].

5.3.5 Effect of Clay Loading

The above-mentioned analysis on EPDM/organoclay nanocomposites was conducted at 10phr organoclay loading. In this chapter the effect of the clay loading will be investigated, mainly on the mechanical performance. The accelerator used in the vulcanization recipe was ZDEC. Investigating the tensile properties of the rubber nanocomposites containing the MA group (yields better clay intercalation/exfoliation) and organoclay bearing the ODA and the ODTMA intercalant, of primary and quaternary nature, respectively, the choice of 10 phr clay appears to be, indeed, optimum. Note that the tensile strength of the nanocomposites reaches a maximum at about 10 phr organoclay content (Fig. 5.25a). It is interesting to observe the different trend of the curves for these two types of nanocomposites. The EPDM-MA/MMT-ODA presents a plateau as a function of increasing organoclay content,

whereas for the EPDM-MA/MMT-ODTMA deterioration in the ultimate strength occurs at high organoclay loading. Pronounced are also the differences in the elongation at break values versus clay loading (Fig. 5.25b). The EPDM-MA/MMT-ODA nanocomposite above 10 phr organoclay content has surprisingly high strain values. On the contrary, for the EPDM-MA/MMT-ODTMA a decrease in the elongation at break can be found, which is likely related with agglomeration phenomena. This agglomeration results in premature failure, owing to which both ultimate stress and elongation at break are reduced. Similar stress-strain behavior has been reported for various rubber nanocomposites [52-53, 67, 69, 71, 77]. Usually, at favorable matrix/organoclay interactions and relatively low organoclay content, both tensile strength and elongation at break increase [67, 53, 71]. Further increase of the organoclay content produces a plateau (saturation) or a reduction in the ultimate stress and strain values [67, 69, 71]. This rather typical behavior was found for the EPDM-MA/MMT-ODTMA nanocomposite (Fig. 5.25).

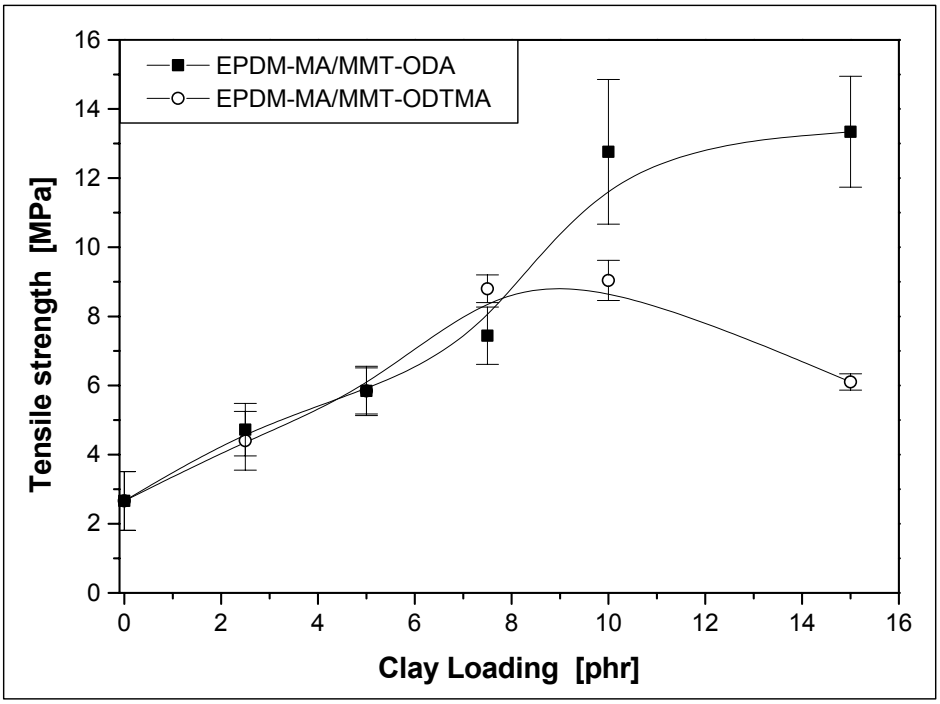

a)

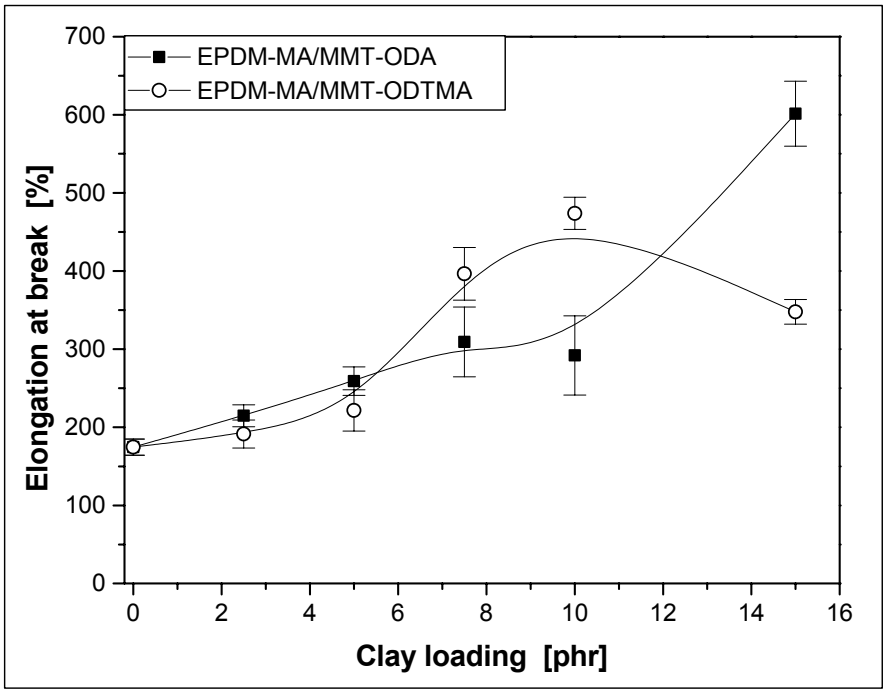

b)

Figure 5.25: a) Tensile strength and b) elongation at break vs. clay loading for the EPDM-MA/MMT- ODA and EPDM-MA/MMT-ODTMA nanocomposites

The tensile strength improvement, which was accompanied by an increase at the elongation at break for these compounds, seems to be an interesting side effect. This phenomenon, which has been appeared also in other rubber compounds, was attributed to the synergistic action of platelet orientation and chain slippage [61]. In order to elucidate this observation, the mechanisms developed for polymer/filler composites [16, 136] should be taken into account.

In general, the reinforcing efficiency of CB filled rubbers increases as the CB particles agglomerate (chain-like filler structure at high filler amounts). At the same time, the degree of bound rubber (as measured in the respective uncured specimens) increases [137]. As shown in the TEM images (e.g. Figures 5.23), the dispersion of the silicate platelets (for the examined 10phr clay loading) seems to create a ‘secondary structure’. This structure is analogous to the so-called ‘secondary structure’ of the CB appearing usually in highly filled rubbers (cf. chapter 2.2.1). To attain such morphology at a low organoclay content a good dispersion of the clay is required in the rubber matrix.

In Figure 5.26 the poor and good dispersion of the same amount of layered silicate is depicted under high deformation of the rubber. Although the filler volume in both cases supposed to be the same (cf. same number of plates in Figures 5.26a and b), the effective volume of the filler differs strongly as a function of the dispersion grade. The reason for this difference can be related with parameters like the bound rubber, rubber shell creation in the vicinity of each silicate platelet (cf. dark grey areas in Figure 5.26) and the occlusion of rubber within the clay galleries. Thus, a modulus increase is expected at low organoclay content when the clay layers are well dispersed.

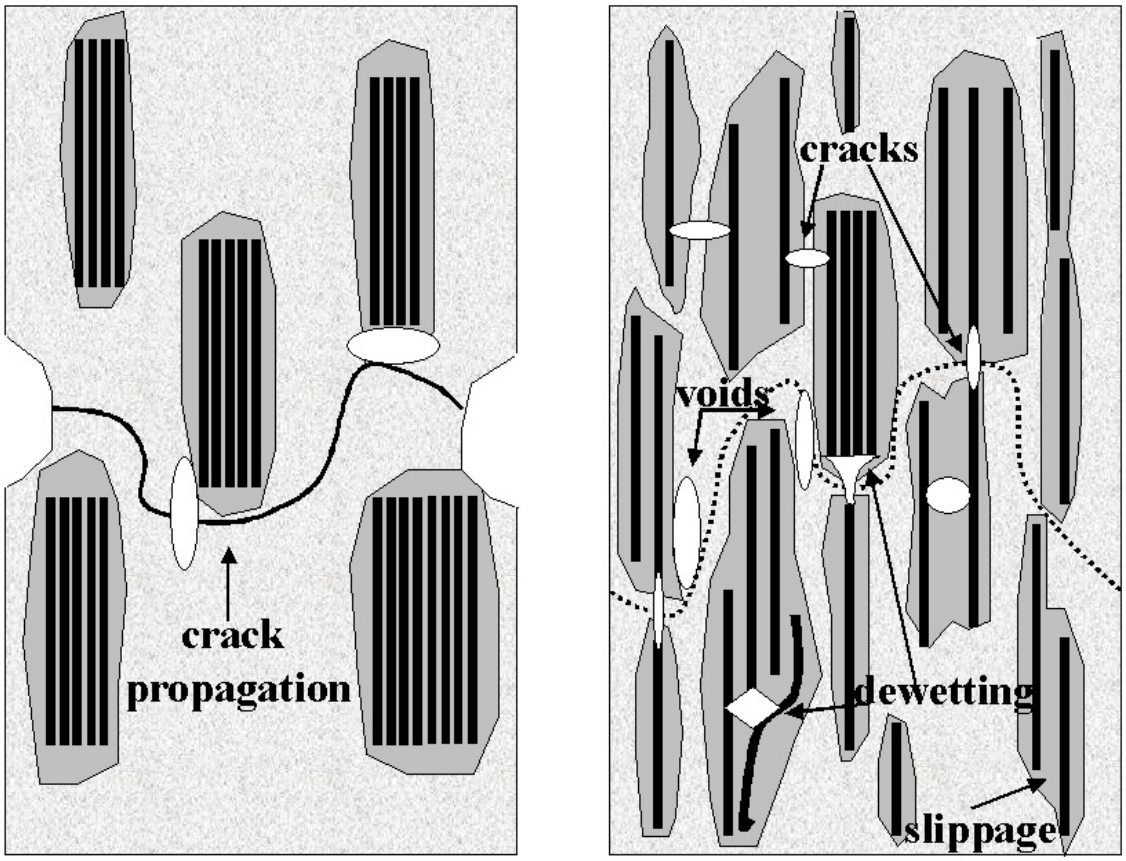

a) b)

Figure 5.26: Scheme of failure development in rubber/organoclay mixes with poor (a) and good (b) dispersion of the clay layers due to high strain at uniaxial loading: a) fast crack growth after surface cracking b) slow crack growth via void coalescence

The failure of the rubber specimens upon tensile loading starts with crack initiation. If the elastomeric network is capable of dissipating the input energy (e.g. by converting into heat), then it can suffer higher stresses up to break. In rubber/layered silicate

nanocomposites, first the orientation of the clay platelets takes place during uniaxial drawing [51]. At sufficient high strain, cracks can be generated by the fillers (via voiding, dewetting phenomena, chain slippage etc.). As the dispersion of the platelets allows the creation of numerous of voids (subcritical cracks) in their vicinity (Fig. 5.26b), the amount of dissipated energy is high enough to withstand higher values of strain than before. Note that shortening of the aggregate-aggregate distance (free ligament) can lead to greater resistance against crack propagation. Furthermore, the increased length of the crack path as the crack spreads around the platelets ("zig-zag" route) can also be considered as a mechanism of energy dissipation.

By this model the increase in both tensile strength and elongation at break can be explained for rubber/layered silicate nanocomposites. Furthermore, the deterioration (that usually noticed) or levelling off in the mechanical performance with increasing organoclay loading [53, 67] can be explained by the onset of big agglomerates, which favor the initiation of catastrophic failure.

5.4 HNBR/Organoclay Nanocomposites

Having already analysed several parameters affecting the intercalation/exfoliation phenomena on EPDM/organoclay nanocomposites, investigation was conducted on HNBR bearing a rather polar chain backbone (43% acrylonitrile content). In the following experiments, further aspects are clarified and categorized regarding the vulcanization system involved (sulfur or peroxide).

5.4.1 Clay Dispersion in Sulfur Cured Systems

As discussed previously, the maleic anhydride group (used for EPDM) has been identified to be involved in complexes with primary and secondary amines [134]. Although that may act beneficially for the organoclay dispersion in rubber nanocomposites, the possible interactions with a primary amine intercalant (ODA) cannot be disregarded (cf. chapter 5.3.4). To clarify the mechanisms involved in sulfur-cured rubber/organoclay nanocomposites, HNBR was chosen and the properties of the respective compounds were tested. In this system no chemical bonding between the rubber and the organoclay intercalant can be assumed, and thus a clearer view on the effect of the sulfur curing on the nanocomposite formation can be received.

5.4.1.1 Effect of Type of Organoclay Intercalant

To investigate the effect of the clay modification on the organoclay dispersion in sulfur cured HNBR, three types of clay intercalants, holding different degree of functionality, were used. The microstructure was initially tested by means of XRD scattering. Figure 5.27 presents the related XRD spectra of the HNBR mixed with different types of organo-MMTs. Apart from the MMT-ODA, which has a primary amine surfactant, MMT-ODTMA and MMT-MTH having less reactive quaternary ammonium surfactant were selected. The latter (MTH) intercalant has two hydroxyl groups (OH). Note that the hydroxyl groups are capable to create hydrogen bonds with the acrylonitrile groups (-CN…H-O-) of the HNBR. The length of the alkyl tail of the intercalants used proved to be appropriate to produce polymer/nanocomposites [35, 71, 96].

The XRD spectra taken from the compounds after mixing with all the additives show that the MMT-ODA and MMT-ODTMA have been intercalated (Fig. 5.27a and b). It is interesting to observe that the MMT-ODA presents higher basal spacing than the MMT-ODTMA albeit the initial basal spacing of the latter was higher. This may be related to the higher adsorption of the curatives within the galleries in case of the primary amine intercalant. For the MMT-MTH compound, the mixing produced exfoliated structure (or *d*-spacing not detectable by the XRD equipment) based on the fact that no XRD peak of the clay was resolved (Fig. 5.27c). It is obvious that the chemical treatment of the clay and the rubber are highly compatible and thus exfoliation of the silicate layers was favored [46].

As far as melt-compounding concerns intercalated (MMT-ODA, MMT-ODTMA) and exfoliated structures (MMT-MTH) were achieved. The vulcanization changed the clay dispersion tremendously. As can be seen in Figure 5.27 for the HNBR with MMT-ODA, the vulcanization resulted in two clay populations. One of them was intercalated showing an interlayer spacing of 3.10 nm (less than the 3.85 nm that was before curing) while the other was de-intercalated exhibiting an interlayer spacing of 1.70 nm (less than the initial value, viz. 2.10 nm of this organoclay). Note that this claim is based on the fact that the (002) and further basal reflections do not fit either in respect to their position or their relative intensities. For the MMT-ODTMA

compound a highly intercalated population was produced with a basal spacing of 3.87 nm (higher than the 3.53 nm that was before curing).

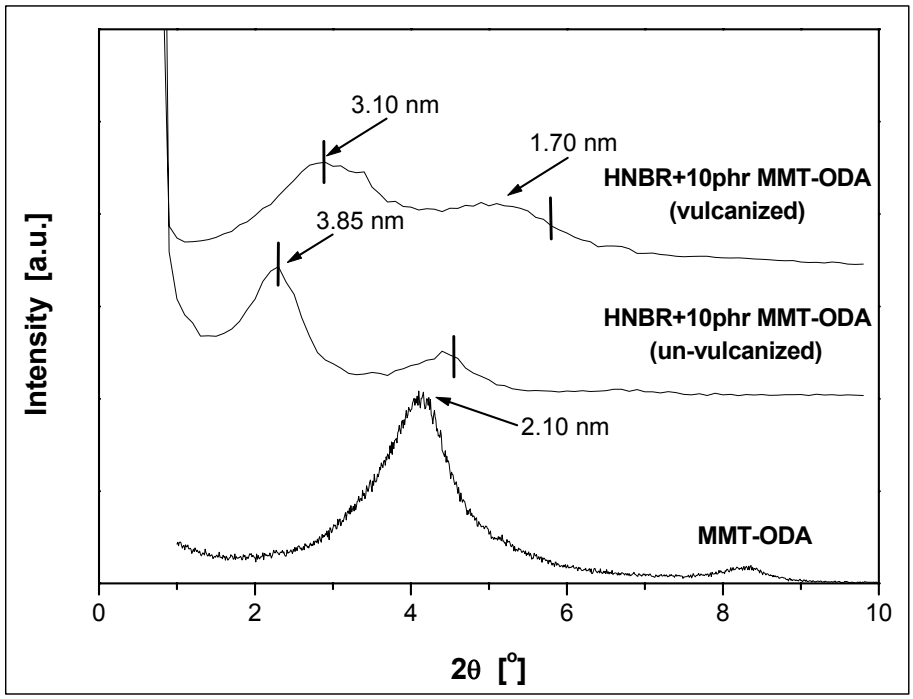

a)

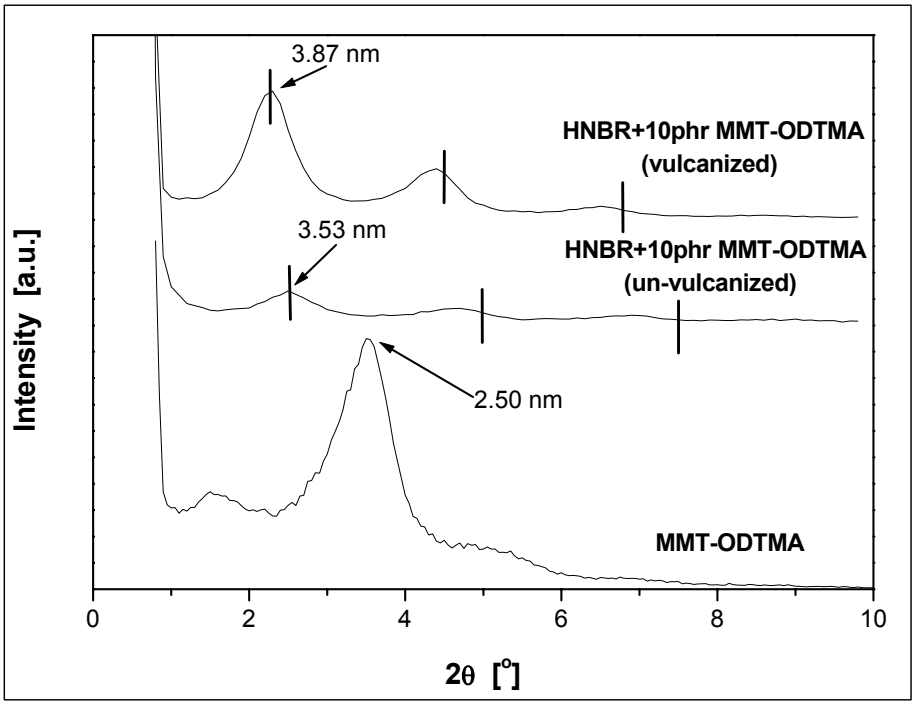

b)

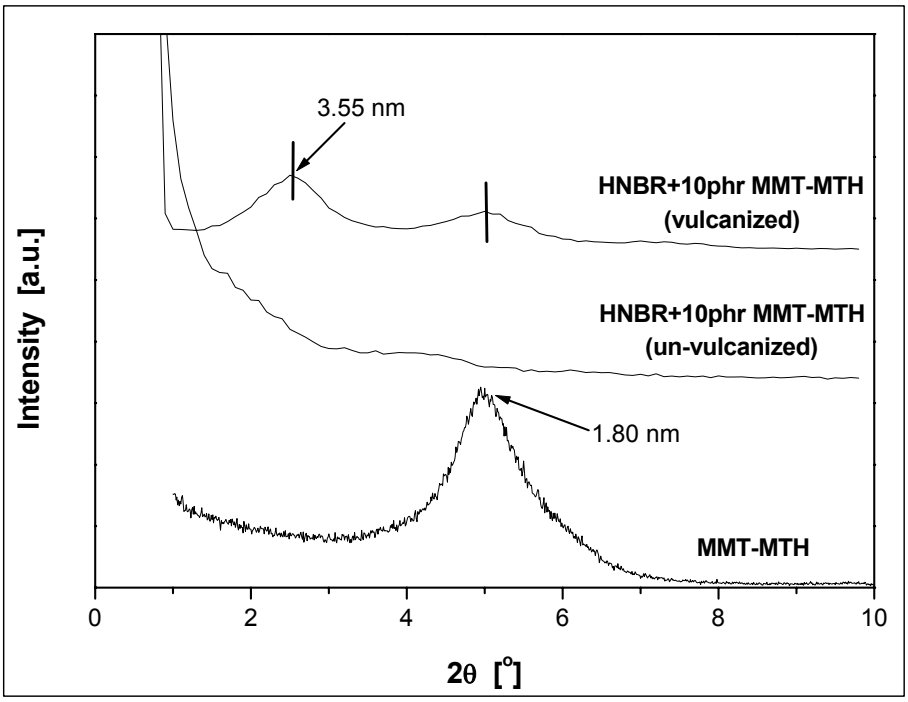

c)

Figure 5.27: XRD spectra of HNBR reinforced with different types of organically modified montmorillonite before and after vulcanization: a) HNBR mixed with MMT-ODA, b) HNBR mixed with MMT-ODTMA and c) HNBR mixed with MMT-MTH. Notes: The spectra of the related organoclays are also contained. The position of the (001), (002) and (003) reflexes is indicated by lines

The reason for the difference between MMT-ODA and MMT-ODTMA can be attributed to the different reactivity of the primary and the quaternary amines upon curing (as discussed in section 5.3.4). They are involved in a generation of vulcanization intermediates in which the clay intercalant and the curatives participate (cf. Fig. 5.24). In case of MMT-ODTMA we are faced to a regular intercalated organoclay structure. This is corroborated by the appearance of the XRD peaks representing correctly the higher order basal reflections (position and intensity ratio). Interesting to observe that the quaternary ammonium of MMT-MTH did not retain the exfoliated structure upon curing (Fig. 5.27c). Instead of that an intercalated structure with an interlayer spacing of 3.55 nm appeared (less than the 3.87 nm of the MMT-ODTMA and more than the 3.10 nm of the MMT-ODA cured compounds). Note that

in this case also a well-ordered intercalated clay structure must be present based on the higher order XRD peaks.

The quaternary ammonium ions enabled to avoid the de-intercalation phenomena upon curing for the MTH intercalant, as they remained tethered on the silicate surface. Recall that for the MMT-ODTMA the curing resulted in a slight layer expansion (possibly due to crosslinking of chains within the galleries irrespective to the presence of ODTMA). In case of the MMT-MTH the reordered clay structure can likely be related again to the H-bonding (between the CN group of the rubber and the OH of the MTH) which is still at work during intergallery crosslinking.

Direct evidence for the organoclay dispersion in the HNBR matrix can be derived from TEM images. As can be observed in Figure 5.28 both MMT-ODA and MMT-ODTMA present well-dispersed structures showing intercalated (mostly) and exfoliated (scarcely) populations. Figure 5.28d suggests that the mechanism of peeling apart of the platelet stacks upon shear might be at work. This has been proposed for high molecular mass polymer/layered silicate systems during compounding [88].

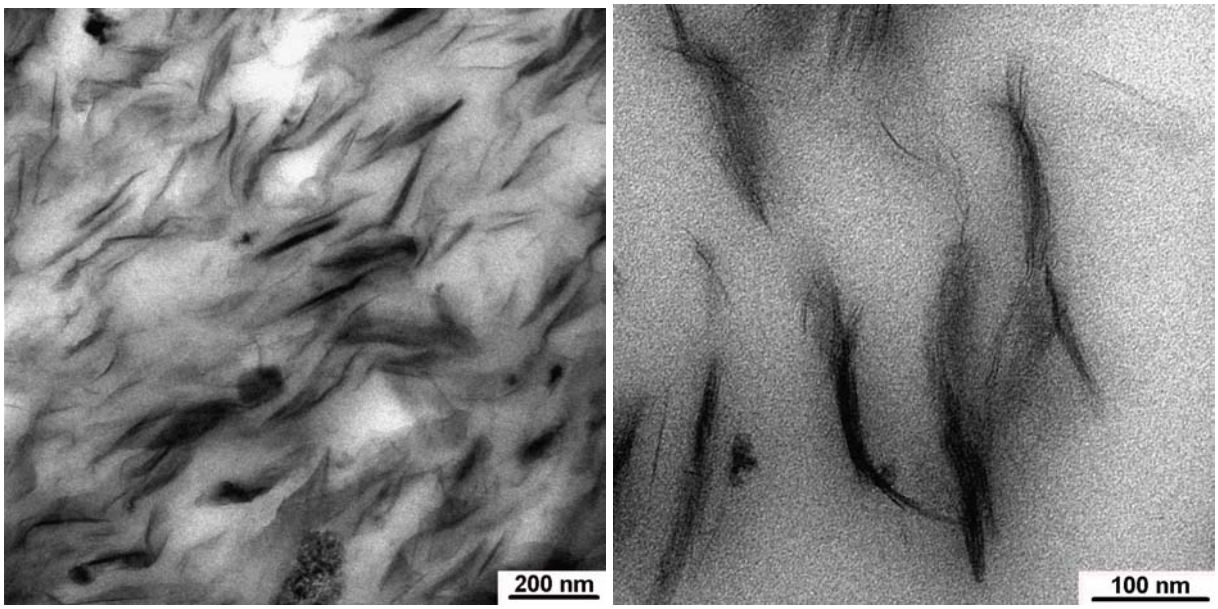

a) b)

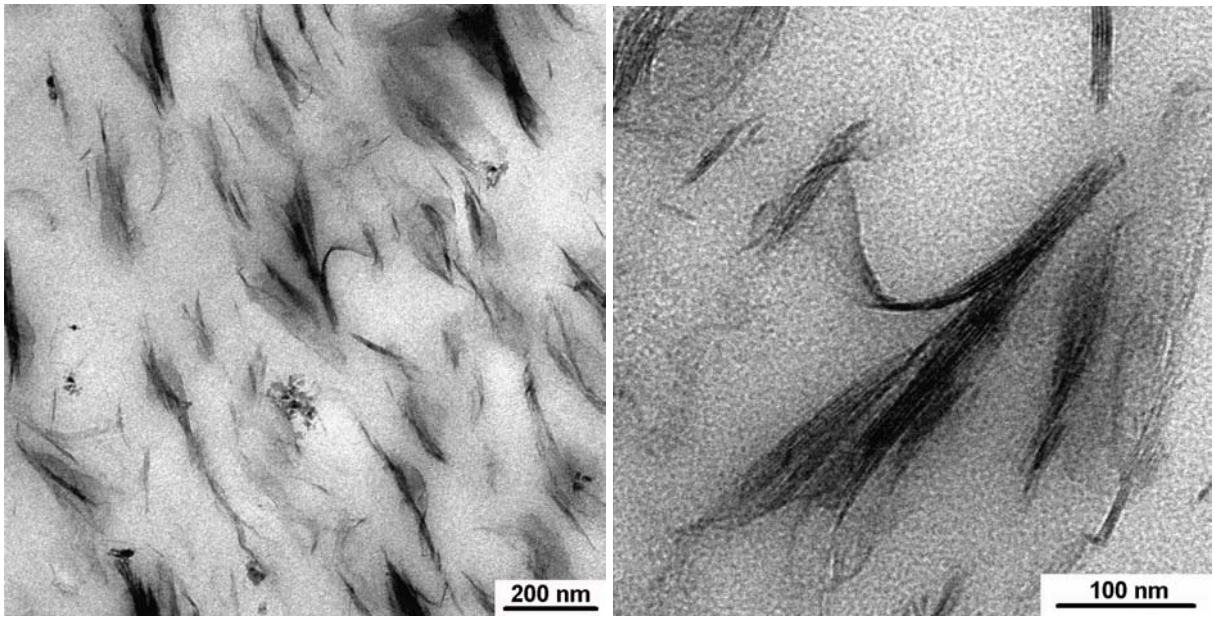

c) d)

Figure 5.28: TEM images of HNBR mixed with MMT-ODA (a and b), as well as, MMT-ODTMA (c and d) after vulcanization and at different magnifications

The variation in the degree of intercalation of the organoclays in the vulcanized HNBR (cf. XRD data) should manifest in the mechanical performance of the rubber nanocomposites. Figure 5.29 presents the DMTA spectra of the respective compounds. The storage modulus (E') of the nanocomposites lies markedly higher compared to the neat HNBR or HNBR filled with unmodified MMT (bentonite) (Fig. 5.29a). Having in mind that the working temperature of rubbers is usually above their glass transition (T_g), the plateau values of the E' in this region is of great importance. As shown in Figure 5.29a, the stiffness of the HNBR/organo-MMTs compounds above the T_g is significantly higher compared to the conventional filler (cf. bentonite). The best performance is reached with MMT-MTH. Recall that this is traced to the OH groups of this intercalant that may create a stronger interphase between the rubber and the silicate surface via H-bonding.

A further hint for the degree of bonding between the matrix and the nano-filler can be derived from the tanδ vs temperature curves. For NBR filled with carbon black (CB) it was shown that the lowering of the diameter of the CB particle is well reflected in the tanδ peak, which strongly decreased [138]. As shown in Figure 5.29b for the unmodified MMT (bentonite) the tanδ peak is identical with that of the neat rubber (T_g

appears at about –4.5°C because of the high acrylonitrile content of the HNBR used) [139]. This fact is related with the poor interaction between HNBR and bentonite. For the HNBR/organo-MMT mixes the tanδ peaks were strongly reduced in intensity. This suggests the onset of a filler network, which is able to withstand dynamic deformations [16]. HNBR/MMT-MTH compound presents the lowest T_g peak intensity. Thus, it can be concluded that the interphase in this case is the best among the compounds examined. A strong interphase guarantees a good stress transfer from the matrix to the filler. When the mechanical performance of the nanocomposites with only 10phr (or less) organoclay is similar to that of rubber with 30-40 phr CB [78] (note that the diameter of the CB particle can be in the order of nano-dimensions), then the clay platelets are treated as very efficient nanoreinforcements.

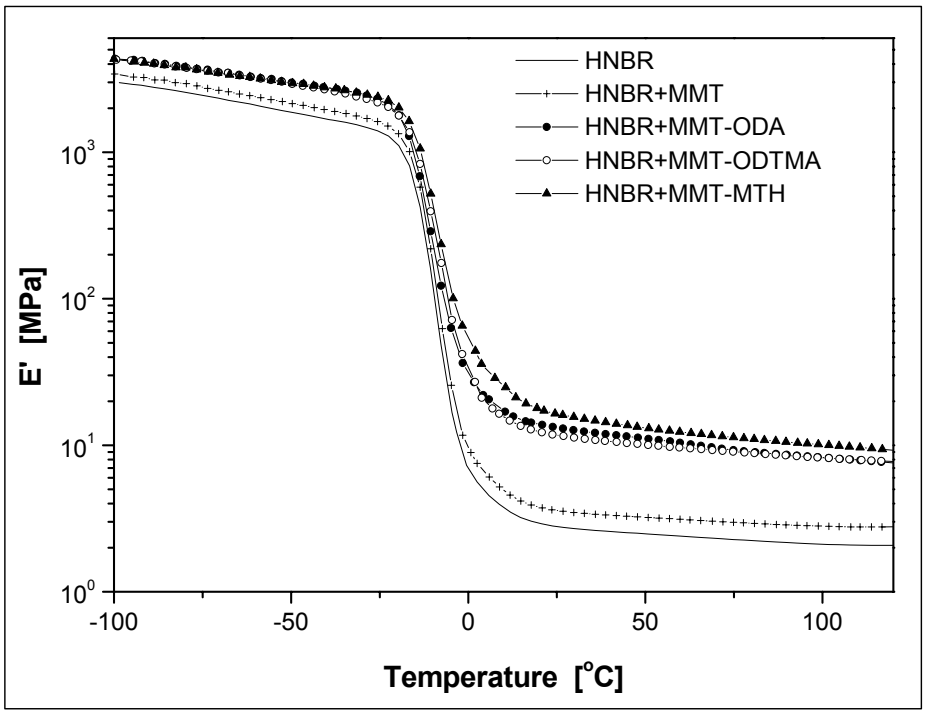

a)

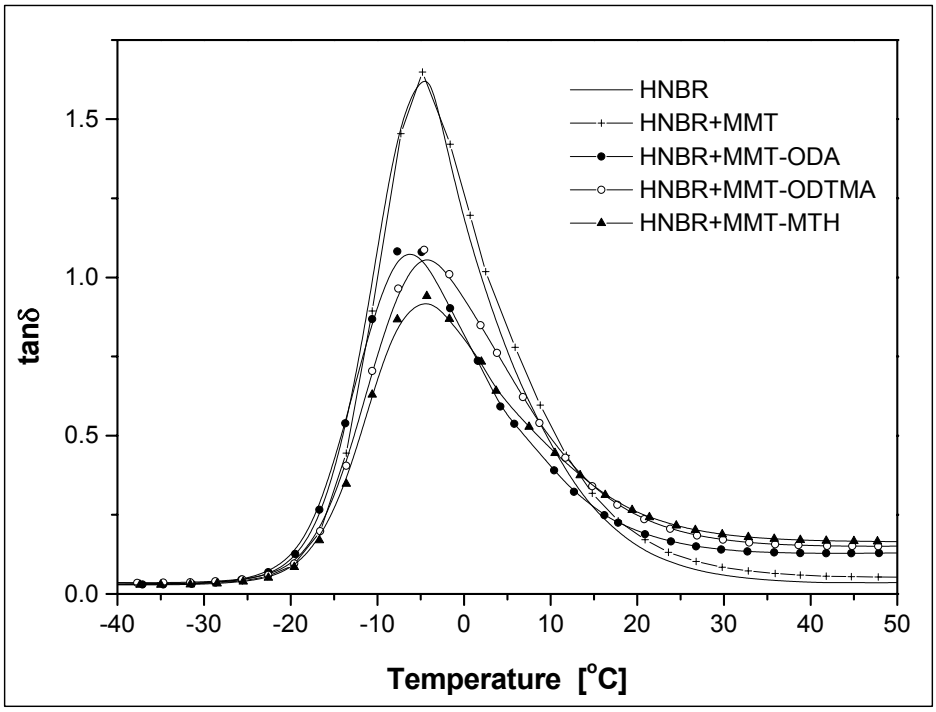

b)

Figure 5.29: a) Storage modulus (E') and b) mechanical loss factor (tanδ) as a function of temperature for the HNBR and HNBR containing various fillers in 10 phr amount (sulfur cured)

As the thermal stability is crucial for rubber applications, the thermal degradation of the HNBR nanocomposites was investigated by thermogravimetric analysis (TGA). As shown in Figure 5.30, the 85% weight loss value shifted from 418 °C measured for the HNBR or HNBR reinforced with unmodified filler, to 430 °C for MMT-ODTMA and MMT-MTH filler. The MMT-ODA organoclay yielded the best thermal behavior because the 85% weight loss value was found at 442 °C. The observed beneficial action of the organoclay on the heat stability of the rubber matrix is in accordance with results obtained in literature for other polymers, like ethylene-co-vinylacetate (EVA) [140]. The better behavior of the MMT-ODA filler compared to the MMT-ODTMA or MMT-MTH can be attributed to the ODA intercalant. Recall that in this case deintercalated clay stacks dispersed in the HNBR matrix were also received. These clay stacks do not bear any thermally instable tethered organic intercalant, fact that prolongs the onset of the thermal degradation of the matrix.

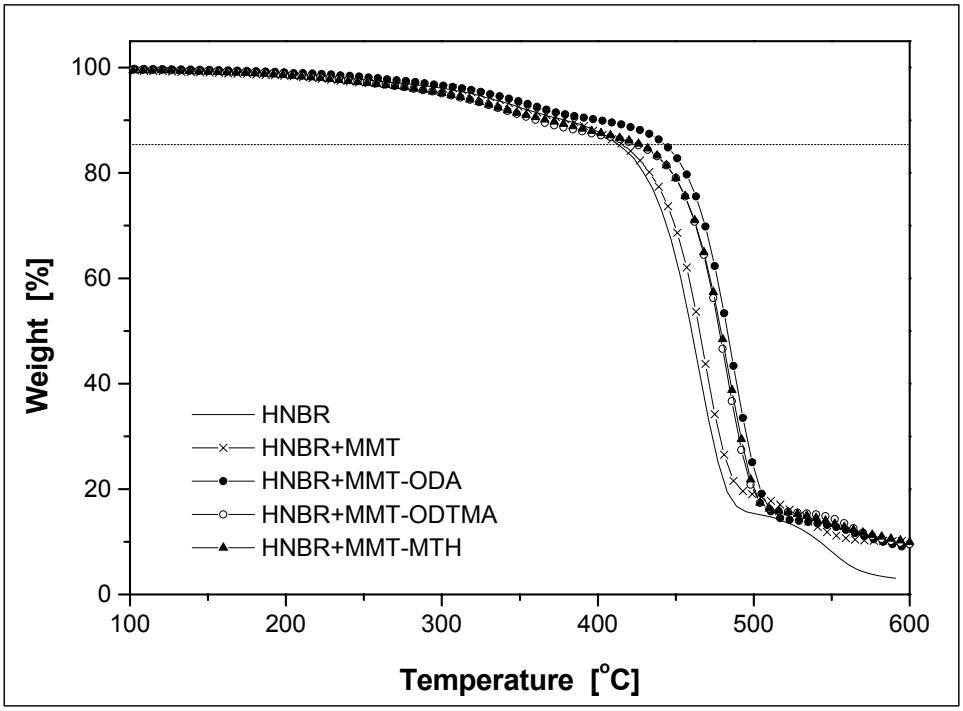

Figure 5.30: Thermal stability of the HNBR nanocomposites

Investigating the specimens in static tensile experiments, the stiffness increase noticed in DMTA test (cf. Figure 5.29) should reappear. In Figure 5.31 characteristic stress-strain curves are presented for the HNBR/organo-MMT mixtures. It is obvious that the bentonite has the lowest reinforcing effect in HNBR (cf. curves 1 and 2 in Figure 5.31). For all organo-MMTs both ultimate tensile strength and elongation at break values were enhanced. At the same time a prominent modulus improvement was found for the HNBR-organo-MMT mixtures in comparison to the neat HNBR or HNBR filled with MMT (cf. Fig. 5.31b). The best performance was obtained by MMT-ODA and MMT-MTH, which doubled the tensile strength of the neat HNBR. The tensile strength improvement, which was accompanied by an increase at the elongation at break for these compounds, is attributed to the phenomenological model/explanation discussed in chapter 5.3.5.

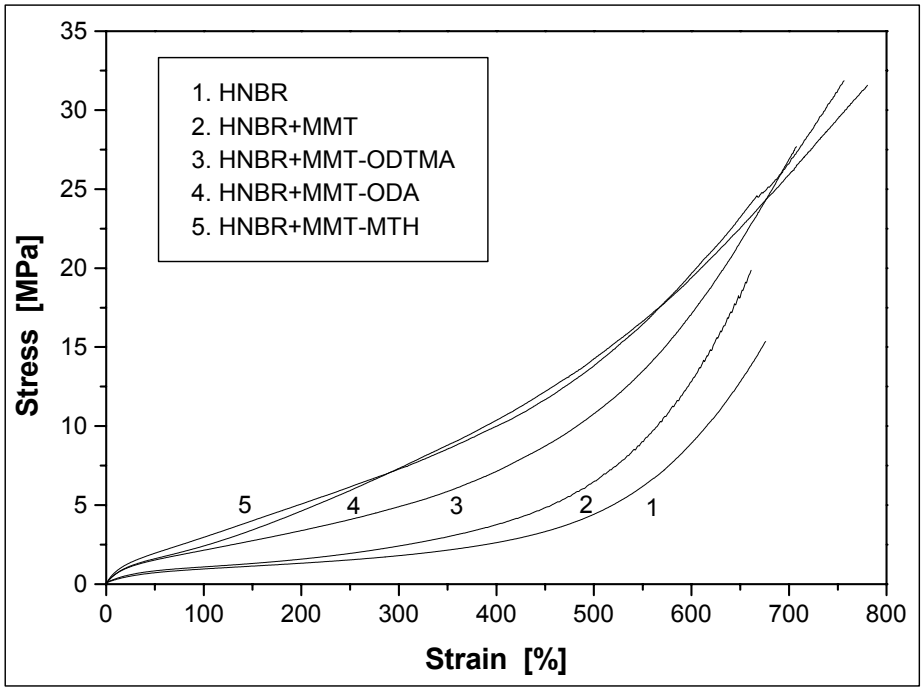

a)

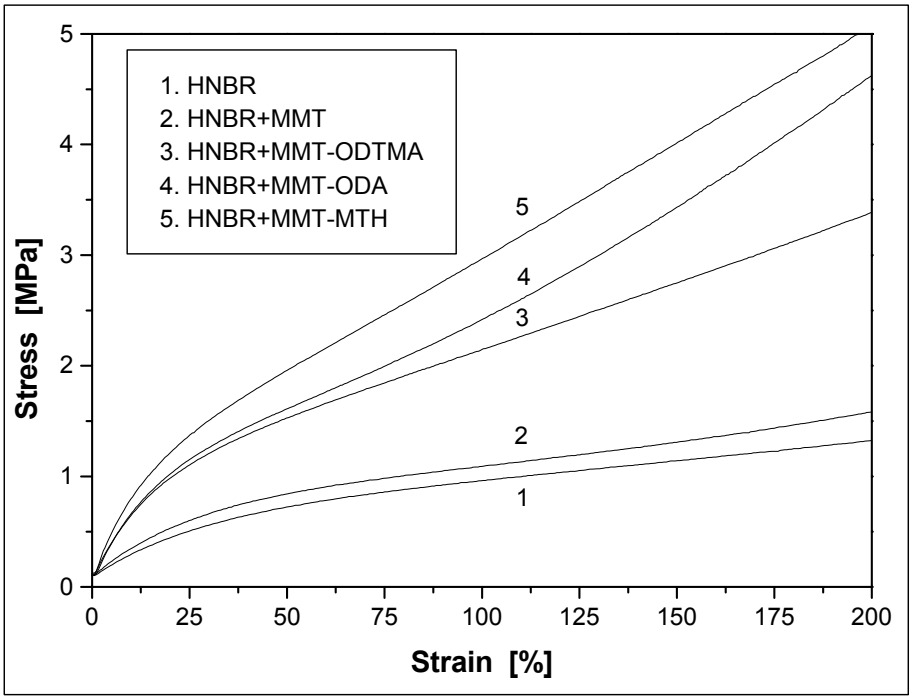

b)

Figure 5.31: Stress-strain curves of the vulcanized HNBR containing various organoclays in 10 phr amount: a) full curves and b) initial sections

The mechanical performance (including the tear strength and hardness) of the above-mentioned HNBR nanocomposites is summarized in Table 5.2. Note that MMT-MTH, which bears a polar quaternary intercalant, presents the highest stiffness values. The MMT-ODA shows extraordinary improvement on the tear strength. This fact should be related with the reactivity of the ODA intercalant, since the clay origin (MMT) is the same for all the three organoclays tested.

Table 5.2: Mechanical properties of HNBR/organo-MMTs at 10 phr filler amount

Properties	Mixes				
	HNBR	HNBR/ MMT	HNBR/ MMT-ODA	HNBR/MMT-ODTMA	HNBR/ MMT-MTH
Tensile strength (MPa)	15.2 ±1.8	19.8 ± 2.0	31.5 ± 1.4	27.6 ± 2.0	31.8 ± 1.0
Modulus at (MPa					
100% Elong.	0.9 ± 0.1	0.9 ± 0.1	2.4 ± 0.2	2.1 ± 0.1	2.9 ± 0.1
200% Elong.	1.3 ± 0.2	1.5 ± 0.1	4.6 ± 0.2	3.4 ± 0.2	5.1 ± 0.2
300% Elong.	1.8 ± 0.3	2.4 ± 0.2	7.3 ± 0.3	4.9 ± 0.2	7.3 ± 0.2
Elong. at break (%)	675 ±107	660 ± 26	780 ± 26	707 ± 45	756 ± 40
Tear strength (kN/m)	8.8 ± 1.3	10.3 ± 1.0	42.6 ± 0.6	24.7 ±1.0	38.6 ± 2.0
Hardness (Shore A)	60	64	76	75	78

5.4.1.2 Effect of Aspect Ratio of Clay Platelet

In order to examine the effect of the type of the layered silicate on their dispersion, montmorillonite (MMT) and fluorohectorite (FHT) bearing the same organic modifier (ODA) were selected. These silicates of natural (MMT) and synthetic (FHT) origin have a platelet aspect ratio of >200 and >400, respectively. By this way, the analysis will be connected directly with the platelet aspect ratio, as their cation exchange capacity (CEC) and organophilic modification appear alike. As shown in Figure 5.32,

the XRD-related microstructure of the HNBR/FHT-ODA is indeed similar to that of HNBR/MMT-ODA (cf. Fig. 5.27a). The vulcanizate HNBR/FHT-ODA present peaks that correspond to intercalated (3.04 nm) and deintercalated structures (1.77 nm).

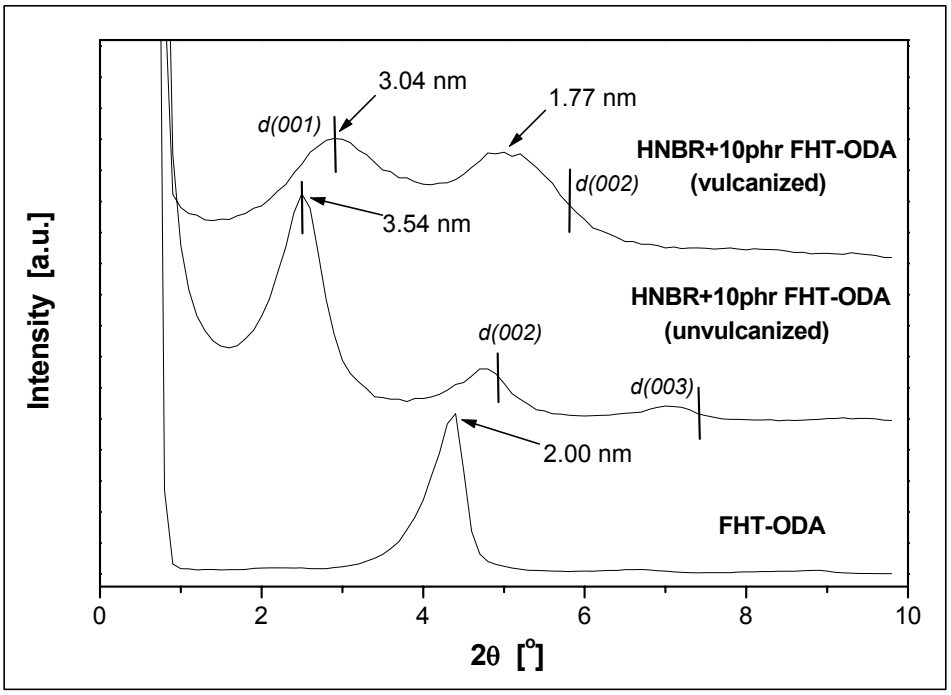

Figure 5.32: HNBR/FHT-ODA nanocomposites (10phr filler amount) recorded from different stages of processing. The position of the (001), (002) and (003) reflexes is indicated by vertical lines

TEM images in Figure 5.33 show a dispersion of exfoliated and intercalated stacks of the organophilic silicates. This dispersion is again similar to that received by MMT-ODA organoclay (Fig 5.28a and b). A closer look at both Figures (i.e. compare Figure 5.28a and b with 5.33) reveals the differences in the aspect ratio. However, as the platelets are stacked their aspect ratio appears far smaller than the initially expected one.

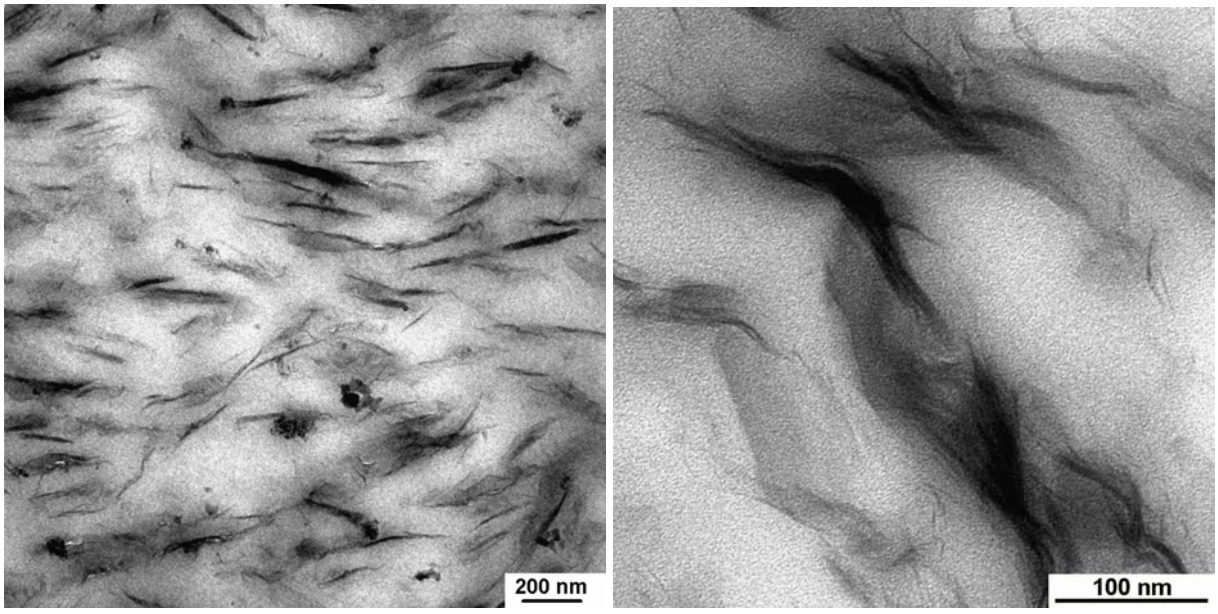

a) b)

Figure 5.33: TEM images of HNBR mixed with FHT after vulcanization and at different magnifications

The mechanical performance as it is indicated by the dynamic mechanical thermal analysis spectra, showed for both vulcanizates similar reinforcing grade (Fig. 5.34).

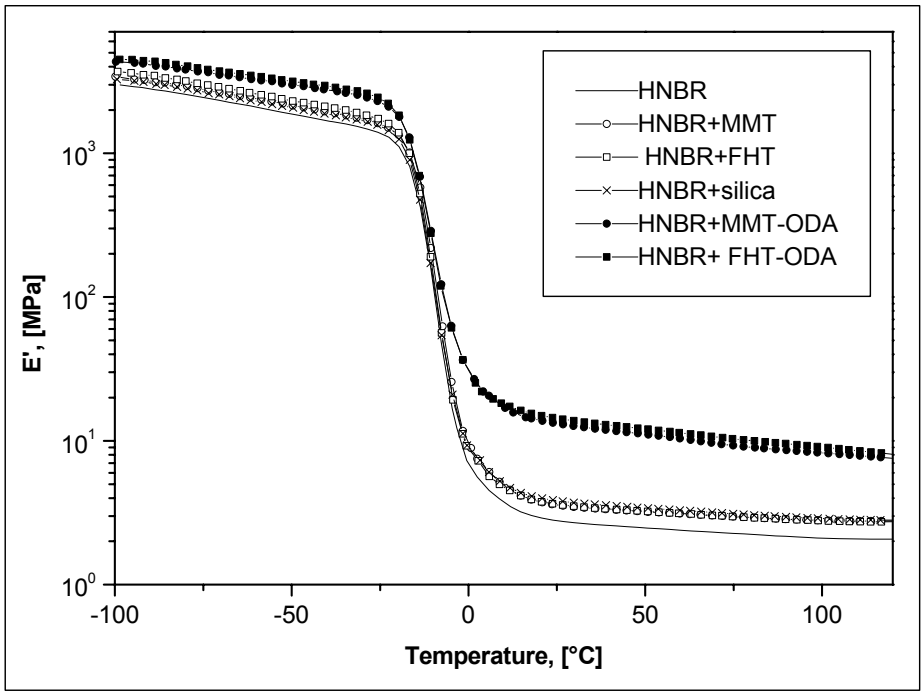

a)

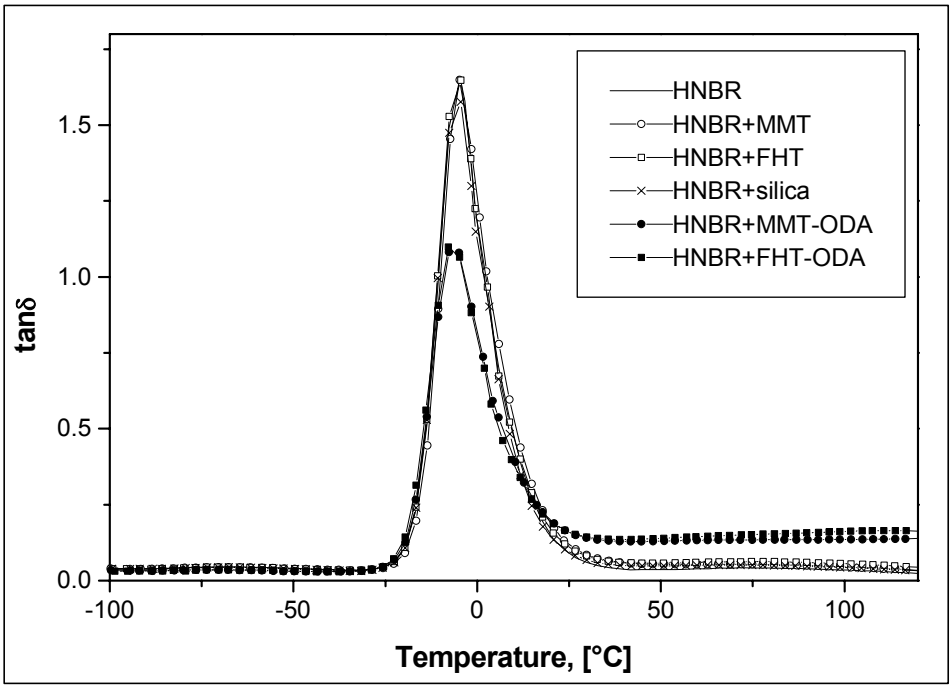

b)

Figure 5.34: DMTA spectra of the HNBR nanocomposites (a) the storage modulus and (b) mechanical loss factor versus temperature

The storage moduli of the HNBR with MMT-ODA and FHT-ODA are quite similar (slightly higher values for FHT-ODA) and far better than those containing MMT, FHT, or the conventional silica filler (Fig. 5.34a). Furthermore, the interphase quality, as suggested by the tanδ-spectra (Fig. 5.34b), appears the same for the organophilic MMT and FHT irrespective their different aspect ratio. Both present far better interfacial bonding with the HNBR matrix than the MMT, FHT, or silica.

The heat degradation shielding of the HNBR vulcanizates emanated by the dispersion of the platelets of high aspect ratio was checked by TGA measurements. In Figure 5.35, the smooth weight loss after 200 ^{o}C for all the compounds, which ends in a plateau at about 400 ^{o}C showing ca. 10% weight reduction, can be attributed to the evaporation of the processing oil (8 phr in the vulcanization recipe). For the organoclay reinforced HNBR, the possible degradation of the organoclay intercalant should be also considered (its weight loss corresponds to ca. 3% when incorporating 10 phr organoclay). The heat resistance yielded by the MMT-ODA or the FHT-ODA appears similar. The 85% weight loss value was shifted from the initial 418 ^{o}C (for the HNBR or HNBR reinforced with unmodified filler) to 445 ^{o}C. Thus, the

heat stability is governed mostly by the dispersion grade (compare the effects of the FHT and the FHT-ODA) and the filler weight percentage (similar behavior for MMT-ODA and FHT-ODA), than by platelet aspect ratio.

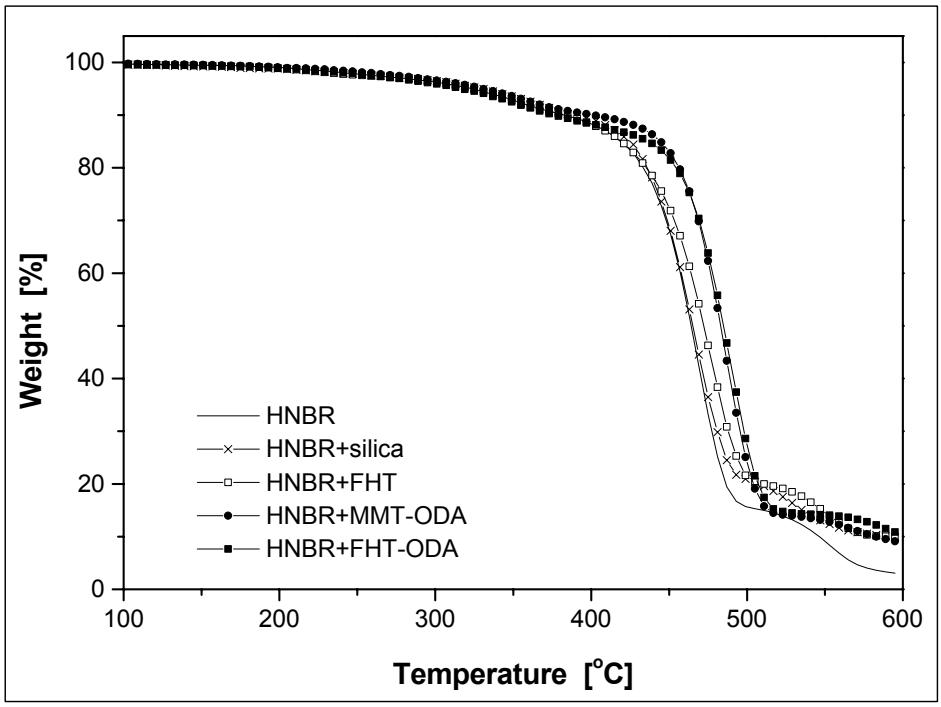

Figure 5.35: TGA spectra for the HNBR reinforced with layered silicate of different aspect ratio

Considering the smooth stiffness increase noticed in the DMTA spectra, for the HNBR/FHT-ODA (Fig. 5.34a), this has to be turned out even clearer in the tensile experiments. As shown in Figure 5.35, the HNBR/FHT-ODA presents, indeed, the highest moduli at all elongation values.

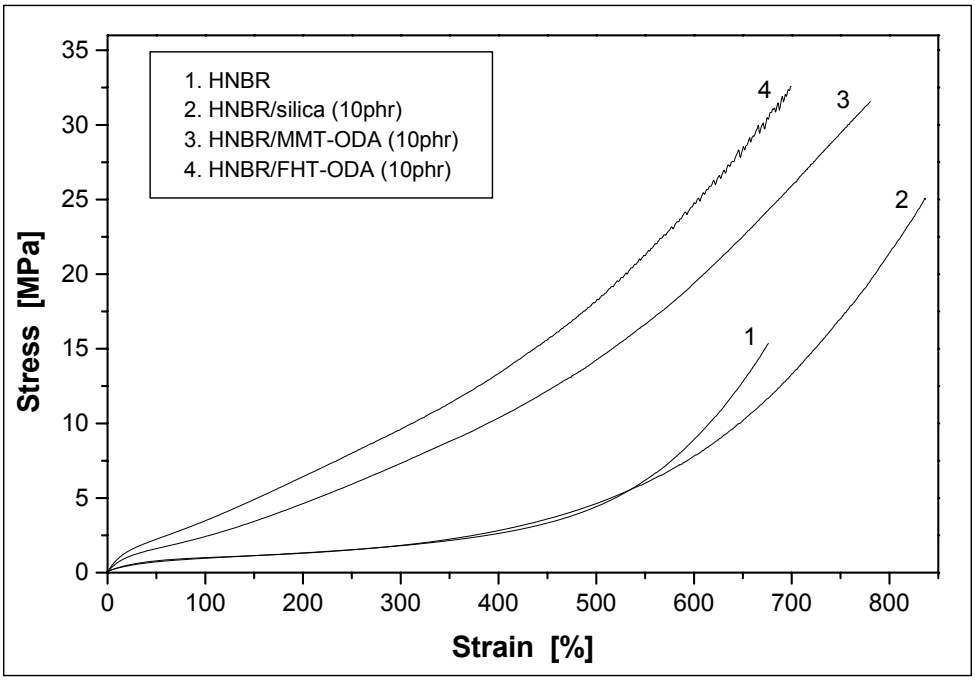

Figure 5.36: Tensile curves of HNBR reinforced with silica and organoclays of different aspect ratio (i.e. MMT-ODA and FHT-ODA)

Summarizing the mechanical performance in Table 5.3, one can notice that the HNBR/FHT-ODA presents improved stiffness characteristics (i.e. modulus values, hardness). On the contrary, the effect of the FHT-ODA on the tear strength is matched with that of the MMT-ODA and both are by far better than the silica or unmodified FHT. The fillers resulting in nanodispersion (i.e. MMT-ODA, FHT-ODA) and showing high aspect ratio (i.e. FHT-ODA) exhibit higher hysteresis data compared to the microcomposites with FHT or silica. This is directly related with the "secondary filler structure" created. As the strain level increases, the "secondary structure" starts to break up (slippage phenomena, silicate surface dewetting, etc.). The relative high hysteresis value for the neat HNBR vulcanizate at the 300% strain level can likely be attributed to the breakage of the sulfid bonds at such high deformations. This value is obviously lower for the HNBR elongated up to 100% strain. Considering the difference between the hysteresis values at 300% and 100% strain (HNBR=14<silica=20<FHT=22<MMT-ODA=23<FHT-ODA=25) one can notice that it is more or less constant. It is speculated that this effect is linked with the HNBR behavior. The normalized hysteresis values (viz. divided with the hysteresis values of the matrix) at 100% strain present the following ranking:

HNBR=1<FHT=1.4<silica=1.5<MMT-ODA=3.1<FHT-ODA=3.2. Comparing them with the normalized values at 300% strain (HNBR=1<silica=1.4<FHT=1.5<MMT-ODA=2.4<FHT-ODA=2.6), one can observe that they have similar trend and somewhat lower values for the organoclay compounds than those calculated at 100% level of strain. Thus, there is a pronounced contribution of the strong interface bonding (high normalized hysteresis values for the organoclays) to the hysteresis.

Table 5.3: Mechanical properties of HNBR/organoclay at 10 phr filler amount (aspect ratio effect)

Properties	Mixes				
	HNBR	HNBR/ silica	HNBR/ FHT	HNBR/ MMT-ODA	HNBR/ FHT-ODA
Tensile strength (MPa)	15.2 ±1.8	25.0 ± 3.4	20.5 ± 2.0	31.5 ± 1.4	32.5 ± 1.7
Modulus at (MPa					
100% Elong.	0.9 ± 0.1	0.9 ± 0.1	1.1 ± 0.1	2.4 ± 0.2	3.5 ± 0.3
200% Elong.	1.3 ± 0.2	1.2 ± 0.2	1.5 ± 0.1	4.6 ± 0.2	6.5 ± 0.5
300% Elong.	1.8 ± 0.3	1.8 ± 0.4	2.1 ± 0.2	7.3 ± 0.3	9.6 ± 0.6
Elong. at break (%)	675 ±107	836 ± 97	770 ± 37	780 ± 26	700 ± 28
Tear strength (kN/m)	8.8 ± 1.3	14.5 ± 1.8	12.3 ± 1.2	42.6 ± 0.6	42.7 ± 1.3
Hardness (Shore A)	60	65	65	76	78
Hysteresis,100 % strain (%)	17	25	24	53	56
Hysteresis,300 % strain (%)	31	45	46	76	81

Based on the mechanical performance the “secondary structure” was best developed when FHT-ODA served as filler. This should appear even more pronounced in the permeability measurements. As shown in Figure 5.37, the oxygen permeation

coefficient for the unfilled HNBR is 87 and 94cm^3.mm/m^2.day.bar for dry and wet conditions, respectively. The permeability increase with increasing humidity is usual considering the polar character of HNBR. As water molecules attach on the acrylonitrile group, the rubber cohesion is weakened, thus, higher oxygen transmission occurs. The unmodified fluorohectorite compound (FHT) reduces slightly the permeability of the film. On the contrary, the modified platy fillers (i.e. MMT-ODA and FHT-ODA) reduced the permeation markedly. The best oxygen barrier property was achieved by FHT-ODA. This can be traced to its highest aspect ratio (compared to MMT-ODA) and to the nano-dispersion (compared to FHT) formed.

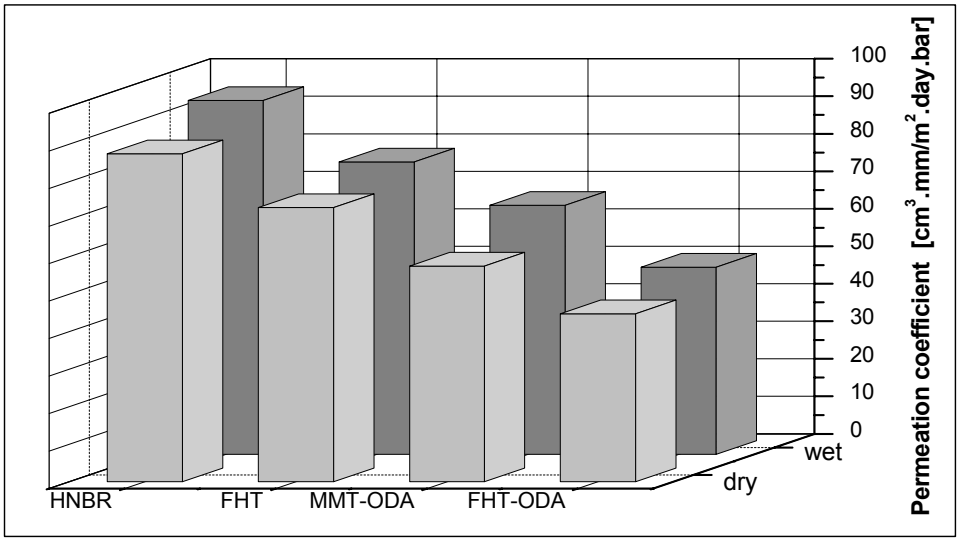

Figure 5.37: Oxygen permeability measurements for the HNBR vulcanizates as a function of the filler aspect ratio

5.4.2 Clay Dispersion in Peroxide Cured Systems and Properties

It has been previously presented (chapter 5.4.3.1) that sulfur vulcanization strongly affects the nanocomposite formation in rubber/clay systems. Primary amine intercalant of the organoclay (ODA) was found to interact with the sulfur curatives resulting in confined/deintercalated clay structures (cf. Fig. 5.27a), apart from intercalated/exfoliated ones (cf. Figure 5.28a). That was traced to a Zn-containing complex (cf. Fig. 5.24) in which the primary amine intercalant and the sulfur were participating. In order to overcome the confinement/deintercalation phenomena

observed for primary amine intercalated clay/rubber, during sulfur vulcanization, peroxide curing of the rubber appears as a possible way. In that case, no Zn/amine complexes should appear as the mechanism for peroxide vulcanization differs from the sulfur one [10]. Note that HNBR is usually cured either by sulfur or peroxide [141]. To investigate the clay dispersion in peroxide cured HNBR compounds, the same types of organoclay as those used in the chapter 5.4.3.1 were involved.

The XRD spectra of the HNBR mixed with the three organo-MMTs are depicted in Figure 5.38. As presented in Figure 5.38a, after compounding the interlayer spacing of the MMT-ODA increased up to 3.60 nm. At the same time, there is a prominent scattering at low angles, which may indicate some irregular packing of the silicate layers and their exfoliation (delamination), as well. After vulcanization, well-ordered intercalated organoclay structure appears. This claim is based on the fact that the d(002) and further basal reflections fit in respect to both their position and intensity. The interlayer spacing slightly increased due to curing. This is in contrast to sulfur vulcanization for the same compound, in which confinement and deintercalation was found (cf. Figure 5.27a). So, during peroxide curing the primary amine intercalant remained tethered on the MMT layers and was not removed (“extracted”). For the HNBR/MMT-ODTMA compound (Figure 5.38b), the basal spacing increased from 2.50 nm to 3.20 nm after mixing. The following vulcanization resulted in an even higher increase of the latter (up to 3.98 nm). The situation is somewhat different for the MMT-MTH, which contains hydroxyl groups (OH) in the galleries. The OH groups form hydrogen bonds with the nitrile ones (CN) of the HNBR. The related polymer-clay compatibility supports the exfoliation (at least in terms of missing peaks characteristic for a layered structure- cf. Figure 5.38c). The appearance, however, of a well-ordered highly intercalated structure after vulcanization (having interlayer spacing of 4.26 nm-cf. Figure 5.38c) supports that the structure before curing constituted of disordered layers with high basal spacing in between.

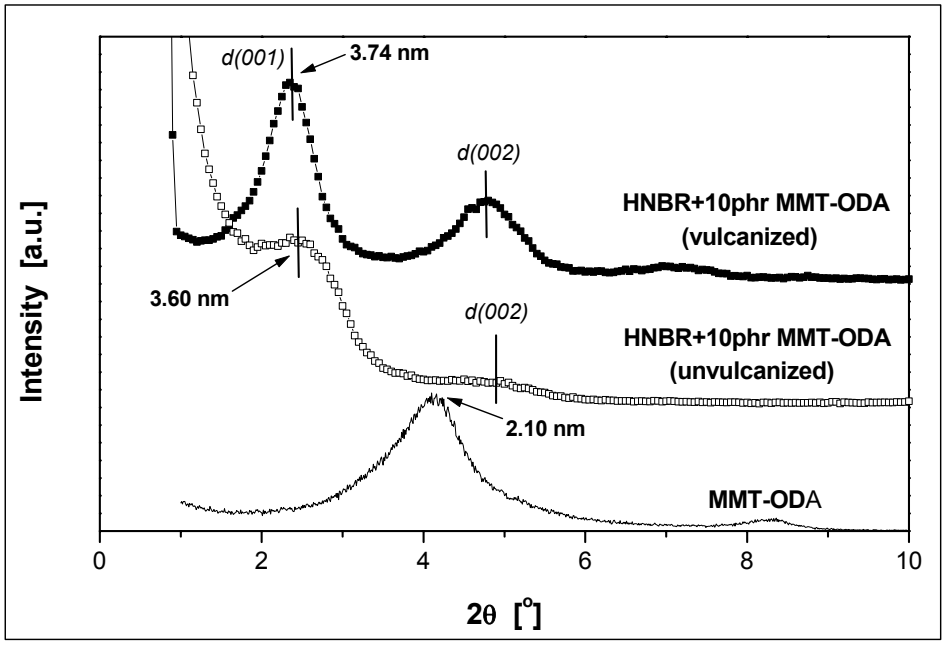
d(001)
3.74 nm
d(002)
HNBR+10phr MMT-ODA
(vulcanized)
3.60 nm
d(002)
HNBR+10phr MMT-ODA
(unvulcanized)
2.10 nm
MMT-ODA
Intensity [a.u.]
0
2
4
6
8
10
2θ [°]

a)

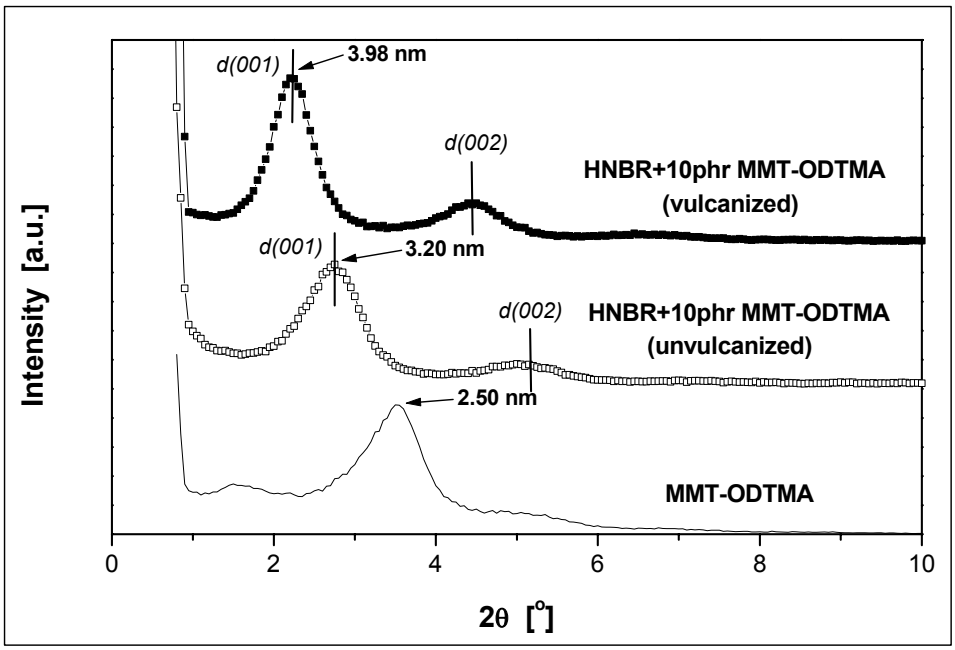
d(001)
3.98 nm
d(002)
HNBR+10phr MMT-ODTMA
(vulcanized)
d(001)
3.20 nm
d(002)
HNBR+10phr MMT-ODTMA
(unvulcanized)
2.50 nm
MMT-ODTMA
Intensity [a.u.]
0
2
4
6
8
10
2θ [°]

b)

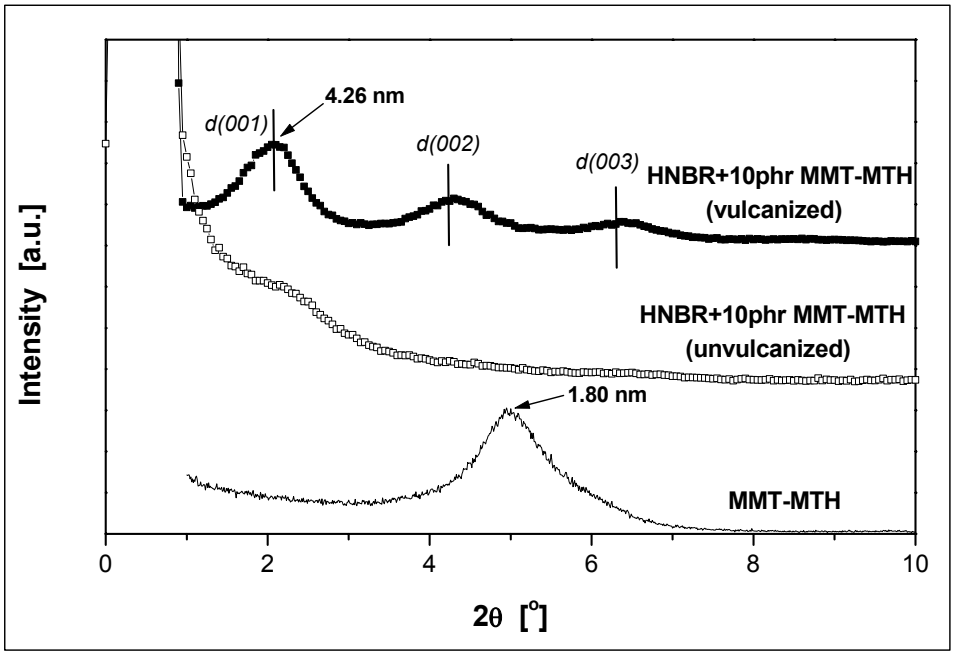

c)

Figure 5.38: XRD spectra of HNBR reinforced with different types of organically modified montmorillonite before and after vulcanization: a) HNBR mixed with MMT-ODA, b) HNBR mixed with MMT-ODTMA and c) HNBR mixed with MMT-MTH. Notes: The spectra of the related organoclays are also contained. The position of the (001), (002) and (003) reflexes is indicated by line marks

The superior action of the organoclays appears also in the dynamic mechanical thermal response of the HNBR compounds (Fig. 5.39). The HNBR/organo-MMT nanocomposites show enhanced storage moduli (Fig. 5.39a), the best improvement yielded the MMT-MTH. The reduction in mechanical loss factor was almost identical for all three organo-MMTs, showing the lowest tanδ peak value for the MMT-MTH (Fig. 5.38b). Recall that for sulfur cured HNBR nanocomposites the best interphase quality was also formed for MMT-MTH, at least when considered the changes in the tanδ vs. temperature traces (cf. Fig. 5.29b).

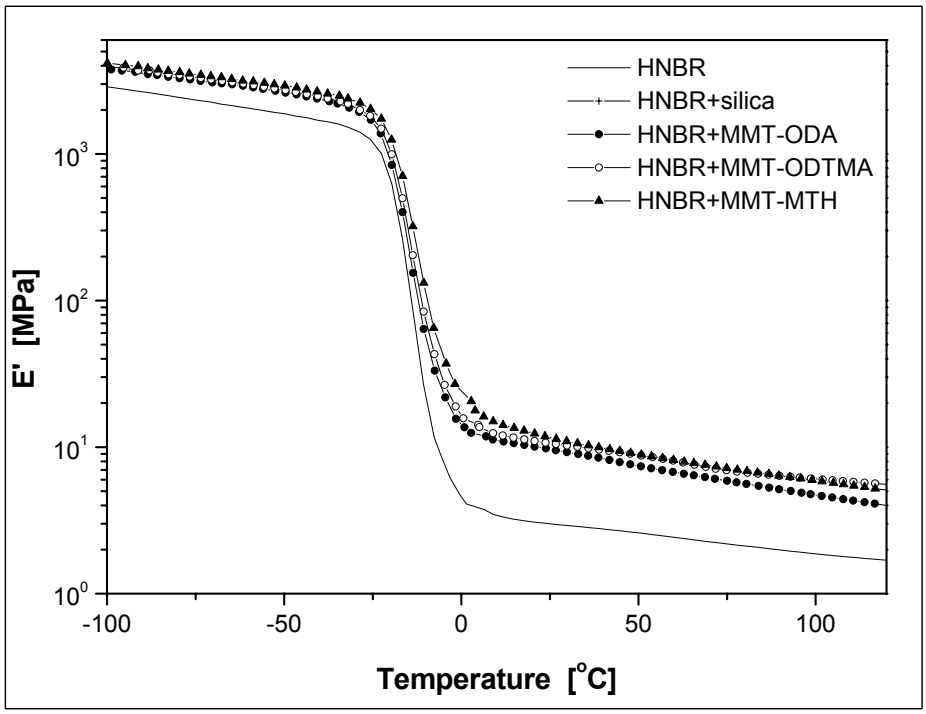

a)

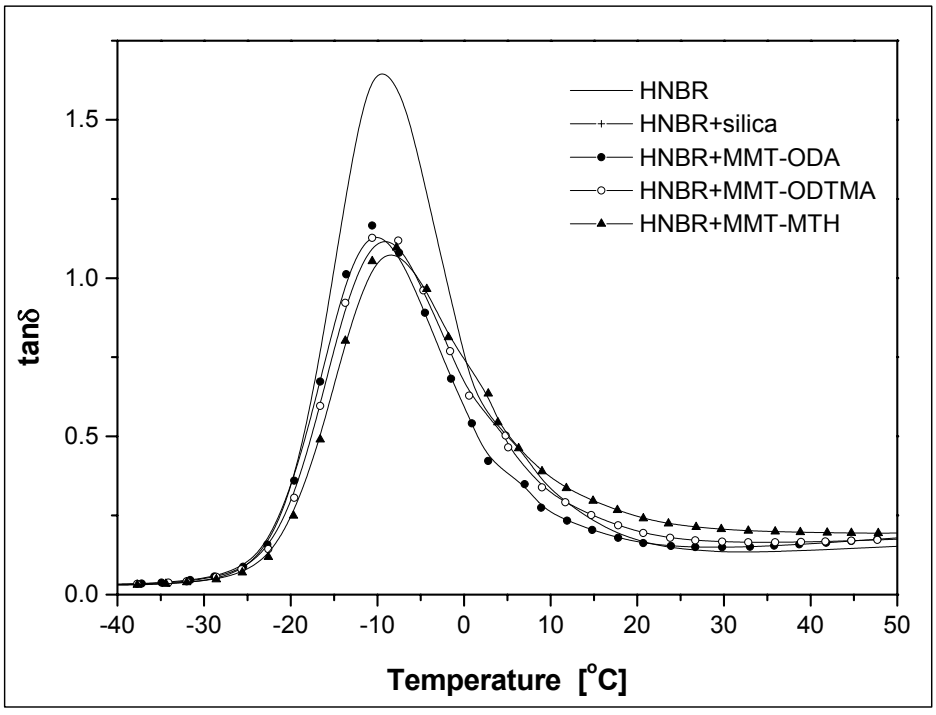

b)

Figure 5.39: a) Storage modulus (E') and b) mechanical loss factor (tanδ) as a function of temperature for the HNBR and HNBR containing various fillers in 10 phr amount (peroxide cured)

The heat stability of the peroxide cured HNBR/organo-MMT nanocomposites is presented in Figure 5.40. Similarly to the sulfur cured systems, the organoclay delayed the degradation of the vulcanizates. The 85% weight loss value is shifted from the initial 420 ^{o}C (measured for the HNBR or HNBR reinforced with silica) up to 440 ^{o}C for the organo-MMTs versions. This is comparable with that of the earlier presented sulfur cured HNBR/organoclay nanocomposites (Fig 5.30). This finding supports that the rubber and filler type instead of the vulcanization system are those parameters, which govern the heat degradation and stability.

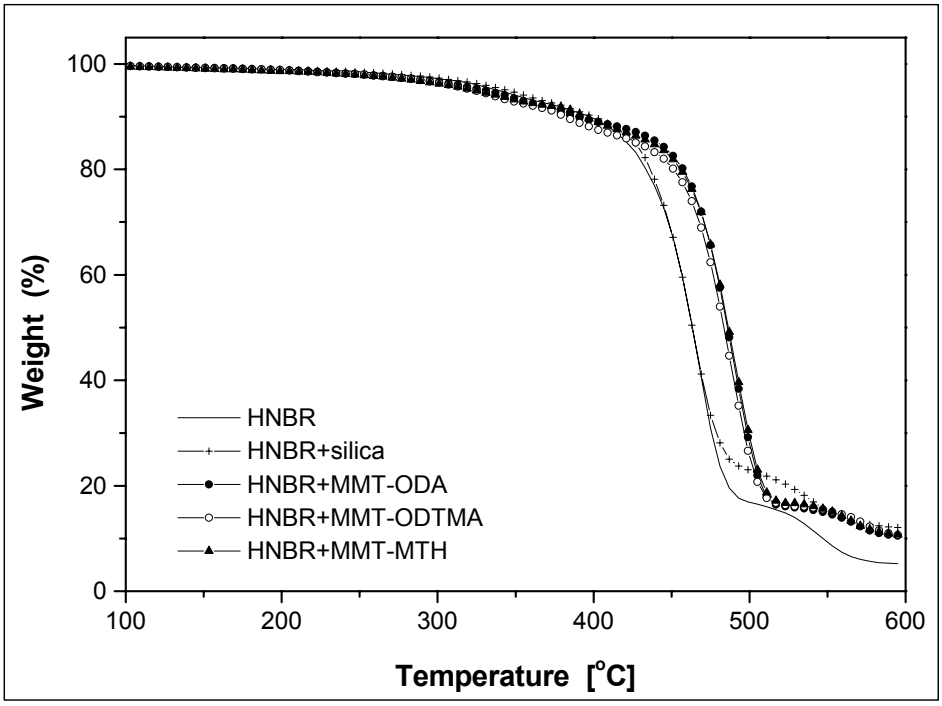

Figure 5.40: TGA thermographs of the HNBR/organoclay nanocomposites (peroxide cured). HNBR and HNBR reinforced with silica are also given for comparison purposes

It has been argued that no chemical interactions between the organoclay intercalant and the HNBR matrix occur during peroxide vulcanization (Fig. 5.38). Thus, the mechanical performance of the vulcanizates should be directly related with the nature of the intercalant type (i.e. polarity, number of alkyl tails and length, etc.). As shown in Table 5.4, the effect of the organo-MMTs is less reflected in the tensile strength and elongation at break values when compared to the silica filled systems. On the other hand, the moduli at various deformations were enhanced. Note that for the MMT-MTH filler the moduli are more than two and four times higher than the silica

filled and plain HNBR, respectively. The strong matrix-filler interaction via H-bonding in this HNBR/MMT-MTH compound is responsible for the observed reinforcing effect. The occlusion of rubber within the galleries and creation of a “rubber shell” in the vicinity of the platelets (because of the favorable H-bonds) are the major factors for the stiffness upgrade. This stiffness enhancement is well reflected also in the hardness values. Interesting to observe that the effects of MMT-ODA and MMT-ODTMA on the tensile properties are similar (recall that both amine tethered heads bear non-polar groups). The superior behavior of the organo-MMTs is well reflected in the tear resistance, too. The zig-zag route of the crack path (cf. Fig. 5.26) produced more than two times higher value for MMT -ODA and –ODTMA than for silica. For the MMT-MTH the combined action of filler dispersion and optimum interphase gave the best tear resistance among the nanocomposites tested.

Table 5.4: Mechanical properties of HNBR/organo-MMTs at 10 phr filler amount

Properties	Mixes				
	HNBR	HNBR/ silica	HNBR/ MMT-ODA	HNBR/MMT-ODTMA	HNBR/ MMT-MTH
Tensile strength(MPa)	9.8 ± 1.1	19.1 ± 2.4	17.3 ± 1.0	18.6 ± 1.0	19.0 ± 0.6
Modulus at (MPa):					
100% Elong.	0.6 ± 0.1	0.9 ± 0.1	1.6 ± 0.1	1.6 ± 0.1	2.3 ± 0.1
200% Elong.	0.9 ± 0.1	1.5 ± 0.1	2.3 ± 0.1	2.3 ± 0.2	3.8 ± 0.2
300% Elong.	1.3 ± 0.3	2.7 ± 0.1	3.3 ± 0.1	3.0 ± 0.4	5.5 ± 0.3
Elong. at break (%)	577 ± 46	646 ± 25	707 ± 22	626 ± 61	588 ± 25
Tear strength (kN/m)	8.0 ± 1.1	11.8 ± 0.9	27.4 ± 0.8	21.2 ±1.2	31.5 ± 2.2
Hardness (Shore A)	62	65	72	72	74

The relative oxygen permeation behavior of the respective films at 0% and 60% relative humidity is depicted in Figure 5.41. The oxygen permeability coefficient of the HNBR in dry and wet conditions was 119 and 129 $cm^3.mm/m^2.day.bar$, respectively. As the humidity increased higher oxygen permeation was obtained similar to the sulfur cured HNBR compounds (cf. Fig. 5.37). As shown in Figure 5.41, the decrease of the permeability coefficient ratio in dry and wet conditions is almost the same for all compounds tested. The silica filler, being isometric, only slightly reduced the oxygen transmission rate. The improvement in the barrier properties of the organoclays is due to tortuosity of the penetration path given by the impermeable clay layers and stacks. The difference in the relative oxygen permeation depends on the dispersion grade of the clay and interphase formed. Assuming some similarities in respect of the interphase for MMT-ODA and MMT-ODTMA (in peroxide cured HNBR) the small divergence may be attributed to the marginal difference in their interlayer spacing [142] (Figure 5.38a and b). Further, the slight difference between MMT-ODA and MMT-ODTMA suggests that the intercalated part of the clay does not contribute much to the barrier improvement [143]. The good dispersion grade and strong interphase for MMT-MTH resulted in the lowest oxygen permeability coefficient ratio (Figure 5.41). With increasing humidity the rubber nanocomposites films maintained their good barrier properties, as the tortuous path given by the MMT platelets [117] compensated the moisture susceptibility of the matrix [144].

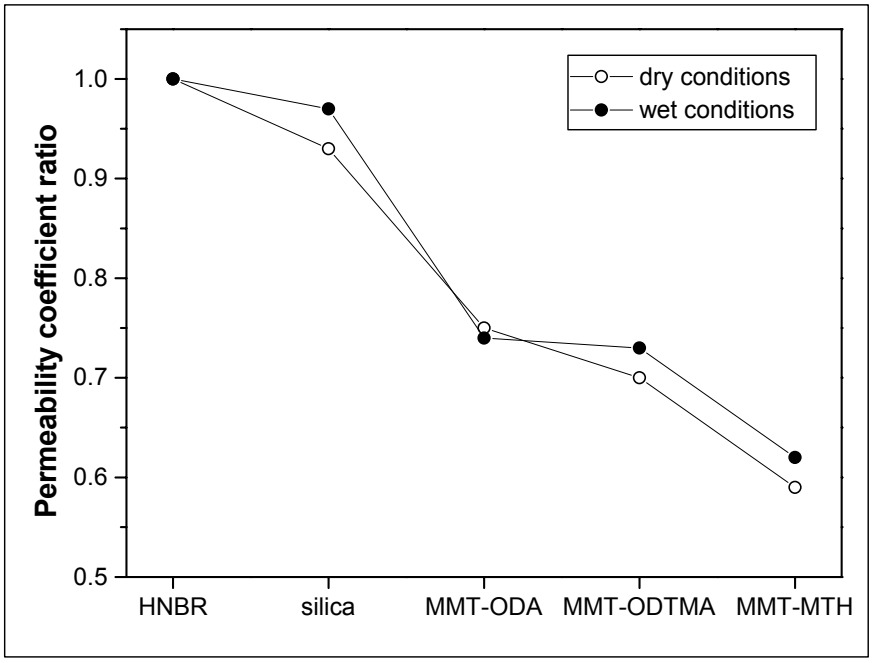

Figure 5.41: Oxygen permeability coefficient ratio for the different HNBR films tested at 0% and 60% relative humidity (dry and wet conditions, respectively). Both measurements conducted at room temperature. (Note that the oxygen permeability coefficient value for HNBR was 119 and 129 $cm^3.mm/m^2.day.bar$ for the dry and wet conditions, respectively)

5.5 Modeling the Rubber/organoclay Nanocomposite Behavior

The mechanical performance and the gas permeation properties of the rubber/organoclay nanocomposites are modeled. For that purpose test results on HNBR/FHT-ODA at varying organoclay content were considered. Note that this mix delivered the best performance (cf. chapter 5.4.1.2).

5.5.1 Mechanical Properties

The Guth equation (eq. 2.5) valid for rubber containing rod-like particles depends strongly on the shape factor f value (as presented in the Appendix-chapter 7). Thus, to proceed further, the aspect ratio of the dispersed phyllosilicate should be determined. Using the “a4i” image analysis program (Aquinto AG, Landshut, Germany), thirty objects in Figure 5.33 were analyzed and the mean aspect ratio of the dispersed FHT-ODA stacks was found to be in the order of 50 presenting a rather

wide scatter (cf. Figure 7.3). Although the aspect ratio of individual fluorohectorite platelets is in the range of more than 200, in the rubber matrix stacks of platelets appear rather than well-resolved exfoliated (individual) platelets. This finding is in accordance with previous investigations using image analysis. It was reported that the mean value of the organo-MMT dispersed in the polymer matrix is less than 50 [114, 145]. As the contribution of the platelet-like filler to the modulus of the rubber/organoclay nanocomposite is expected to be lower than for fiber-like filler (at the same filler volume), Wu et al. [114] introduced a modulus reduction factor (MRF) in the Guth equation (eq. 2.5). Its value was estimated to be 0.66 and it was multiplied by the shape factor *f*:

$$E_c = E_m\left[1 + 0.67(MRF)f \cdot c + 1.62(MRF)^2 f^2 \cdot c^2\right] \tag{5.4}$$

It has been presented that the values of the elastic modulus obtained after dynamic cycling loading can replace the E value (Young's or shear modulus) in the Guth's equation [15]. As the Young's modulus evaluation for rubbers is controversial, the complex modulus (E*) values measured by dynamic mechanical thermal analysis (DMTA) at room temperature (30^{o}C) are used in this analysis. As shown in Figure 5.42, the ratio of the complex modulus of the HNBR/FHT-ODA nanocomposite (E^*_c) divided by the complex modulus of the HNBR matrix (E^*_m) increases with the filler volume. The Guth's equation (plotted in Figure 5.42) fails to predict the experiment at high filler volume. On the contrary, the corrected Guth's equation describes excellently the modulus enhancement of the nanocomposites in the whole filer range studied.

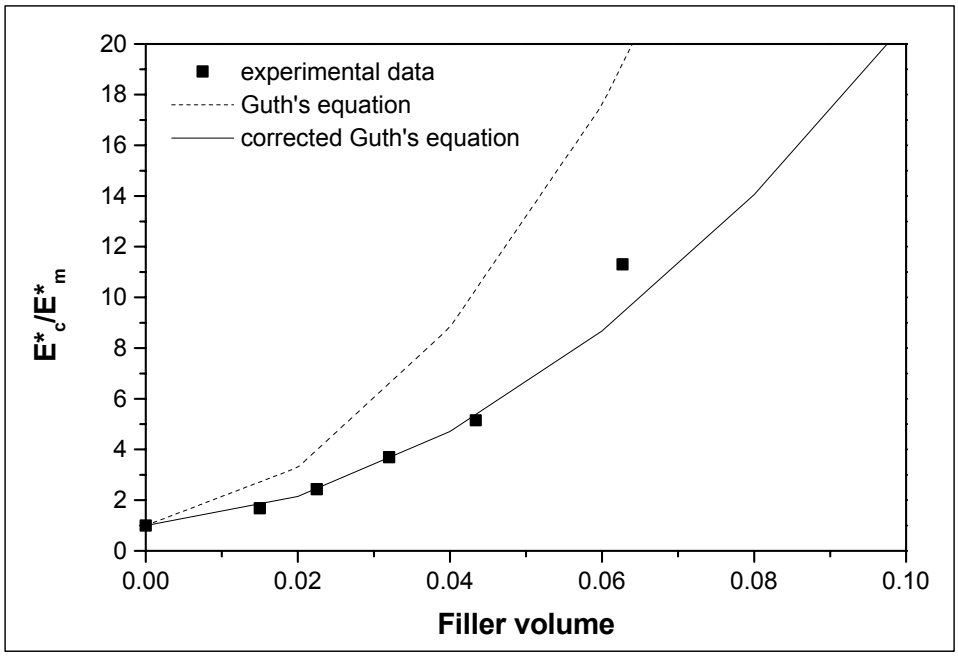

Figure 5.42: Experimentally measured complex modulus and theoretical predictions by Guth's and corrected Guth's model

As the Young's modulus ratio of the nanocomposite to the neat matrix is a measure of the stiffness enhancement, this parameter should also hold for the ratio of the respective complex moduli. Thus, the above experimental data were treated also by Halpin-Tsai (eq. 2.7) model, as well. When the Young modulus of the FHT-ODA filler is much higher than that of the HNBR matrix ($E_f >> E_m$), the η parameter in the equation 2.8 turns to 1. For discontinuous oriented square fiber-reinforced composites ζ has been estimated to be equal to 2(a/b), where a and b are the length and thickness of the fiber, respectively. Replacing the ratio a/b with the estimated aspect ratio of the FHT-ODA in the nanocomposite, correlation between the experimental data and those produced by the Halpin-Tsai equation is shown in Figure 5.43. According to Wu et al. [114] the modulus reduction factor (MRF) should also be active for the Halpin-Tsai model. Therefore, the corrected Halpin-Tsai fitting (eq. 5.5) is also depicted in Figure 5.43.

$$\frac{E_c^*}{E_m^*} = \frac{1+\zeta(MRF)\varphi_f}{1-\varphi_f} \tag{5.5}$$

As presented in Figure 5.43, both models are inadequate at high filler volume fractions. The introduction of the MRF in the Halpin-Tsai equation (corrected Halpin-Tsai model) improved the agreement between experiments and therory at low filler loadings.

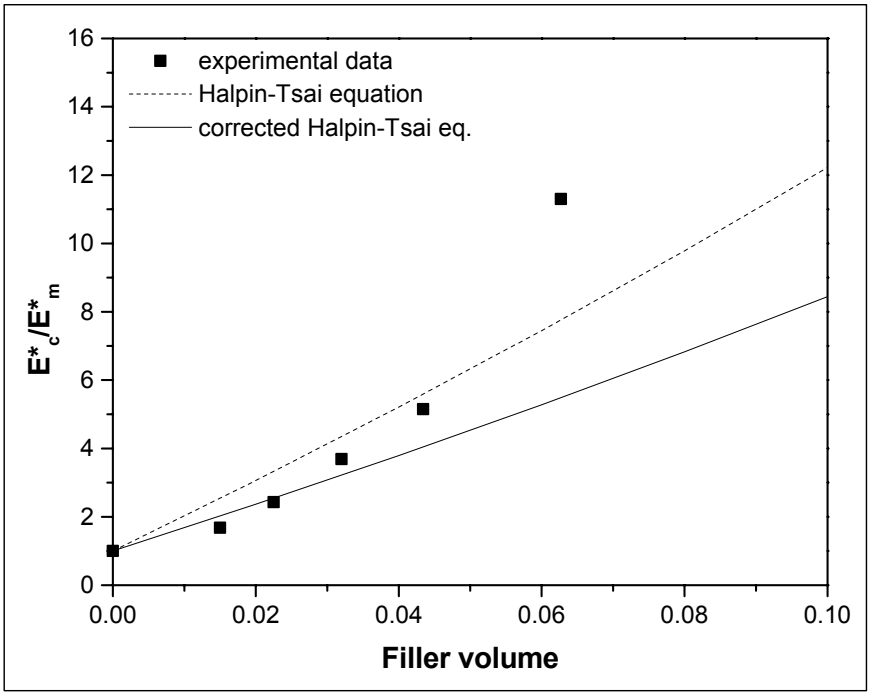

Figure 5.43: Ratio of the experimentally measured complex moduli (nanocomposite/matrix) and its theoretical prediction via the Halpin-Tsai and corrected Halpin-Tsai models

The best fit for the experimental data stiffness of HNBR/FHT-ODA nanocomposites was delivered by the corrected Guth's model. Recall that this was developed for soft matrices and anisometric fillers. The Halpin-Tsai model failed to predict the experimental data likely due to the fact that it is performed for rigid matrices.

5.5.2 Gas Permeation

In order to model the oxygen permeability of the HNBR/FHT-ODA nanocomposites, the Nielsen's (eq. 2.9) and the Bharadwaj's equations (eq. 2.10) were adopted. As shown in Figure 5.44, the experimental data are well predicted by the Nielsen's equation and some discrepancy only at high filler volume fractions occurs. Fitting the Bharadwaj's equation on the experimental data the best match is obtained when the

order parameter (*S*) of the equation 2.10 gets the value of 0.90 (cf. chapter 2.4.2.). Note that this correction means that the platelets of the HNBR/FHT-ODA nanocomposite are not fully horizontally oriented i.e. traverse to the penetration route (*S*=1) in the HNBR matrix but possess some misalignment (*S*=0.90).

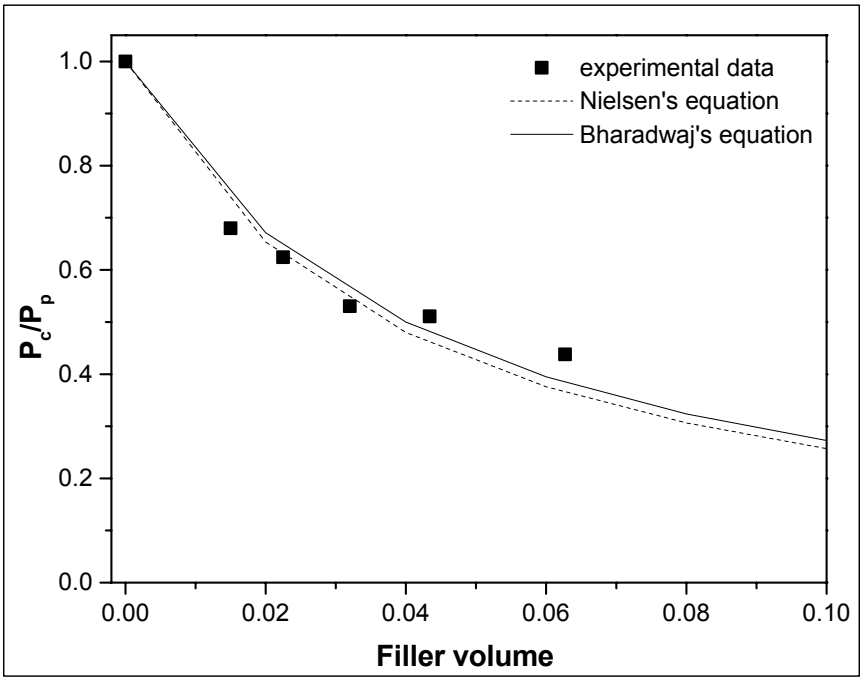

Figure 5.44: Experimentally measured oxygen permeation coefficient at dry conditions and theoretical predictions by Nielsen's and corrected Nielsen's (Bharadwaj's) models

Based on Figure 5.33 (or in the Appendix Figure 7.2), one can state that the orientation of the FHT-ODA platelets has a lower order parameter (S) than the calculated value of 0.90. As there is indeed a preferably horizontally orientation of the platy fillers initially due to calendaring and later due to compression moulding, an order parameter of 0.60 appears as more reasonable. Taking advantage of the interplay of the order parameter with the platelet aspect ratio in equation 2.10 and setting *S*=0.60, the best fit on the experimental data results in an aspect ratio of 60.
The mean value of the aspect ratio of the dispersed stacks has been found to be in the order of 50 by means of image analysis. Although either more TEM images should be analyzed and/or more platelets have to be measured (in order to get reliable statistics), the aspect ratio determined was in accordance with the permeability model. Note that the oxygen permeability is directly related with the

platelet dispersion and their aspect ratio. This is due to the fact that the highly anisometric (phylloid) and impermeable platy surface of the dispersed FHT-ODA in the HNBR matrix controls the oxygen permeation behavior.

6. Summary and Outlook

In the current work, firstly, a method to estimate the optimum vulcanization time for rubbers using a Plate-Plate Rheometer was proposed. Accordingly, making use of the mechanical loss factor versus time curves, a formula for the t_{90} determination was recommended. Afterwards, the work was focused to detect and analyze aspects related with the structural development in rubber/organoclay nanocomposites.

On the example of an EPDM rubber the effects of mixing procedure (mixing techniques, parameters) were identified. It was established that by increasing the shear forces and the compounding temperature the organoclay can be dispersed better in the rubber matrix. By defining a procedure suitable to yield rubber/organoclay nanocomposites of enhanced mechanical performance (i.e. 10 min mixing in the internal mixer at 100^{o}C and at 60 rpm), effects of the rubber polarity on intercalation/exfoliation mechanisms were investigated.

For EPDM rubber, bearing polar MA or GMA groups, better intercalated silicate structures were resolved compared to the plain EPDM. The simultaneous appearance of intercalated/exfoliated and deintercalated clay populations, which were detected for several EPDM/MMT-ODA nanocomposites, were attributed to the primary amine (ODA) intercalant, which may participate in the formation of sulfur-rich Zn-complexes during sulfur vulcanization. It was proposed that the ODA intercalant leaves the silicate surface and migrates in the rubber matrix. This causes the deintercalation of the clay. This phenomenon was amplified when Zn-type accelerators were used for the sulfur vulcanization of EPDM instead of dithiocarbamate or benzothiazole types. For the first accelerator type (i.e. ZDEC), however, a better mechanical performance was observed when compared to CBS or MBT. This was attributed to the pronounced exfoliated clay populations in the vulcanizate, which were also formed apart from the deintercalated ones.

The deintercalation phenomena detected for the EPDM/MMT-ODA nanocomposites were controlled by the type of the clay intercalant. MMT-ODTMA produced exfoliated and intercalated structures in the corresponding rubber mixes. As this organoclay contains a quaternary amine it could be demonstrated in an indirect way that the primary amine intercalant is that one which participate in the formation of the sulfur-rich transitional Zn-complexes (catalytic activation of the sulfur).

Increasing the organoclay content an optimum in the mechanical performance was found for nanocomposites containing 7-10 phr organoclay. The high tensile strength associated with high elongation at break, were attributed to the dispersion grade of the organoclay platelets. The related “platelet network” can dissipate the input energy in the bulk efficiently (creation of subcritical cracks in the vicinity of the platelets). Therefore, higher strains and at the same time enhanced moduli could be observed for the EPDM nanocomposites.

Armored with the knowledge obtained on EPDM/organoclay nanocomposites, a polar rubber was chosen to perform further experiments. Selecting a HNBR matrix, the effects of the intercalant type on the organoclay dispersion were explored. The best performance was recorded for a quaternary ammonium intercalant (i.e. MTH) bearing polar groups (i.e. OH). It was presumed that this is due to hydrogen bonding (CN…H-O) yielding better interphase coupling between the silicates and the rubber. This resulted in superior performance (e.g. tensile strength, storage modulus, hardness, tear resistance, low oxygen permeation).

Increasing the aspect ratio of the silicate by using fluorohectorite (FHT) instead of montmorillonite (MMT) but keeping the same type of clay intercalant (i.e. ODA), a further improvement in the performance was achieved. The effect of the aspect ratio was best reflected in the oxygen permeation measurements.

The clay deintercalation detected for sulfur cured HNBR/MMT-ODA compounds was suppressed by peroxide curing. This finding provides a tool to control the dispersion of the organoclay. For that purpose the interaction of the intercalant in the formation of Zn-sulfur complex has to be considered.

As the prediction of the behavior of rubber/organoclay nanocomposites is of great significance, the mechanical and permeation properties were modeled. Varying the FHT-ODA volume content in the HNBR matrix, the mechanical performance follows the modified Guth’s equation. Thus, the restrained action of the platelet type versus rod-like fillers in rubber matrices is underlined. The Nielsen’s model for gas permeation fitted excellently the experimental data of the oxygen permeation for the HNBR/FHT-ODA vulcanizates. By introducing the order parameter making use of the Bharadwaj’s model, the aspect ratio was deduced and verified the image analysis.

Continuing the work presented in the current thesis, simple recipes for rubber vulcanization could be investigated applying methods capable to reveal insights in

the speculated reactions responsible for the deintercalation of the organoclay. These may include the model compound vulcanization (MCV) method or the reaction-stage modeling (RSM). Moreover, combining the layered silicates with fillers like carbon black (CB), carbon nanotubes or silica (i.e. hydrid reinforcement) synergetic effects may appear. These might include reduced permeability (due to the layered silicate) linked with low rolling resistance (due to the silica particles) and/or semi-conductive properties (due to the carbon compound).

7. Appendix

The behavior of the Guth equation (eq. 2.5) for rod-like particles embedded in the rubber matrix depends strongly on the value of the shape factor (f). As shown in Figure 7.1 with increasing f increases the modulus ratio (E_c/E_m) at a given filler volume fraction.

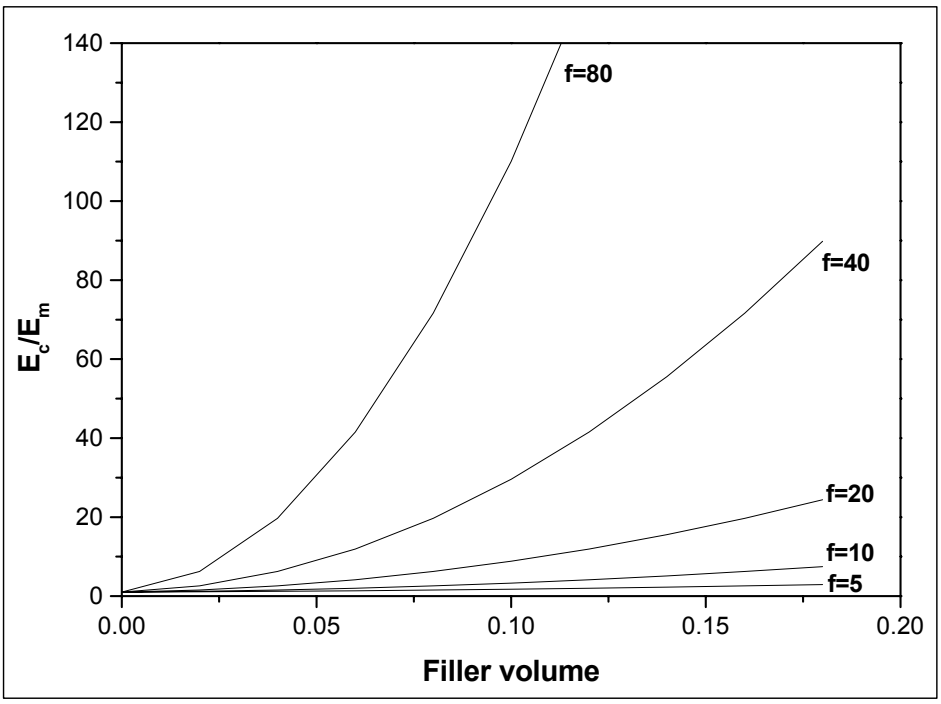

Figure 7.1: Effect of the shape factor on the Guth equation for rod-like particles in rubber matrix

In order to evaluate the aspect ratio of the HNBR/FHT-ODA nanocomposite a TEM image taken at high magnification of this vulcanizate (i.e. Fig. 5.33b) was inspected by means of image analysis. The program used was the “a4i” image analysis (Aquinto AG, Landshut, Germany). Thirty objects were selected (indicated in Figure 7.2) and their length and thickness were measured. Note that in the same Figure (Fig. 7.2), the permeation direction during the oxygen permeation measurements is indicated by arrow. This was done to give an idea to the reader about the tortuous path that the oxygen molecules have to follow around the impermeable silicate stacks after their penetration in the HNBR/FHT-ODA nanocomposite film. At the

same time, the orientation of the FHT-ODA stacks in the HNBR matrix can be identified.

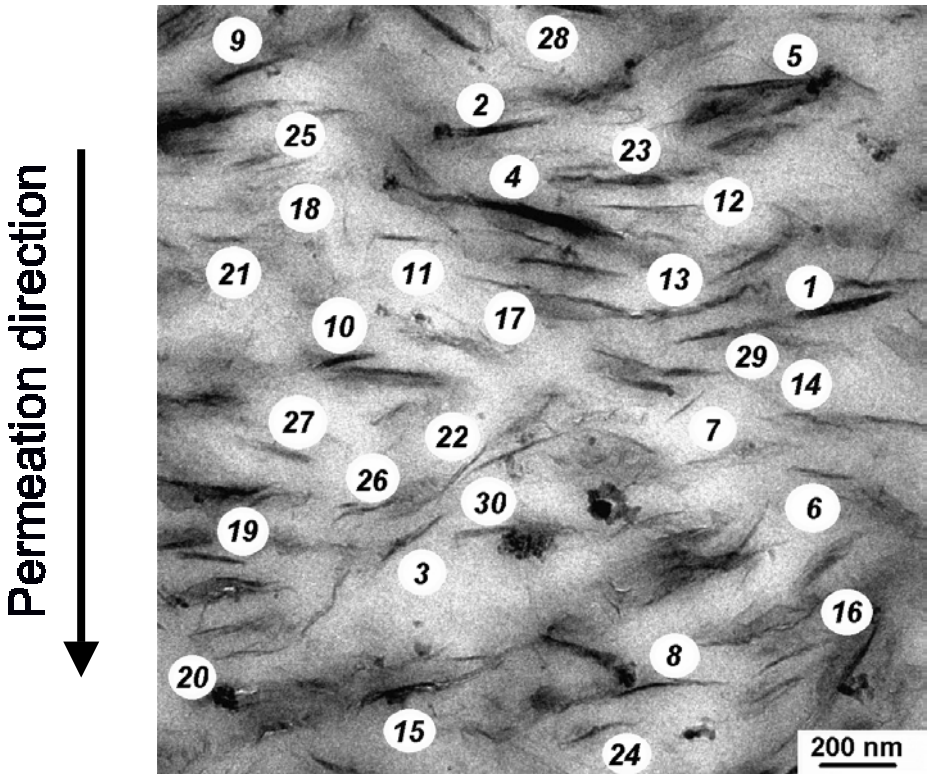

Figure 7.2: TEM image taken from the HNBR/FHT-ODA vulcanizate. Note that numbers indicate the thirty measured stacks of platelets. The permeation direction for the oxygen permeability measurement is also depicted

Considering the silicate stacks, a mean value of about 50 was deduced for the aspect ratio. The frequency that a platelet of a specific aspect ratio appeared in Figure 7.2 is presented schematically in Figure 7.3. It can be easily resolved a rather non-symmetric distribution for the aspect ratio around the mean value of 50.

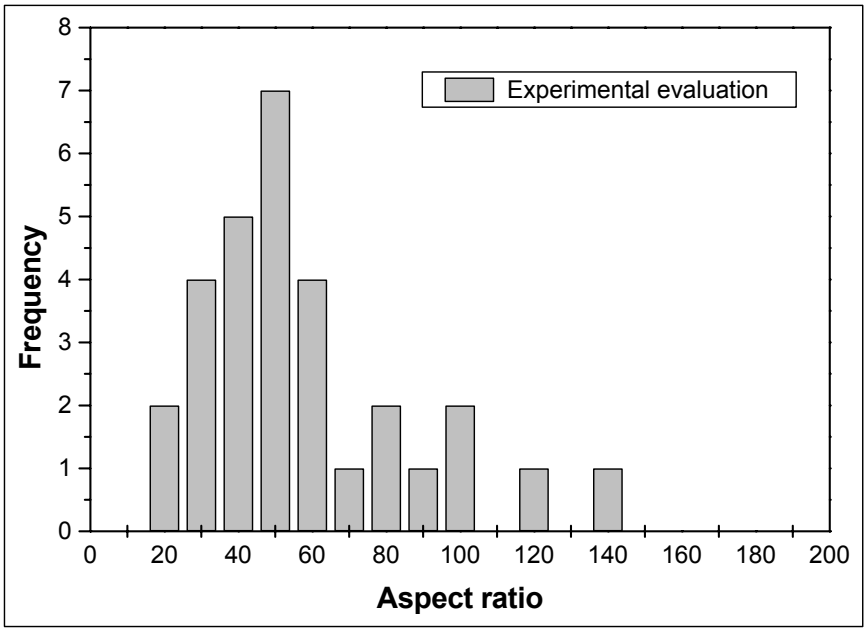

Figure 7.3: Aspect ratio histogram based on Figure 7.2

8. Literature

[1] Röthemeyer, F., Sommer, F.: Kautschuk Technologie. Munich: Hanser 2001.

[2] Akiba, M., Hashim, A.S.: Vulcanization and crosslinking in elastomers. Progress in Polymer Science 22 (1997) pp. 475-521.

[3] Heideman, G., Noordermeer, J.W.M., Datta, R.N., van Baarle, B.: Effect of metal oxides as activator for sulphur vulcanisation in various rubbers. Kautschuk Gummi Kunststoffe 58 (2005) pp.30-42.

[4] Hofmann, W.:Rubber Technology Handbook. Munich:Hanser 1994, pp. 230-231.

[5] Krejsa, M.R., Koenig, J.L.: The nature of sulfur vulcanization. In 'Elastomer Technology Handbook'. Cheremisinoff, N.P. (ed.) Boca Raton, Florida, USA: CRC Press 1993, pp. 475-493.

[6] Coran, A.Y.: Chemistry of the vulcanization and protection of elastomers:a review of the achievements. Journal of Applied Polymer Science 87 (2003) pp. 24-30.

[7] Borrós, S., Agulló, N.: Some contributions to the understanding of the accelerating system during natural rubber vulcanization. Kautschuk Gummi Kunststoffe 53 (2000) pp.131-136.

[8] Nieuwenhuizen, P.J., Timal, S., van Veen, J.M., Haasnoot, J.G., Reedijk, J.: Homogeneous catalysis by zinc complexes during accelerated vulcanization. Kautschuk Gummi Kunststoffe 51 (1998) pp. 336-341.

[9] Hummel, K., Santos Rodríguez, F.J.: Evidence of ionic intermediates in rubber vulcanization detected by on-line electric current measurements in natural rubber/sulfur/tetramethylthiuram monosulfide/zinc oxide and comparison mixtures. Polymer 41 (2000) pp. 3167-3172.

[10] van Duin, M.: Chemistry of EPDM cross-linking. Kautschuk Gummi Kunststoffe 55 (2002) pp.150-156.

[11] Endstra, W.C., Wreesmann, T.J.: Peroxide crosslinking of EPDM rubbers. In 'Elastomer Technology Handbook'. Cheremisinoff, N.P. (ed.) Boca Raton, Florida, USA: CRC Press 1993, pp. 495-518.

[12] Hamed, G.R.: Materials and Compounds. In 'Engineering with rubber' Gent, A.N. (ed.) Munich, Germany: Hanser 1992, pp. 13-31.

[13] Kühner, G., Voll, M.: Manufacture of carbon black. In 'Carbon black' Donnet, J.B., Bansal, R.C., Wang, M.J. (eds.) New York, USA: Dekker 1993, pp. 1-66.

[14] Hess, W.M., Herd, C.R.: Microstructure, morphology and general physical properties. In 'Carbon black' Donnet, J.B., Bansal, R.C., Wang, M.J. (eds.) New York, USA: Dekker 1993, pp. 89-173.

[15] Medalia, A.I.: Effect of carbon black on dynamic properties of rubber vulcanizates. Rubber Chemistry and Technology 51 (1978) pp. 437-523.

[16] Wolff, S., Wang, M.J.: Carbon black reinforcement of elastomers. In 'Carbon black' Donnet, J.B., Bansal, R.C., Wang, M.J. (eds.) New York, USA: Dekker 1993, pp. 289- 355.

[17] Wang, M.J.: Effect of polymer-filler and filler-filler interactions on dynamic properties of filled vulcanizates. Rubber Chemistry and Technology 71 (1998) pp. 520-589.

[18] Nah, C., Kim, D.H., Kim, W.D., Im, W.B., Kaang, S.: Friction and abrasion properties of in-situ silica-filled natural rubber nanocomposites using sol-gel process. Kautschuk Gummi Kunststoffe 57 (2004) pp.224-226.

[19] Murakami, K., Lio, S., Tanahashi, T., Kohjiya, S., Kajiwara, K., Ikeda, Y.: Reinforcement of NR by silica generated in situ: comparison with carbon black stock. Kautschuk Gummi Kunststoffe 54 (2001) pp.668-672.

[20] Smallwood, H.M.: Limited law of the reinforcement of rubber. Journal of Applied Physics 15 (1944) pp.758-766.

[21] Theng, B.K.G.: Formation and properties of clay-polymer complexes. Amsterdam: Elsevier 1979.

[22] Van Olphen, H.: An introduction to clay colloid chemistry. New York: Wiley 1977.

[23] Kühner, G., Voll, M.: Manufacture of carbon black. In 'Carbon black' Donnet, J.B., Bansal, R.C., Wang, M.J. (eds.) New York, USA: Dekker 1993, pp. 1- 66.

[24] Lin, C.J., Hogan, T.E., Hergenrother, W.L.: On the filler flocculation in silica and carbon black filled rubbers: Part II. Filler flocculation and polymer-filler interaction. Rubber Chemistry and Technology 76 (2004) pp. 90-114.

[25] Sae-Oui, P., Sirisinha, C., Hatthapanit, K., Thepsuwan, U.: Comparison of reinforcing efficiency between Si-69 and Si-264 in an efficient vulcanization system. Polymer Testing 24 (2005) pp. 439-446.

[26] Galanti, A., Laus, M., Fiorini, M.: Reinforcement of SBS by organophilic clay fillers. Kautschuk Gummi Kunststoffe 52 (1999) pp. 21-25.

[27] Alexandre, M., Dubois, P.: Polymer-layered silicate nanocomposites: Preparation, properties and uses of a new class of materials. Materials Science and Engineering Reviews 28 (2000) pp. 1-63.

[28] LeBaron, P.C., Wang, Z., Pinnavaia, T.J.: Polymer-layered silicate nanocomposites: An overview. Applied Clay Science 15 (1999) pp. 11-29.

[29] Sinha Ray, S., Okamoto, M.: Polymer/layered silicate nanocomposites: A review from preparation to processing. Progress in Polymer Science 28 (2003) pp. 1539-1641.

[30] Kojima, Y., Usuki, A., Kawasumi, M., Okada, A., Fukushima, Y., Kurauchi, T., Kamigaito, O.: Mechanical properties of nylon 6-clay hydrid. Journal of Materials Research 8 (1993) pp. 1185-1189.

[31] Kojima, Y., Usuki, A., Kawasumi, M., Okada, A., Kurauchi, T., Kamigaito, O.: Sorption of water in nylon 6-clay hydrid. Journal of Applied Polymer Science 49 (1993) pp. 1259-1264.

[32] Kojima, Y., Usuki, A., Kawasumi, M., Okada, A., Kurauchi, T., Kamigaito, O.: One-pot synthesis of nylon 6-clay hydrid. Journal of Polymer Science: Part A: Polymer Chemistry 31 (1993) pp. 1755-1758.

[33] Messersmith, P.B., Giannelis, E.P.: Synthesis and characterization of layered silicate-epoxy nanocomposites. Chemistry of Materials 6 (1994) pp. 1719-1725.

[34] Lan, T., Pinnavaia, T.J.: Clay-reinforced epoxy nanocomposites. Chemistry of Materials 6 (1994) pp. 2216-2219.

[35] Lan, T., Kaviratna, P.D., Pinnavaia, T.J.: Mechanism of clay tactoid exfoliation in epoxy-clay nanocomposites. Chemistry of Materials 7 (1995) pp. 2144-2150.

[36] Vaia, R.A., Jandt, K.D., Kramer, E.J., Giannelis, E.P.: Kinetics of polymer melt intercalation. Macromolecules 28 (1995) pp. 8080-8085.

[37] Hackett, E., Manias, E., Giannelis, E.P.: Molecular dynamics simulations of organically modified layered silicates. Journal of Chemical Physics 108 (1998) pp. 7410-7415.

[38] Anastasiadis, S.H., Karatasos, K., Vlachos, G., Manias, E., Giannelis, E.P.: Nanoscopic-confinement effects on local dynamics. Physical Review Letters 84 (2000) pp. 915-918.

[39] Hackett, E., Manias, E., Giannelis, E.P.: Computer simulations studies of PEO/layered silicate nanocomposites. Chemistry of Materials 12 (2000) pp. 2161-2167.

[40] Balazs, A.C., Singh, C., Zhulina, E.: Modeling the interactions between polymers and clay surfaces through self-consistent field theory. Macromolecules 31 (1998) pp. 8370-8381.

[41] Ginzburg, V.V., Singh, C., Balazs, A.C.: Theoretical phase diagrams of polymer/clay composites: Therole of grafted organic modifiers. Macromolecules 33 (2000) pp. 1089-1099.

[42] Garcés, J.M., Moll, D.J., Bicerano, J., Fibiger, R., McLeod, D.G.: Polymeric nanocomposites for automotive applications. Advanced Materials 12 (2000) pp. 1835-1839.

[43] Majumdar, D., Blanton, T.N., Schwark, D.W.: Clay-polymer nanocomposite coatings for imaging application. Applied Clay Science 23 (2003) pp. 265-273.

[44] Giannelis, E.P.: Polymer-layered silicate nanocomposites: Synthesis, properties and applications. Applied Organometallic Chemistry 12 (1998) pp. 675-680.

[45] Njuguna, J., Pielichowski, K.: Polymer nanocomposites for aerospace applications: Fabrication. Advanced Engineering Materials 6 (2004) pp. 193-203.

[46] Dennis, H.R., Hunter, D.L., Chang, D., Kim, S., White, J.L., Cho, J.W., Paul, D.R.: Effect of melt processing conditions on the extent of exfoliation in organoclay-based nanocomposites. Polymer 42 (2001) pp. 9513-9522.

[47] Zhu, L., Xanthos, M.: Effects of process conditions and mixing protocols on structure of extruded polypropylene nanocomposites. Journal of Applied Polymer Science 93 (2004) pp. 1891-1899.

[48] Kojima, Y., Fukumori, K., Usuki, A., Okada, A., Kurauchi, T.: Gas permeabilities in rubber-clay hydrid. Journal of Materials Science Letters 12 (1993) pp. 889-890.

[49] Burnside, S.D., Giannelis, E.P.: Synthesis and properties of new poly(dimethylsiloxane) nanocomposites. Chemistry of Materials 7 (1995) pp. 1597-1600.

[50] Akelah, A., Salahuddin, N., Hiltner, A., Baer, E., Moet, A.: Morphological hierarchy of butadieneacrylonitrile/montmorillonite nanocomposite. Nanostructured Materials 4 (1994) pp. 965-978.

[51] Ganter, M., Gronski, W., Reichert, P., Mülhaupt, R.: Rubber nanocomposites: Morphology and mechanical properties of BR and SBR vulcanizates reinforced by organophilic layered silicates. Rubber Chemistry and Technology 74 (2001) pp. 221-235.

[52] Burnside, S.D., Giannelis, E.P.: Nanostructure and properties of polysiloxane-layered silicate nanocomposites. Journal of Polymer Science: Part B: Polymer Physics 38 (2000) pp. 1595-1604.

[53] Mousa, A., Karger-Kocsis, J.: Rheological and thermodynamical behavior of styrene/butadiene rubber-organoclay nanocomposites. Macromolecular Materials and Engineering 286 (2001) pp. 260-266.

[54] Vu, Y.T., Mark, J.E., Pham, L.H., Engelhardt, M.: Clay nanolayer reinforced of cis-1,4-polyisoprene and epoxidized natural rubber. Journal of Applied Polymer Science 82 (2001) pp. 1391-1403.

[55] Wang, Y., Zhang, L., Tang, C., Yu, D.: Preparation and characterization of rubber-clay nanocomposites. Journal of Applied Polymer Science 78 (2000) pp. 1879-1883.

[56] Zhang, L., Wang, Y., Wang, Y., Sui, Y., Yu, D.: Morphology and mechanical properties of clay/styrene-butadiene rubber nanocomposites. Journal of Applied Polymer Science 78 (2000) pp. 1873-1878.

[57] Sadhu, S., Bhowmick, A.K.: Preparation and properties of styrene-butadiene rubber based nanocomposites: The influence of the structural and processing parameters. Journal of Applied Polymer Science 92 (2004) pp. 698-709.

[58] Schön, F., Gronski, W.: Filler networking of silica and organoclay in rubber composites: Reinforcement and dynamic-mechanical properties. Kautschuk Gummi Kunststoffe 56 (2003) pp. 166-171.

[59] Song, M., Wong, C.W., Jin, J., Ansarifar, A., Zhang, Z.Y., Richardson, M.: Preparation and characterization of poly(styrene-co-butadiene) and polybutadiene rubber/clay nanocomposites. Polymer International 54 (2005) pp. 560-568.

[60] Zhang, Z., Zhang, L., Li, Y., Xu, H.: New fabrication of styrene-butadiene rubber/montmorillonite nanocomposites by anionic polymerization. Polymer 46 (2005) pp. 129-136.

[61] Wu, Y.P., Ma, Y., Wang, Y.Q., Zhang, L.Q.: Effects of characteristics of rubber, mixing and vulcanization on the structure and properties of rubber/clay nanocomposites by melt blending. Macromolecular Materials and Engineering 289 (2004) pp. 890-894.

[62] Liang, Y.R., Lu, Y.L., Wu, Y.P., Ma, Y., Zhang, L.Q.: Pressure, the critical factor governing final microstructures of cured rubber/clay nanocomposites. Macromolecular Rapid Communications 26 (2005) pp. 926-931.

[63] Zheng, H., Zhang, Y., Peng, Z., Zhang, Y.: Influence of clay modification on the structure and mechanical preperties of EPDM/montmorillonite nanocomposites. Polymer Testing 23 (2004) pp. 217-223.

[64] Usuki, A., Tukigase, A., Kato, M.: Preparation and properties of EPDM-clay hydrids. Polymer 43 (2002) pp. 2185-2189.

[65] Zheng, H., Zhang, Y., Peng, Z., Zhang, Y.: A comparison between cure systems for EPDM/montmorillonite nanocomposites. Polymer and Polymer Composites 12 (2004) pp. 197-206.

[66] Ahmadi, S.J., Yudong, H., Li, W.: Synthesis of EPDM/organoclay nanocomposites: Effect of the clay exfoliation on structure and physical properties. Iranian Polymer Journal 13 (2004) pp. 415-422.

[67] Chang, Y.W., Yang, Y., Ryu, S., Nah, C.: Preparation and properties of EPDM/organomontmorillonite hydrid nanocomposites. Polymer International 51 (2002) pp. 319-324.

[68] Kader, M.A., Nah, C.: Influence of clay on the vulcanization kinetics of fluoroelastomers. Polymer 45 (2004) pp. 2237-2247.

[69] Hwang, W.G., Wei, K.H., Wu, C.M.: Mechanical, thermal, and barrier properties of NBR/organosilicate nanocomposites. Polymer Engineering and Science 44 (2004) pp. 2117-2124.

[70] Nah, C., Ryu, H.J., Han, S.H., Rhee, J.M., Lee, M.H.: Fracture behaviour of acrylonitrile-butadiene rubber/clay nanocomposites. Polymer International 50 (2001) pp. 1265-1268.

[71] Kim, J.T., Oh, T.S., Lee, D.H.: Preparation and characteristics of nitrile rubber (NBR) nanocomposites based on organophilic layered clay. Polymer International 52 (2003) pp. 1058-1063.

[72] Joly, S., Garnaud, G., Ollitrault, R., Bokobza, L.: Organically modified layered silicates as reinforcing fillers for natural rubber. Chemistry of Materials 14 (2002) pp. 4202-4208.

[73] Magaraphan, R., Thaijaroen, W., Lim-Ochakun, R.: Structure and properties of natural rubber and modified montmorillonite nanocomposites. Rubber Chemistry and Technology 76 (2003) pp. 406-418.

[74] Varghese, S., Karger-Kocsis, J.: Melt-compounded natural rubber nanocomposites with pristine and organophilic layered silicates of natural and synthetic origin. Journal of Applied Polymer Science 91 (2004) pp. 813-819.

[75] López-Manchado, M.A., Herrero, B., Arroyo, M.: Organoclay-natural rubber nanocomposites synthesized by mechanical and solution mixing methods. Polymer International 53 (2004) pp. 1766-1772.

[76] Teh, P.L., Mohd Ishak, Z.A., Hashim, A.S., Karger-Kocsis, J., Ishiaku, U.S.: On the potential of organoclay with respect to conventional fillers (carbon black, silica) for epoxidized natural rubber compatibilized natural rubber vulcanizates. Journal of Applied Polymer Science 94 (2004) pp. 2438-2445.

[77] Bala, P., Samantaray, B.K., Srivastava, S.K., Nando, G.B.: Organomodified montmorillonite as filler in natural and synthetic rubber. Journal of Applied Polymer Science 92 (2004) pp. 3583-3592.

[78] Arroyo, M., López-Manchado, M.A., Herrero, B.: Organo-montmorillonite as substitute of carbon black in natural rubber compounds. Polymer 44 (2003) pp. 2447-2453.

[79] Teh, P.L., Mohd Ishak, Z.A., Hashim, A.S., Karger-Kocsis, J., Ishiaku, U.S.: Effects of epoxidized natural rubber as a compatibilizer in melt compounded natural–organoclay nanocomposites. European Polymer Journal 40 (2004) pp. 2513-2521.

[80] Pramanik, M., Srivastava, S.K., Samantaray, B.K., Bhowmick, A.K.: Synthesis and characterization of organosoluble, thermoplastic elastomer/clay nanocomposites. Journal of Polymer Science: Part B: Polymer Physics 40 (2002) pp. 2065-2072.

[81] Jeon, H.S., Rameshwaram, J.K., Kim, G., Weinkauf, D.H.: Characterization of polyisoprene-clay nanocomposites prepared by solution blending. Polymer 44 (2003) pp. 5749-5758.

[82] Wang, Y., Zhang, L., Tang, C., Yu, D.: Preparation and characterization of rubber-clay nanocomposites. Journal of Applied Polymer Science 78 (2000) pp. 1879-1883.

[83] Wu, Y.P., Zhang, L.Q., Wang, Y.Q., Liang, Y., Yu, D.S.: Structure of carboxylated acrylonitrile-butadiene rubber (CNBR)-clay nanocomposites by co-coagulating rubber latex and clay aqueous suspensions. Journal of Applied Polymer Science 82 (2001) pp. 2842-2848.

[84] Varghese, S., Karger-Kocsis, J.: Natural rubber-based nanocomposites by latex compounding with layered silicates. Polymer 44 (2003) pp. 4921-4927.

[85] Wu, Y.P., Wang, Y.Q., Zhang, H.F., Wang, Y.Z., Yu, D.S., Thang, L.Q., Yang, J.: Rubber-pristine clay nanocomposites prepared by co-coagulating rubber latex and clay aqueous suspensions. Composites Science and Technology 65 (2005) pp. 1195-1202.

[86] Hwang, W.G, Wei, K.H., Wu, C.M.: Preparation and mechanical properties of nitrile butadiene rubber/silicate nanocomposites. Polymer 45 (2004) pp. 5729-5734.

[87] Karger-Kocsis, J., Wu, C.M.: Thermoset rubber/layered silicate nanocomposites. Status and future trends. Polymer Engineering and Science 44 (2004) pp. 1083-1093.

[88] Fornes, T.D., Yoon, P.J., Keskkula, H., Paul, D.R.: Nylon 6 nanocomposites: The effect of matrix molecular weight. Polymer 42 (2001) pp. 9929-9940.

[89] Kawasumi, M., Hasegawa, N., Kato, M., Usuki, A, Okada, A.: Preparation and mechanical properties of polypropylene-clay hydrids. Macromolecules 30 (1997) pp. 6333-6338.

[90] Lan, T., Kaviratna, P.D., Pinnavaia, T.J.: Epoxy self-polymerization in smectite clays. Journal of Physics and Chemistry of Solids 57 (1996) pp. 1005-1010.

[91] Kornmann, X., Thomann, R., Mülhaupt, R., Finter, J., Berglund, L.A.: High performance epoxy-layered silicate nanocomposites. Polymer Engineering and Science 42 (2002) pp. 1815-1826.

[92] Wang, K.H., Xu, M., Choi, Y.S., Chung, I.J.: Effect of aspect ratio of clay on melt extensional process of maleated polyethylene/clay nanocomposites. Polymer Bulletin 46 (2001) pp. 499-505.

[93] Chang, J.H., An, Y.U., Cho, D., Giannelis, E.P.: Poly(lactic acid) nanocomposites: Comparison of their properties with mantmorillonite and synthetic mica (II). Polymer 44 (2003) pp. 3715-3720.

[94] Kornmann, X., Lindberg, H., Berglund, L.A.: Synthesis of epoxy-clay nanocomposites: Influence of the nature of the clay. Polymer 42 (2001) pp. 1303-1310.

[95] Miyagawa, H., Rich, M.J., Drzal, L.T.: Amine-cured epoxy/clay nanocomposites. II. The effect of the nanoclay aspect ratio. Journal of Polymer Science: Part B: Polymer Physics 42 (2004) pp. 4391-4400.

[96] Zilg, C., Thomann, R., Finter, J., Mülhaupt, R.: The influence of silicate modification and compatibilizers on mechanical properties and morphology of anhydride-cured epoxy nanocomposites. Macromolecular Materials and Engineering 280/281 (2000) pp. 41-46.

[97] Fornes, T.D., Hunter, D.L., Paul, D.R.: Nylon-6 nanocomposites from alkylammonium-modified clay: The role of alkyl tails on exfoliation. Macromolecules 37 (2004) pp. 1793-1798.

[98] Fornes, T.D., Yoon, P.J., Hunter, D.L., Keskkula, H., Paul, D.R.: Effect of organoclay structure on nylon 6 nanocomposite morphology and properties. Polymer 43 (2002) pp. 5915-5933.

[99] Nieuwenhuizen, P.J., Haasnoot, J.G., Reedijk, J.: Model-compound vulcanization-an established technique for the next century. Kautschuk Gummi Kunststoffe 53 (2000) pp. 144-152.

[100] Heideman, G., Noordermeer, J.W.M., Datta, R.N., van Baarle, B.: Effect of metal oxides as activator for sulfur vulcanisation in various rubbers. Kautschuk Gummi Kunststoffe 58 (2005) pp. 30-42.

[101] Nieuwenhuizen, P.J.: Zinc accelerator complexes. Versatile homogeneous catalysts in sulfur vulcanization. Applied Catalysis A: General 207 (2001) pp. 55-68.

[102] Coran, A.Y.: Chemistry of the vulcanization and protection of elastomers: A review of the achievements. Journal of Applied Polymer Science 87 (2003) pp. 24-30.

[103] Dirksen, A., Nieuwenhuizen, P.J., Hoogenraad, M., Haasnoot, J.G., Reedijk, J.: New mechanism for the reaction of amines with zinc dithiocarbamates. Journal of Applied Polymer Science 79 (2001) pp. 1074-1083.

[104] Hummel, K., Santos Rodríguez, F.J.: Electrochemical evidence of transitory ionic species in the vulcanization of natural rubber with sulfur, 2-mercaptobenzothiazole and zinc oxide: the activator effect of stearic acid. Kautschuk Gummi Kunststoffe 54 (2001) pp. 122-126.

[105] Nieuwenhuizen, P.J., Ehlers, A.W., Hofstraat, J.W., Janse, S.R., Nielen, M.W.F., Reedijik, J., Baerends, E.J.: The first theoretical and experimental proof of polythiocarbamatozinc(II) complexes, catalysts for sulfur vulcanization. Chemistry-A European Journal 4 (1998) pp. 1816-1821.

[106] Elías-Zúñiga, A.: A phenomenological energy-based model to chracterize stress-softening effect in elastomers. Polymer 46 (2005) pp. 3496-3506.

[107] Kaliske, M.: Finite element approach to evaluate fracture sensitivity of elastomeric material. Kautschuk Gummi Kunststoffe 58 (2005) pp. 186-190.

[108] Klüppel, M.: Hyperelasticity and stress softening of filler reinforced polymer networks. Macromolecular Symposia 200 (2003) pp. 31-43.

[109] Guth, E.: Theory of filler reinforcement. Journal of Applied Physics 16 (1945) pp. 20-25.

[110] Payne, A.R., Whittaker, R.E., Smith, J.F.: Effect of vulcanization on the low-strain dynamic properties of filled rubbers. Journal of Applied Polymer Science 16 (1972) pp. 1191-1212.

[111] Mullins, L., Tobin, N.R.: Stress softening in rubber vulcanizates. Part I. Use of a strain amplification factor to describe the elastic behavior of filler-reinforced vulcanized rubber. Journal of Applied Polymer Science 9 (1965) pp. 2993-3009.

[112] Wolff, S., Donnet, J.B.: Characterization of fillers in vulcanizates according to the Einstein-Guth-Gold equation. Rubber Chemistry and Technology (1990) pp. 32-45.

[113] Shia, D., Hui, C.Y., Burnside, S.D., Giannelis, E.P.: An interface model for the prediction of Young's modulus of layered silicate-elastomer nanocomposites. Polymer Composites 19 (1998) pp. 608-617.

[114] Wu, Y.P., Jia, Q.X., Yu, D.S., Zhang, L.Q.: Modeling Young's modulus of rubber-clay nanocomposites using composite theories. Polymer Testing 23 (2004) pp. 903-909.

[115] Bissot, T.C.: Performance of high-barrier resins with platelet-type fillers. In 'Barrier Polymers and Structures'. Koros, W.J. (ed.) Washington, DC, USA: ACS 1990, pp. 225-238.

[116] Lan, T., Kaviratna, P.D., Pinnavaia, T.J.: On the nature of polyimide-clay hydrid composites. Chemistry of Materials 6 (1994) pp. 573-575.

[117] Bharadwaj, R.K.: Modeling the barrier properties of polymer-layered silicate nanocomposites. Macromolecules 34 (2001) pp. 9189-9192.

[118] Papke, N.: Neue thermoplastische elastomere mit co-kontinuierlicher phasenstruktur auf basis von polyester/elastomer blends unter verwendung gezielt chemisch funktionalisierter elastomere. PhD Thesis, Institut für Verbundwerkstoffe – Schriftreihe, Band 13 (2000).

[119] Papke, N., Karger-Kocsis, J.: Determination methods of the grafting yield in glycidyl methacrylate-grafted ethylene/propylene/diene rubber (EPDM-g-GMA): correlation between FTIR and ^{1}H-NMR analysis. Journal of Applied Polymer Science 74 (1999) pp. 2616-2624.

[120] Brown, R.P.: Physical Testing of Rubbers. London: Applied Science Publishers Ltd 1979, pp. 93-96.

[121] Jiang, P., See, H., Swain, M.V., Phan-Thien, N.: Using oscillatory squeezing flow to measure the viscoelasticic properties of dental composite resin cements during curing. Rheologica Acta 42 (2003) pp. 118-122.

[122] da Costa, H.M., Visconte, L.L.Y., Nunes, R.C.R., Furtado, C.R.G.: Rice husk ash filled natural rubber. I. Overall rate constant determination for the vulcanization process from rheometric data. Journal of Applied Polymer Science 87 (2003) pp. 1194-1203.

[123] Raghavan, S.R., Chen, L.A., McDowell, C., Khan, S.A., Hwang, R., White, S.: Rheological study of crosslinking and gelation in chlorobutyl elastomer systems. Polymer 37 (1996) pp. 5869-5875.

[124] Vlassopoulos, D., Chira, I., Loppinet, B., McGrail, P.T.: Gelation kinetics in elastomer/thermoset polymer blends. Rheologica Acta 37 (1998) pp. 614-623.

[125] Lin, Y.G., Mallin, D.T., Chien, J.C.W., Winter, H.H.: Dynamic mechanical measurements of crystallization-induced galation in thermoplastic elastomeric poly(propylene). Macromolecules 24 (1991) pp. 850-854.

[126] Richtering, H.W., Gagnon, K.D., Lenz, R.W., Fuller, R.C., Winter, H.H.: Physical gelation of a bacterial thermoplastic elastomer. Macromolecules 25 (1992) pp. 2429-2433.

[127] Yoon, J.T., Jo, W.H., Lee, M.S., Ko, M.B.: Effects of comonomers and shear on the melt intercalation of styrenics/clay nanocomposites. Polymer 42 (2001) pp. 329-336.

[128] Lindgreen, H, Drits, V.A., Sakharov, B.A., Salyn, A.L., Wrang, P., Dainyak, L.G.: Illite-smectite structural changes during metamorphism in black Cambrian Alum shales from the Baltic area. American Mineralogist 85 (2000) pp. 1223-1238.

[129] Meunier, A., Lanson, B., Beaufort, D.: Vermiculation of smectite interfaces and illite layer growth as a possible dual model for illite-smectite illitization in diagenetic environments: a synthesis. Clay Minerals 35 (2000) pp. 573-586.

[130] Lagaly, G., Ziesmer, S.: Colloid chemistry of clay minerals: the coagulation of montmorillonite dispersions. Advances in Colloid and Interface Science 100-102 (2003) pp. 105-128.

[131] Pozsgay, A., Fráter, T., Százdi, L., Müller, P., Sajó, I., Pukánszky, B.: Gallery structure and exfoliation of organophilized montmorillonite: effect on composite properties. European Polymer Journal 40 (2004) pp. 27-36.

[132] Németh, J., Rodríguez-Gattorno, G., Díaz, D., Vázquez-Olmos, A.R., Dékány, I.: Synthesis of ZnO nanoparticles on a clay mineral surface in dimethyl sulfoxide medium. Langmuir 20 (2004) pp. 2855-2860.

[133] Zaborski, M., Donnet, J.B.: Activity of fillers in elastomernetworks of different structure. Macromolecular Symposia 194 (2003) pp. 87-99.

[134] van Duin, M., Borggreve, R.J.M.: Blends of polyamides and maleic-anhydride-containing polymers: interfacial chemistry and properties. In 'Reactive Modifiers for Polymers'. Al-Malaika, S. (ed) London, UK: Blackie Academic 1997, pp. 133-162.

[135] Chow, W.S., Mohd-Ishak, Z.A., Karger-Kocsis, J., Apostolov, A.A., Ishiaku, U.S.: Compatibilizing effect of maleated polypropylene on the mechanical properties and morphology of injection molded polyamide 6/polypropylene/organoclay nanocomposites. Polymer 44 (2003) pp. 7427-7440.

[136] Karger-Kocsis, J.: Microstructure and fracture mechanical performance of short-fibre reinforced thermoplastics. In 'Application of fracture mechanics to composite materials' Friedrich, K. (ed.) Amsterdam, The Netherlands: Elsevier 1989, pp. 189-247.

[137] Leblanc, J.L.: Elastomer-filler interactions and the rheology of filled rubber compounds. Journal of Applied Polymer Science 78 (2000) pp.1541-1550.

[138] Sirisinha, C., Prayoonchatphan, N.: Study of carbon black distribution in BR/NBR blends based on damping properties: Influences of carbon black particle size, filler, and rubber polarity. Journal of Applied Polymer Science 81 (2001) pp. 3198-3203.

[139] Severe, G., White, J.L.: Transition behavior of hydrogenated acrylonitrile-butadiene rubber. Kautschuk Gummi Kunststoffe 55 (2002) pp. 144-148.

[140] Zanetti, M., Camino, G., Thomann, R., Mülhaupt, R.: Synthesis and thermal behaviour of layered silicate-EVA nanocomposites. Polymer 42 (2001) pp. 4501-4507.

[141] Mezger, M., Eisele, U., Rohde, E.: The performance of hydrogenated nitrile rubber (HNBR) under various dynamic stresses. Kautschuk Gummi Kunststoffe 44 (1991) pp. 341-347.

[142] Osman, M.A., Mittal, V., Lusti, H.R.: The aspect ratio and gas permeation in polymer-layered silicate nanocomposites. Macromolecular Rapid Communications 25 (2004) pp. 1145-1149.

[143] Osman, M.A., Mittal, V., Morbidelli, M., Suter, U.W.: Epoxy-layered silicate nanocomposites and their gas permeation properties. Macromolecules 37 (2004) pp. 7250-7257.

[144] Grunlan, J.C., Grigorian, A., Hamilton, C.B., Mehrabi, A.R.: Effect of clay concetration on the oxygen permeability and oprical properties of a modified poly(vinyl alcohol). Journal of Applied Polymer Science 93 (2004) pp. 1102-1109.

[145] Fornes, T.D., Paul, D.R.: Modeling properties of nylon 6/clay nanocomposites using composite theories. Polymer 44 (2003) pp. 4993-5013.

List of Publications

1. Varghese, S., Karger-Kocsis, J., Gatos, K.G.: Melt compounded epoxidized natural rubber/layered silicate nanocomposites: structure-properties relationships. Polymer 44 (2003), pp. 3977-3983.

2. Gatos, K.G., Kandilioti, G., Galiotis, C., Gregoriou, V.G.: Mechanically and thermally induced chain conformational transformations between helical form I and trans-planar form III in syndiotactic polypropylene using FT-IR and Raman spectroscopic techniques. Polymer 45 (2004), pp. 4453-4464.

3. Varghese, S., Gatos, K.G., Apostolov, A.A., Karger-Kocsis, J.: Morphology and mechanical properties of layered silicate reinforced natural and polyurethane rubber blends produced by latex compounding. Journal of Applied Polymer Science 92 (2004), pp. 543-551.

4. Gregoriou, V.G., Kandilioti, G., Gatos, K.G.: An infrared spectroscopic approach to the polymorphic behavior of syndiotactic polypropylene and its crystal-crystal transformations during mechanical stretching. Vibrational Spectroscopy 34 (2004), pp. 47-53.

5. Gatos, K.G., Thomann, R., Karger-Kocsis, J.: Characteristics of ethylene propylene diene monomer rubber/organoclay nanocomposites resulting from different processing conditions and formulations. Polymer International 53 (2004), pp. 1191-1197.

6. Gatos, K.G., Karger-Kocsis, J.: Estimation of the vulcanization time for rubbers by considering their linear viscoelastic response assessed by a plate-plate rheometer. Kautschuk Gummi Kunststoffe 57 (2004), pp. 350-354.

7. Gatos, K.G., Sawanis, N.S., Apostolov, A.A., Thomann, R., Karger-Kocsis, J.: Nanocomposite formation in hydrogenated nitrile rubber (HNBR)/organo-montmorillonite as a function of the intercalant type. Macromolecular Materials and Engineering 289 (2004), pp. 1079-1086.

8. Gatos, K.G., Apostolov, A.A., Karger-Kocsis, J.: Compatibilizing effect of grafted glycidyl methacrylate on EPDM/organoclay nanocomposites. Materials Science Forum 482 (2005), pp.347-350.

9. Tsotra, P., Gatos, K.G., Gryshchuk, O., Friedrich, K.: Hardener type as critical parameter for the electrical properties of epoxy resin/polyaniline blends. Journal of Materials Science 40 (2005), pp. 569-574.

10. Gatos, K.G., Karger-Kocsis, J.: Effects of primary and quaternary amine intercalants on the organoclay dispersion in a sulfur-cured EPDM rubber. Polymer 46 (2005), pp.3069-3076.

11. Gatos, K.G., Százdi, L., Pukánszky, B., Karger-Kocsis, J.: Controlling the deintercalation in hydrogenated nitrile rubber (HNBR)/organo-montmorillonite nanocomposites by curing with peroxide. Macromolecular Rapid Communications 26 (2005), pp. 915-919.

12. Minogianni, C., Gatos, K.G., Galiotis, C.: Estimation of crystallinity in isotropic isotactic polypropylene with Raman spectroscopy. Applied Spectroscopy 59 (2005), pp. 1141-1147.

13. Mohd Ishak, Z.A., Gatos, K.G., Karger-Kocsis, J.: On the in-situ polymerization of cyclic butylene terephthalate (CBT) oligomers: DSC and rheological study. Polymer Engineering and Science 46 (2006), in press.

14. Gatos, K.G., Martínez Alcázar, J.M., Psarras, G.C., Karger-Kocsis, J.: Polyurethane latex/water dispersible boehmite alumina nanocomposites: thermal, mechanical and dielectrical properties. submitted.

List of Students Support Works

1. Sawanis, N.S.: Compounding and characterization of hydrogenated nitrile rubber (HNBR)/organoclay nanocomposites. Studienarbeit, Technische Universität Kaiserslautern (2004).

2. Martínez Alcázar, J.G.: Effect of aspect ratio on the nanoreinforcement of rubber latex/alumina nanocomposites. Praktikum, Technische Universität Kaiserslautern (2005).